ADVANCED ENERGY MATERIALS
www.advenergymat.de

Self-Supported Electrocatalysts for Practical Water Electrolysis

Hongyuan Yang, Matthias Driess, and Prashanth W. Menezes**

Over the years, significant advances have been made to boost the efficiency of water splitting by carefully designing economic electrocatalysts with augmented conductivity, more accessible active sites, and high intrinsic activity in laboratory test conditions. However, it remains a challenge to develop earth-abundant catalysts that can satisfy the demands of practical water electrolysis, that is, outstanding all-pH electrolyte capacity, direct seawater splitting ability, exceptional performance for overall water splitting, superior large-current-density activity, and robust long-term durability. In this context, considering the features of increased active species loading, rapid charge, and mass transfer, a strong affinity between catalytic components and substrates, easily-controlled wettability, as well as, enhanced bifunctional performance, the self-supported electrocatalysts are presently projected to be the most suitable contenders for practical massive scale hydrogen generation. In this review, a comprehensive introduction to the design and fabrication of self-supported electrocatalysts with an emphasis on the design of deposited nanostructured catalysts, the selection of self-supported substrates, and various fabrication methods are provided. Thereafter, the recent development of promising self-supported electrocatalysts for practical applications is reviewed from the aforementioned aspects. Finally, a brief conclusion is delivered and the challenges and perspectives relating to promotion of self-supported electrocatalysts for sustainable large-scale production of hydrogen are discussed.

1. Introduction

The gradually rising energy and environmental crisis have caused increased global concerns, and therefore, developing renewable and clean emerging energy which can be employed as alternatives to traditional fossil fuels is of extreme necessity.[1–6] In this regard, hydrogen (H_2) is an ideal energy carrier and has received extensive attention due to its high gravimetric energy density (up to 142 MJ kg^{-1}), green combustion products, and recyclable features.[7,8] Currently, the primary methods for H_2 production are based on steam methane reforming, coal gasification, and biomass conversion, which are not only expensive but also emit a significant amount of CO_2 inevitably affecting the greenhouse effect.[9,10] From this perspective, an appealing alternative approach is to split water to produce only clean H_2 and oxygen (O_2) gas through thermocatalytic, photocatalytic, or electrocatalytic techniques.[11–13] Within them, electrocatalytic water splitting has become the worldwide research focus recently as this technology can produce environmental-friendly high-pure H_2 energy from electricity, as well as can be combined with other intermittent energy, such as wind and solar energy, elevating the utilization efficiency of the overall sustainable energy system.[14,15] The fundamental half-reactions which take place on a water electrolyzer involve hydrogen evolution reaction (HER) at the cathode and oxygen evolution reaction (OER) at the anode.[16] Presently, the commercial devices for water electrolysis include acidic proton-exchange membranes (PEMs) electrolyzer and alkaline water electrolyzers (AWEs). Among them, PEMs typically contain precious metal (such as platinum group metals) in their electrodes, leading to the rapid rise of cost and significant limit of further application, while AWEs equipped with non-precious metal-based electrodes usually operate at a low current density, displaying moderate energetic efficiency.[17,18]

To solve these bottlenecks, a considerable amount of research has been dedicated to investigate low-cost but active earth-abundant metal-based catalysts for water electrolyzers, especially transition metal (TM)-based ones, such as, nitrides,[19] oxides,[20] chalcogenides,[21] phosphides,[22] phosphates,[23] carbide,[24] borides,[25] borophosphates,[26,27] and intermetallic compounds.[28–30] Unfortunately, the activity and stability for most of these catalysts are still far from satisfactory from the perspectives of practical application in massive H_2 production, and the main reasons for this being i) the majority of electrocatalysts do not display reasonable activity in all-pH media (especially in neutral media due to the poor electric conductivity of the electrolyte) and the limit on pH ranges creates an increase of the electrolyte expenses for water electrolysis technology and lowers the yield of H_2 production.[31,32] ii) The direct seawater

H. Yang, M. Driess, P. W. Menezes
Department of Chemistry: Metalorganics and Inorganic Materials
Technische Universität Berlin
Straße des 17 Juni 135, Sekr. C2 10623 Berlin, Germany
E-mail: matthias.driess@tu-berlin.de;
prashanth.menezes@mailbox.tu-berlin.de

The ORCID identification number(s) for the author(s) of this article can be found under https://doi.org/10.1002/aenm.202102074.

DOI: 10.1002/aenm.202102074

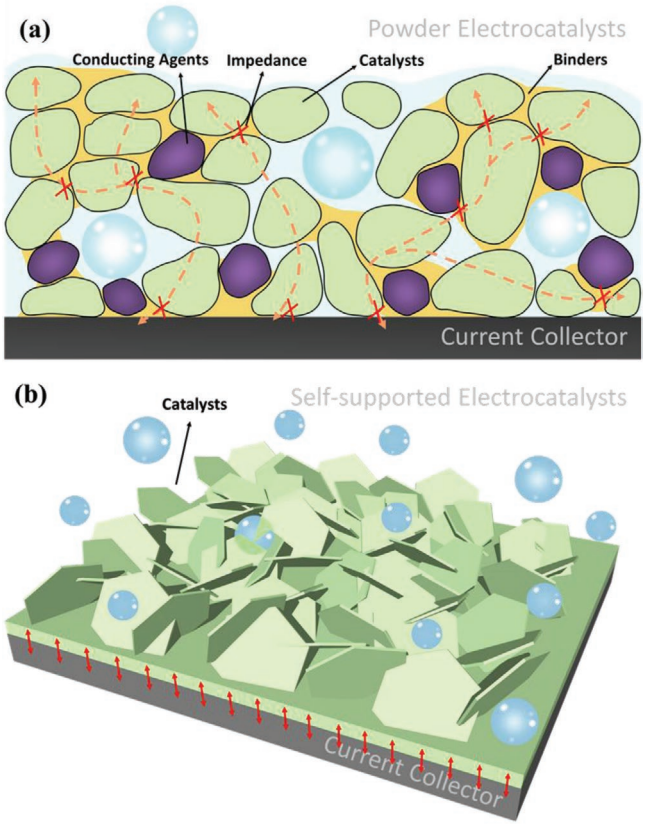

Figure 1. Schematic illustrations of a) powder electrocatalysts deposited on the electrode substrate with conducting additives and binders, and b) self-supported electrocatalysts.

splitting is still inefficient, highly expensive, and unpredictable compared to the purified water, although seawater is the most abundant water resource on earth (≈97%) and of high interest for technologically viable sustainable H_2 production.[33] iii) It is difficult to realize efficient overall water splitting (OWS) in which both HER and OER simultaneously take place in an integrated cell. This may probably be ascribed to the mismatched HER and OER performance in the various pH-value electrolyte, further diminishing the working efficiency of the whole water electrolyzer.[34,35] iv) Most of the reported electrocatalysts show good catalytic activity only at small current densities (≤20 mA cm^{-2}), which hardly meet the requirements of industrially operating electrolyzers (≥500 mA cm^{-2}).[36] v) The vast number of electrocatalysts can only maintain working current density for tens of hours, while the practical application requires up to thousands-of-hours stability.[37] In this regard, the development of noble metal-free catalysts for practical water splitting urgently requires further breakthroughs.

Currently, the most reported nanocatalysts for water electrolysis are synthesized in the form of powders (**Figure 1**a), which are then usually coated on the current collector (electrode substrates) by the addition of polymeric binders (such as Nafion or polytetrafluoroethylene). This inexorably masks the active sites, limits electron conductance, reduces the mass transport due to adverse consequences such as active surface area, microstructural destruction, and a decrease of volume, as well as deteriorates the film stability owing to binder degradation under operating conditions resulting in an overall decline of work efficiency and the rise of the fabrication cost.[38,39] Besides, for the substantial improvement of electrical conductivity of the powders, often conductive additives, especially carbon-based nanomaterials, are additionally added but on the downside, the carbon species have a propensity for corrosion (oxidation) at higher applied potentials or currents undermining the electrode performance.[40] Thus, it is critical to design and fabricate highly functional, electrocatalytically stable, and highly effective binder-free electrodes that can satisfy the required demand of water electrolysis and surmount the shortcomings of powder catalysts. On the other hand, binder-free self-supported electrocatalysts in which the catalytically active species directly grown on the conductive and flexible substrates (Figure 1b) have gained enormous interest and have been sought to be promising electrodes for practical water electrolysis. The main advantages of self-supported electrodes in comparison to the conventional ones include i) anchoring and dispersion of the active catalysts on the substrate promoting larger loading amounts and thus abundant active sites;[41] ii) evasion of polymeric binders and conductive additives to expose more catalytically active sites;[42,43] iii) suitable nanostructured engineering (1D, 2D, or 3D structures) leading to the enhanced electroactive surface area, swift charge and mass transport and superior reaction kinetics;[44] iv) strong adhesion and seamless integration between the electrocatalysts and conducting substrates that can prevent mechanical shedding of the catalysts from the substrates under continuous operation conditions of water splitting at large current densities;[45,46] v) the surface wettability engineering of self-supported electrocatalysts that can be easily controlled by modulating the composition and architecture of the deposited nanocatalysts. Here, the construction of superhydrophilic surface can facilitate the tight contact between active sites on the electrodes and the electrolyte, elevating the resulting catalytic activity. Such electrodes with superaerophobicity can enable the evolved bubbles to smoothly depart from the electrode surface, preventing the accumulation of numerous evolved bubbles on the electrode surface under large current densities, thus protecting active catalysts from shedding and interface resistance from boosting.[47,48] Lastly, vi) the post-coating step, as well as the additional polymeric binders and conductive additives are not required for self-supported electrocatalysts, which is a favorable factor for the simplification of fabrication procedures and the reduction of synthesis expenses.[49] All these factors endow the self-supported electrocatalysts with huge potential for practical water electrolysis to produce massive H_2 fuel to fulfill the anticipated energy demand.

In the past few years, encouraging progress has been continuously made in the development of self-supported electrocatalysts with outstanding activity and durability for water splitting. Accordingly, timely and comprehensive reviews about meaningful works in this area is of significant necessity, providing a useful guide to the following research. Although a limited number of reviews are accessible on the recent development of self-supported electrocatalysts for water electrolysis,[44,50–54] most of them overviewed from the perspectives of various TM-based compounds,[50,51] or geometric constructions,[44] or synthetic methods,[52,53] or

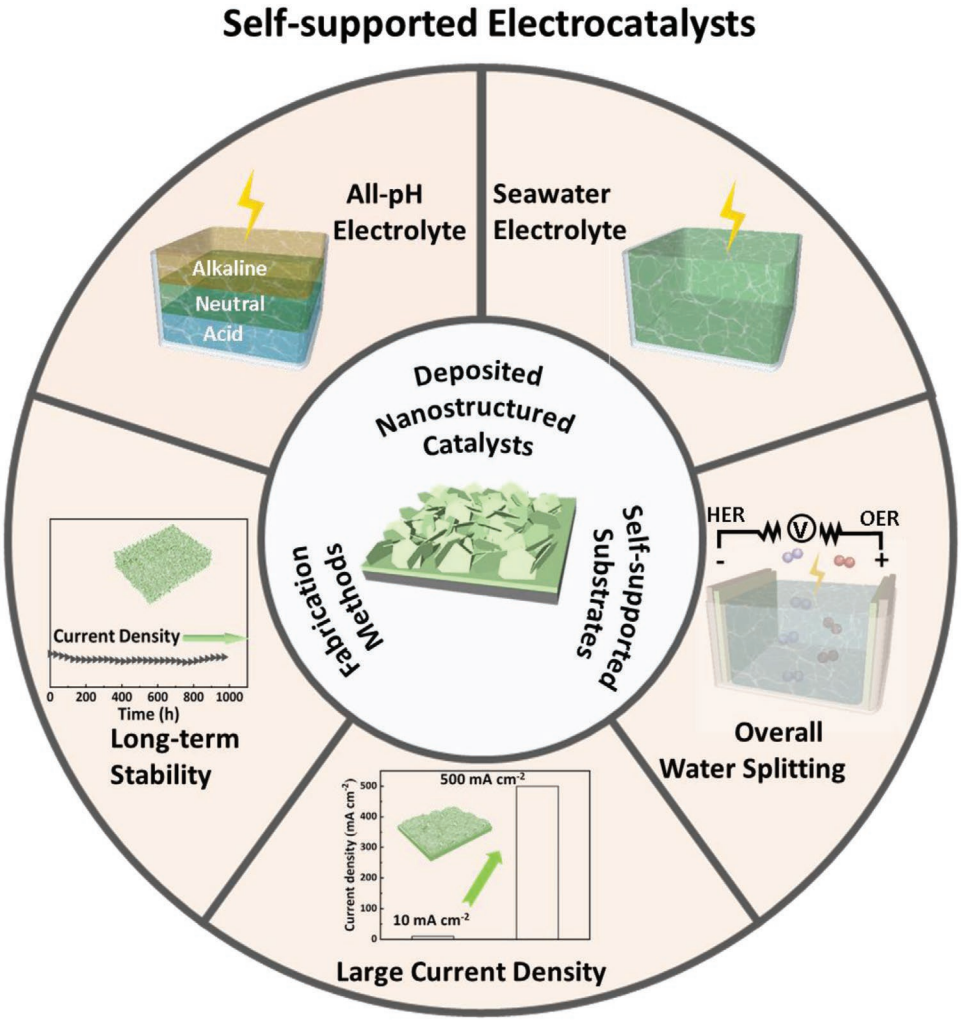

Figure 2. Design strategies of self-supported electrocatalysts and their promising practical application potentials.

selection of supported substrates.[54] Most importantly, an overall systematic and comprehensive review that is dedicated to reveal promising self-supported electrocatalysts for practical water electrolysis is still lacking. In view of this, herein, we conduct a detailed survey on the design and fabrication of self-supported electrocatalysts emphasizing nanostructured catalysts, conductive substrates, and fabrication methods. Based on this, the advanced self-supported electrocatalysts, which are promising for substantial H_2 generation through water electrolysis, are reviewed in the context of performance parameters in all-pH media, in seawater electrolyte, for OWS, under large current density and after long operational conditions, respectively (**Figure 2**). In addition, we also introduce the fundamentals of electrocatalytic water splitting and possible requirements for practical applications. Finally, the current challenges and future perspectives for the development of such catalysts are also highlighted. This review is expected to supply inspiration and guidance for the forthcoming research which is committed to further propel the progress of broad-scale, efficient and low-priced H_2 production by water electrolysis.

2. Fundamentals of Electrocatalytic Water Splitting

As is shown in **Figure 3**a, electrocatalytic water splitting refers to dissociating water to H_2 and O_2 through active catalysts which are coated on two electrodes in an electrolyzer. Therefore, it consists of two half-reactions, HER at the cathode and OER at the anode. The involved chemical reactions are as follows.[16]

Electrocatalytic water splitting reaction

$$2H_2O \rightarrow 2H_2 + O_2 \quad (1)$$

HER at the cathode
In acid electrolyte:

$$2H^+ + 2e^- \rightarrow 2H_2 \quad (2)$$

In alkaline or neutral electrolyte:

$$2H_2O + 2e^- \rightarrow 2H_2 + 2OH^- \quad (3)$$

OER at the anode

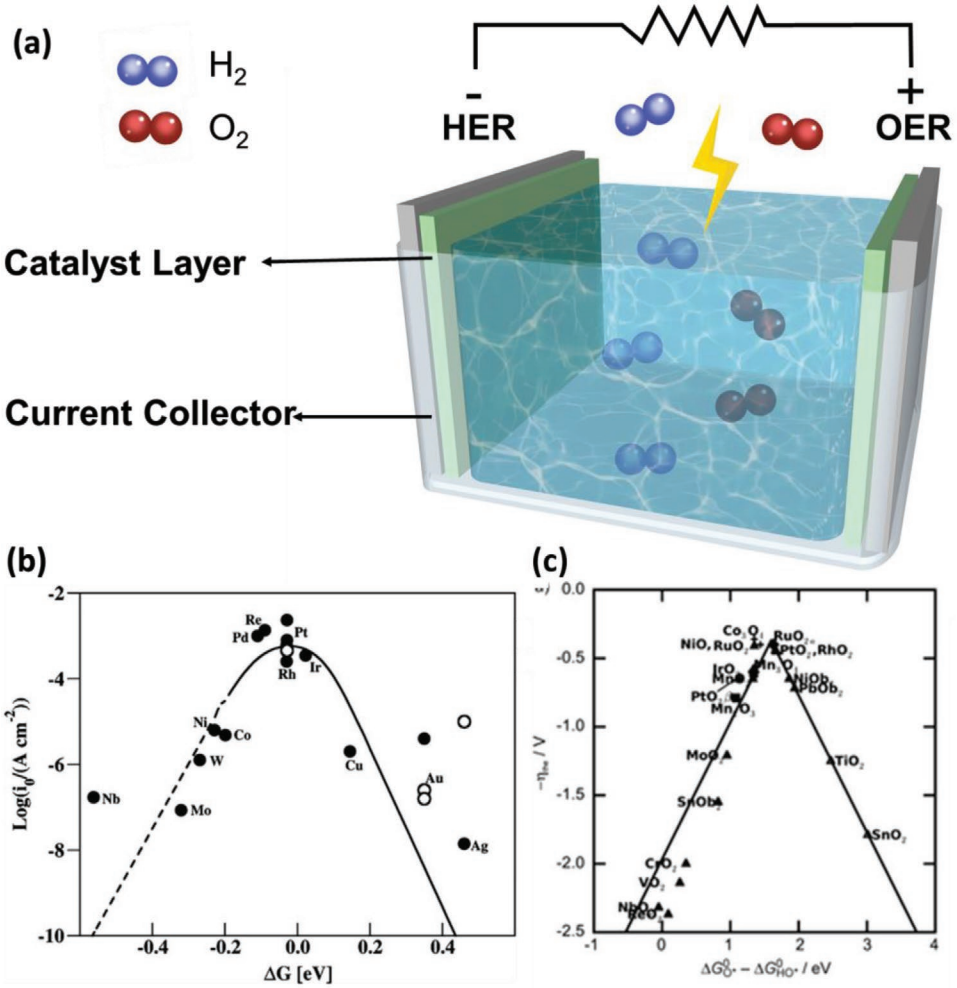

Figure 3. a) Schematic diagram of a water electrolyzer where the half-reactions, HER and OER occur at cathode and anode, respectively. b) HER volcano plot on the relationship between j_0 and ΔG_{*H} for different metals. Reproduced with permission.[56] Copyright 2010, American Chemical Society. c) OER volcano plot on the relationship between theoretical overpotential η and $\Delta G_{*O} - \Delta G_{*OH}$ for different metals oxides. Reproduced with permission.[59] Copyright 2011, Wiley-VCH.

In acid electrolyte:

$$2H_2O \rightarrow O_2 + 4H^+ + 4e^- \quad (4)$$

In alkaline or neutral electrolyte:

$$4OH^- \rightarrow O_2 + 2H_2O + 4e^- \quad (5)$$

2.1. Fundamentals of Hydrogen Evolution Reaction

The HER that takes place at the cathode mainly comprises two steps: i) Volmer reaction and ii) heyrovsky reaction or Tafel reaction. For the first step (Volmer reaction), when in the acid electrolyte, a proton H^+ from the electrolyte and an electron e^- from the electrode combine at the adsorption site of the electrode surface to form an adsorbed H* (* represents the adsorption site). In alkaline or neutral media, an additional dissociation process of water molecules is required, normally causing a corresponding reaction energy barrier.[32,55] For the second step, no matter in which electrolyte, there are two possible reaction pathways: one is that the generated H* is combined with a new pair of H^+ and e^-, thus the H_2 molecule will be obtained, and then desorbed. This step is referred as Heyrovsky reaction. In another case, the H_2 molecules are derived from the recombination of the adsorbed H* and its adjacent H*. This step is the Tafel reaction.[31] In electrolytes with various pH values, the specific HER reaction routes are as follows.[16]

In acid electrolyte:

$$H^+ + e^- + * \rightarrow H* \quad \text{(Volmer reaction)} \quad (6)$$

$$H* + H^+ + e^- \rightarrow H_2 \quad \text{(Heyrovsky reaction)} \quad (7)$$

$$\text{Or} \quad H* + H* \rightarrow H_2 \quad \text{(Tafel reaction)} \quad (8)$$

In alkaline or neutral electrolyte:

$$H_2O + e^- + * \rightarrow H* + OH^- \quad \text{(Volmer reaction)} \quad (9)$$

$$H^* + H_2O + e^- \rightarrow H_2 + OH^- \quad \text{(Heyrovsky reaction)} \tag{10}$$

$$\text{Or} \quad H^* + H^* \rightarrow H_2 \quad \text{(Tafel reaction)} \tag{11}$$

It is generally believed that the dominant reaction pathway for HER can be determined by the value of Tafel slope b from the simplified Tafel formula:[8]

$$\eta = a + b\log(j) \tag{12}$$

In this equation, η, a, b, and j represent overpotential, Tafel constant, Tafel slope, and current density, respectively. When the b value is around 116 mV dec^{-1}, the rate-determining step is the Volmer mechanism, and the HER will be governed by Heyrovsky and Tafel mechanisms when the value of Tafel slope is approximately 38 and 29 mV dec^{-1}, respectively.[8] On the other hand, no matter what the reaction path of HER is, the process of adsorbing H is inevitable. To this end, the free energy of hydrogen adsorption (ΔG_{*H}) is widely accepted as a descriptor that intuitively reflects the efficiency of H_2 evolution.[31] The absolute value of ΔG_{*H} closer to zero means the corresponding catalyst exhibits better HER activity. When ΔG_{*H} is over zero and its value is more positive, the hydrogen adsorption capacity is weaker. In other words, hydrogen desorption is easier. In contrast, when the ΔG_{*H} of a catalyst is less than zero and its value is more negative, the intermediate H has stronger adsorption with the adsorption site, thus the subsequent hydrogen desorption becomes more difficult.[56] As the volcano diagram on the relationship between exchange current density (j_0) of different metal catalysts and the related ΔG_{*H} depicted from the work of Nørskov et al. shows, the precious metal platinum with a ΔG_{*H} close to 0 owns the largest exchange current density, proving that Pt possesses superior HER activity to other metals (Figure 3b).[56]

2.2. Fundamentals of Oxygen Evolution Reaction

Compared with HER at the cathode, OER has larger energy-consumption and more sluggish reaction kinetics owing to its much more complex four discrete electron transfer process, and therefore, anodic OER is considered as the primary bottleneck restricting the development of water electrolysis technology. The elementary steps of OER undergo different mechanisms in different electrolytes.[16,57]

In acid electrolyte:

$$H_2O + * \rightarrow *OH + H^+ + e^- \tag{13}$$

$$*OH \rightarrow *O + H^+ + e^- \tag{14}$$

$$*O + H_2O \rightarrow *OOH + H^+ + e^- \tag{15}$$

$$*OOH \rightarrow *O_2 + H^+ + e^- \tag{16}$$

$$*O_2 \rightarrow * + O_2 \tag{17}$$

In alkaline or neutral electrolyte:

$$OH^- + * \rightarrow *OH + e^- \tag{18}$$

$$*OH + OH^- \rightarrow *O + H_2O + e^- \tag{19}$$

$$*O + OH^- \rightarrow *OOH + e^- \tag{20}$$

$$*OOH + OH^- \rightarrow *O_2 + e^- \tag{21}$$

$$*O_2 \rightarrow * + O_2 \tag{22}$$

However, in all kinds of electrolytes, the OER reaction involves the same four reaction intermediate, namely *OH, *O, *OOH, and *O_2. Correspondingly, the reaction free energy ΔG_1-ΔG_4 is commonly employed to evaluate the reaction kinetics of OER. The reaction step with the largest ΔG value is considered to dominate the entire OER process. In many cases, the conversion from *HO into *O or formation of *OOH from *O requires the greater reaction free energy, hence the larger one between ΔG_2 and ΔG_3 determining the whole OER reaction rate.[57,58] Additionally, Rossmeisl et al. pointed out for OER under ideal equilibrium voltage that the reaction free energy for the formation of the four elementary intermediates is the same, which is 1.23 eV (4.92 eV/4 = 1.23 eV) and the equilibrium voltage of each elementary reaction is 1.23 V (1.23 eV/e = 1.23 V)[59] That is, ideally, OER reaction can occur at the equilibrium voltage. Whereas under practical conditions, the applied voltage which can drive OER is always much greater than equilibrium voltage, and the theoretical overpotential can be obtained via the difference between max[ΔG_2, ΔG_3]/e and equilibrium voltage (1.23 V).[58]

On the other hand, for most metal oxides, there is such a relationship between *OH and *OOH: $\Delta G_{*OOH} - \Delta G_{*OH} = 3.2 \pm 0.2$ eV exist, implying the elementary reaction step of converting *OH into *O can occur at the free energy greater than 1.6 ± 0.1 eV.[59] Based on this, Rossmeisl and co-workers proposed $\Delta G_{*O} - \Delta G_{*OH}$ as a characteristic descriptor and illustrated the volcano map on the change of $\Delta G_{*O} - \Delta G_{*OH}$ against the variation of theoretical overpotential for different metal oxides, in which precious metal-based oxides generally show excellent catalytic performance (Figure 3c).[59]

2.3. Assessment of Electrocatalysts for Practical Water Splitting

Various criteria indexes have been applied to assess the performance of electrocatalysts for water splitting. Especially for those catalysts which are promising for practical application, their evaluation standard should be higher than the laboratory level. Unfortunately, so far, no systematic summary of the evaluation criteria for the performance of these catalysts has been conducted. In view of this, we specifically generalize the assessment standards for electrocatalysts with practical application potential from the perspectives of electrocatalytic activity, stability, and working environment, respectively.

Overpotential (η), Tafel slope (b), and exchange current density (j_0) are the essential indexes for electrocatalytic activity assessment. Among them, overpotential is the most critical parameter. It refers to the difference between the practically applied potential and the equilibrium potential for surmounting the reaction energy barrier which results from three aspects: i) electron transfer, ii) mass diffusion in the electrolyte, and iii) interplay at the electrode surface in the practical electrolyzer. As a result, the overpotential defined from linear sweep voltammetry or cyclic voltammetry (CV) polarization curve is normally composed of activity, concentration, and resistance overpotentials, originating from the electrochemical polarization, concentration polarization as well as resistance from the electrode, solution, and their contact points, respectively.[60] Since only the activity overpotential corresponds to the inherent properties of electrocatalysts, concentration and resistance overpotentials should be excluded for a precise reflection on water electrolysis activity. Working electrode rotation, electrolyte stir, and/or test temperature increment are the effective strategies for eliminating concentration overpotential, while iR_s correction (i and R_s represent working current and internal resistance, respectively) is often used to rule out resistance overpotential.[8] Similarly, the Tafel slope provides insight into the reaction mechanism and the kinetics of the reaction under study and should be performed in steady-state conditions.[61]

On one hand, the overpotential at 10 mA cm^{-2} current density (catalytic current normalized to the geometric area of working electrode) is most frequently selected as the reference to estimate water splitting activity. This criterion derives from the solar to energy efficiency for a one-step photoexcitation system, which should reach around 10%, enabling the solar hydrogen production to be cost-competitive.[62] On the other hand, for evaluating the practical application potential of electrocatalysts, it would be more meaningful to compare overpotential at a much higher current density. According to the industrial application, that is, PEM and AWE, with current densities ranging from 200 to 2000 mA cm^{-2}, the overpotential at above 500 mA cm^{-2} current density are usually taken into consideration to assess the activity of catalysts promising for practical water electrolysis.[32,50,63]

Chronoamperometry (CA), chronopotentiometry (CP), and CV cycles are routine methods to test the durability of electrocatalysts for water splitting. Normally, under the CA test, the constant applied potential is located at the value affording 10 mA cm^{-2} current density, while the applied current density tends to be directly fixed at 10 mA cm^{-2} when CP is carried out. Typically, the duration of these two measurements is expected to be at least above 24 h. Moreover, no less than 1000 times cycles are required for the CV test to define reasonable stability.[8] But such a short-term working period is obviously insufficient for those catalysts which can be utilized in practical H_2 production. In many cases, the electrocatalysts which are energetically efficient and can last thousands of hours with the robust operation are recognized as suitable candidates for practical development.[32,37,50]

The working environment is also a pivotal assessment factor for practical water splitting catalysts. First of all, most reported catalysts just show outstanding activity in half-cell conditions, rather than working as a bifunctional catalyst to achieve efficient HER and OER simultaneously in the same integrated electrolyzer. Thus, the catalyst which exhibits superior bifunctional activity, especially OWS activity, would be considered to have facile applicability and great cost-effectiveness. Besides, given that the utilization of considerable electrocatalysts is confined in the mild electrolyte environment (narrow pH range, room temperature, and moderate concentration), whether the excellent activity and durability of a catalyst can be displayed in different electrolyte conditions (e.g., all pH range, natural seawater, harsh temperature, and concentration) determines its potential to be transferred to the industry.

3. Design and Fabrication of Self-Supported Electrocatalysts

Self-supported electrocatalysts are described as nanostructured catalysts which are deposited on the substrates through various fabrication methods without the utilization of any binders or additives. With that in mind, in order to design and fabricate self-supported electrocatalysts with high working efficiency, low cost, and handy preparation process with three essential factors should be particularly considered, that is, the deposited nanostructured catalysts, the self-supported substrates, and the various fabrication methods. For the deposited nanostructured catalysts, the targeted catalyst components,[50] structure-activity relations,[64] and surface reconstruction during the electrochemical process[65] are responsible for whether their working efficiency can meet the requirement of practical application. Furthermore, different self-supported substrates, including conductive and insulating ones, also influence the nanostructure and performance of the resulting catalyst.[66,67] Lastly, according to various fabrication methods which are employed to deposit the catalytic species on all kinds of selective substrates, the obtained morphology, size distribution, crystalline phase, as well as, accessible and exposed active sites of the nanocatalysts are correspondingly controlled.[68,69] In recent times, extensive efforts have been dedicated to the aforementioned points, aiming at endowing self-supported electrocatalysts with practical application prospects. The following discussion will summarize the above three aspects.

3.1. Design of the Deposited Nanostructured Catalysts

For the nanostructured catalysts which are supported on the substrate, foremost, their components tend to determine the final catalytic performance and the whole preparation cost. Currently, non-noble metal elements, especially those TM ones, that is, Ni, Co, Fe, Cu, W, Mo, Zn, Ti, Mn, and V, are extensively explored for the synthesis of the catalytic species owing to their relatively high catalytic activity, earth abundance, and low price. These elements mainly exist in the various compounds, such as oxides, hydroxides, chalcogenides, pnictides, nitrides, borides, phosphates, and alloys as the principal ingredient in catalytic species.[50,70–75] To enable the water splitting efficiency of TM-based electrocatalysts to be comparable to the benchmark precious metal-based catalysts, two methods are most widely utilized as follows. i) The

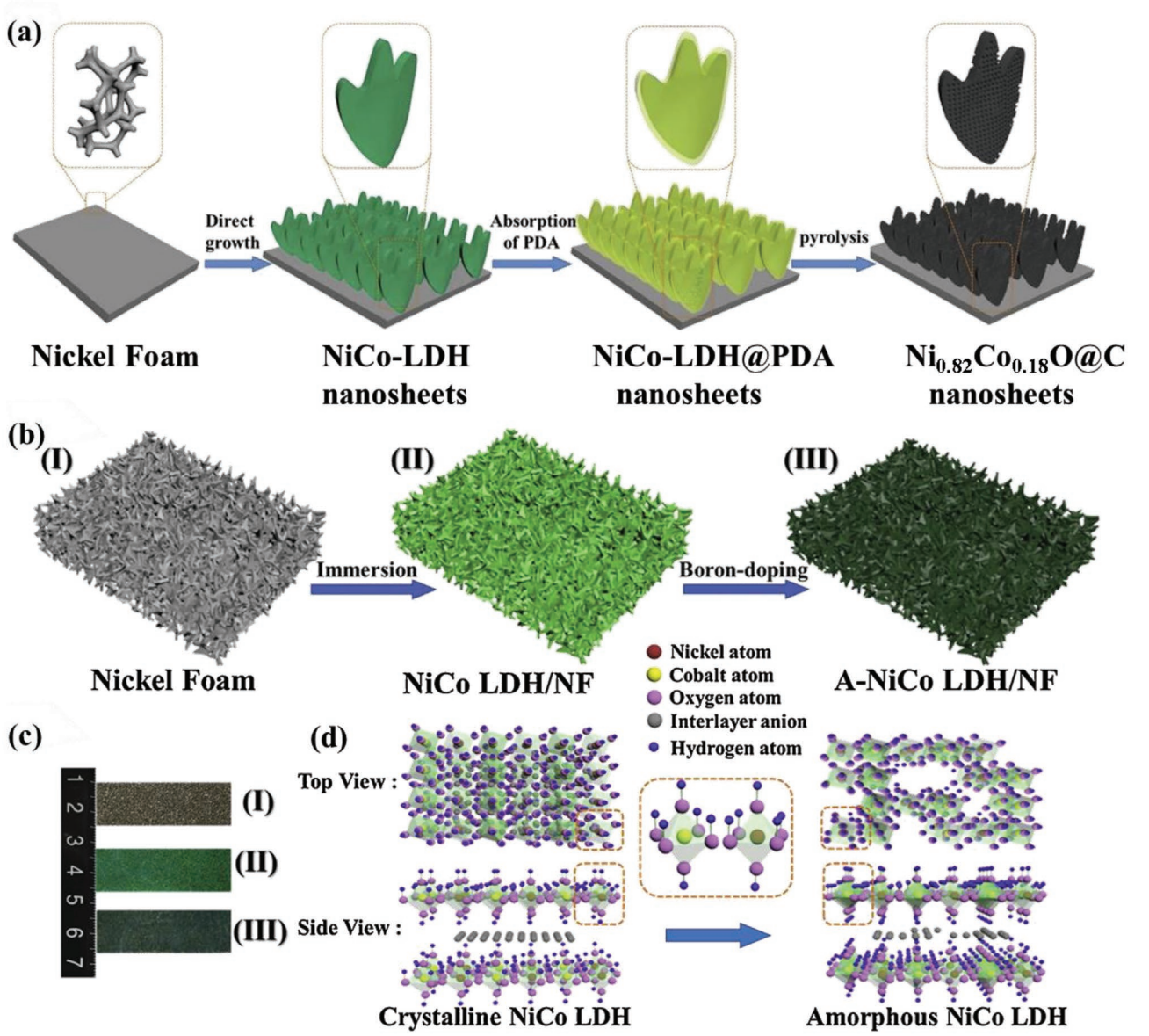

Figure 4. a) The schematic illustration of the synthetic process for the $Ni_{0.82}Co_{0.18}O$@C nanosheets arrays grown on the Ni foam (NF) substrate. Reproduced with permission.[34] Copyright 2019, Elsevier. b) The scheme of the preparation process for the amorphous NiCo LDH (A-NiCo LDH) nanosheet arrays supported on the NF, c) corresponding photographs of bare NF(I), NiCo LDH/NF (II), and A-NiCo LDH/NF (III), and d) the structural transformation of NiCo LDH to A-NiCo LDH. Reproduced with permission.[78] Copyright 2020, Elsevier.

coupling of conductive components (other conductive TM-based compounds or porous carbon substances).[76,77] For example, Wu et al. coupled the nickel foam (NF)-supported NiCo oxides nanosheets with ultrathin porous carbon shell which can facilitate the conductivity and provide more defects as active sites, further boosting the catalytic capability of the hybrid catalyst for OWS (**Figure 4**a).[34] ii) The doping of heteroatoms/groups, for example, metal atoms including various TMs and several rare earth metals, non-metal atoms such as N, P, S, Se, B as well as some small groups.[78–80] For instance, Wu et al. doped small BO_3 groups into crystalline NiCo layered double hydroxide (i.e., LDH, which is composed of metal cations which are located in octahedral brucite-like layers, as well as charge-balancing anions and water molecules in the interlayer spacing) nanosheets on NF, generating amounts of locally additional defects and thus providing more active sites and faster electron transfer. Accordingly, the BO_3-doping displayed much enhanced H_2 evolution ability compared to the pristine catalysts (Figure 4b–d).[78] The above two approaches can distinctly expose more active sites, expedite the ion/electron transfer and optimize the electronic modulation of TM-based nanostructured catalysts, thus improving their water electrolysis activity.

Furthermore, the structure and surface morphology of deposited nanocatalysts are directly related to the resulting water splitting efficiency. Therefore, the regulation of structure

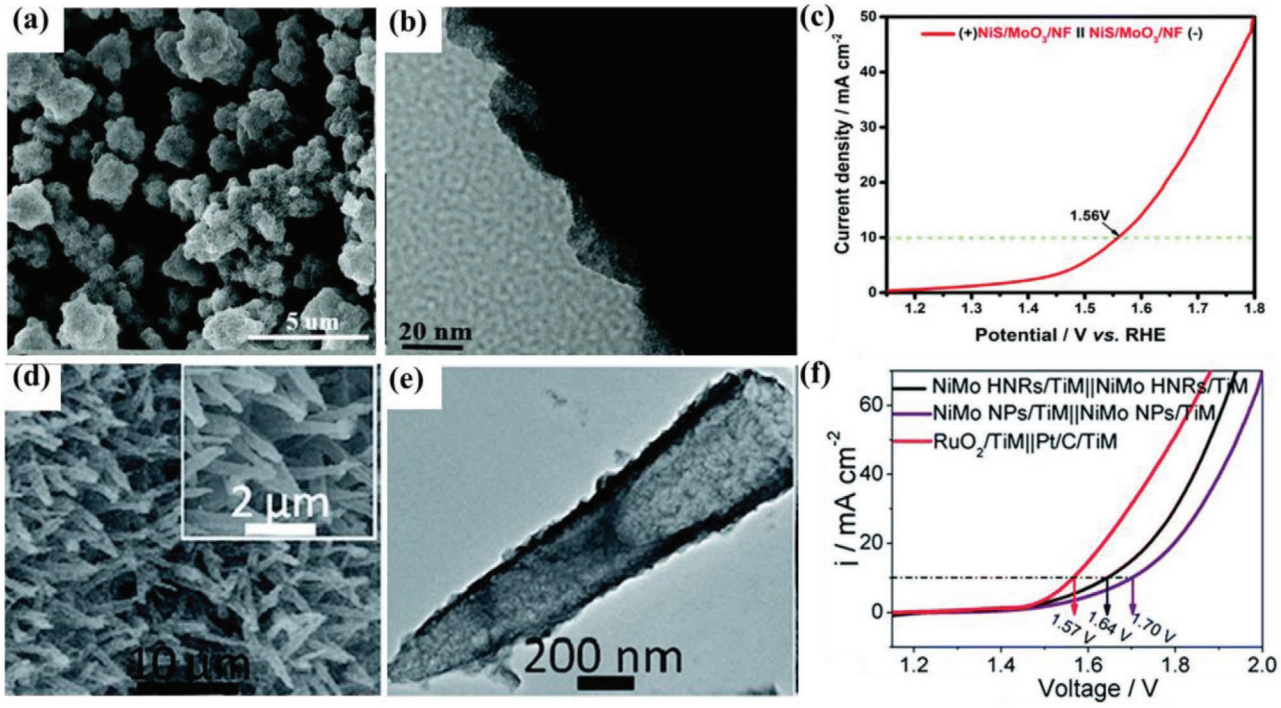

Figure 5. a) Scanning electron microscopy (SEM) image and b) Transmission electron microscopy (TEM) image of $NiS/MoO_3/NF$, c) Linear sweep voltammetry (LSV) polarization curve of $NiS/MoO_3/NF$ as both cathode and anode toward OWS. Reproduced with permission.[93] Copyright 2020, Royal Society of Chemistry. d) SEM image and e) TEM image of hollow NiMo-alloy, f) LSV polarization curve of NiMo HNRs/TiM as both cathode and anode toward OWS. Reproduced with permission.[96] Copyright 2015, Royal Society of Chemistry.

and surface morphology of catalytic species can effectively tune the overall working ability of self-supported electrocatalysts. Such regulations can be mainly divided into two types, that is, geometric dimension modulation and hollow structure construction.[8,81,82] For the former, the geometric dimension of the nanostructured catalyst comprises of 0D (e.g., nanoparticles and nanoclusters).[83,84] 1D (e.g., nanorods, nanotubes, and nanowires),[85–87] 2D (e.g., nanosheets, nanofilms, and nanoflakes),[88–90] 3D (e.g., nanocubes and nanocages) nanocatalysts.[91,92] Among them, 1D and 2D nanostructure are particularly favorable to the improvement of catalytic capacity because these morphologies exhibit larger surface area, more exposed active sites, and faster mass/electron transfer.[44] More intriguingly, the multidimensional integrated architecture can further enhance the merits of individual 1D or 2D nanostructure of nanocatalysts, which can be illustrated by the report of Du et al.[93] As is shown in **Figure 5**a,b, they fabricated a self-supported heterostructured electrocatalyst which consisted of 1D MoO_3 nanorods coupled with 2D NiS nanosheets on NF ($NiS/MoO_3/NF$). This hybrid catalyst owned more accessible active sites, rapid electron transfer, favorable gas bubbles escape, thus driving current density of 10 mA cm^{-2} at the cell voltage of only 1.56 V for OWS in alkaline media (Figure 5c). On the other hand, the hollow structure construction mainly consists of the configuration of the hollow structure and core-shell structure.[8] Their additional void spaces can enlarge the surface area, providing more accessible active sites and efficient mass transport, and thus entitling deposited catalysts with high catalytic activity.[94,95] For example. Sun et al. reported novel hollow NiMo nanorods arrays which were supported on Ti mesh (NiMo HNRs/TiM). Thanks to the merits of the unique 1D hollow structure including rich mass diffusion pathways and large exposed surface area, NiMo HNRs/TiM presented good bifunctional activity, delivering 10 mA cm^{-2} OWS current density at 1.64 V cell voltage (Figure 5d–f).[96] Furthermore, it is important to note that the rationally designed nanostructures and their surface morphology can control the specific surface area (which was normally measured by the Brunauer-Emmet-Teller, BET, method) of the resulting deposited nanocatalysts, and the larger electrochemical specific surface area they exhibit, the more exposed active sites they possess.[13] Increasing the surface porosity, as well as downsizing the structure of the deposited catalysts into ultrasmall nanoscales are the most commonly utilized methods for achieving self-supported nanocatalysts with higher electrochemical specific surface area, thus showing outstanding electrochemical performance.[97,98]

Finally, during the electrochemical process, especially for OER at the anode, the reconstruction of surface structure and crystalline phase inevitably occurs, which has become the recently emerging research focus on catalysts for water electrolysis.[98–100] Interestingly, the self-reconstruction of the surface phase tends to be accompanied by the modification of catalyst morphology into the layer-like structure, both boosting the intrinsic activity of original "pre-catalysts".[99] Therefore, it is believed that the in situ formed (oxy)hydroxides derived from "pre-catalyst" under OER work as the real active species to dominate the water oxidation.[101] For example, our

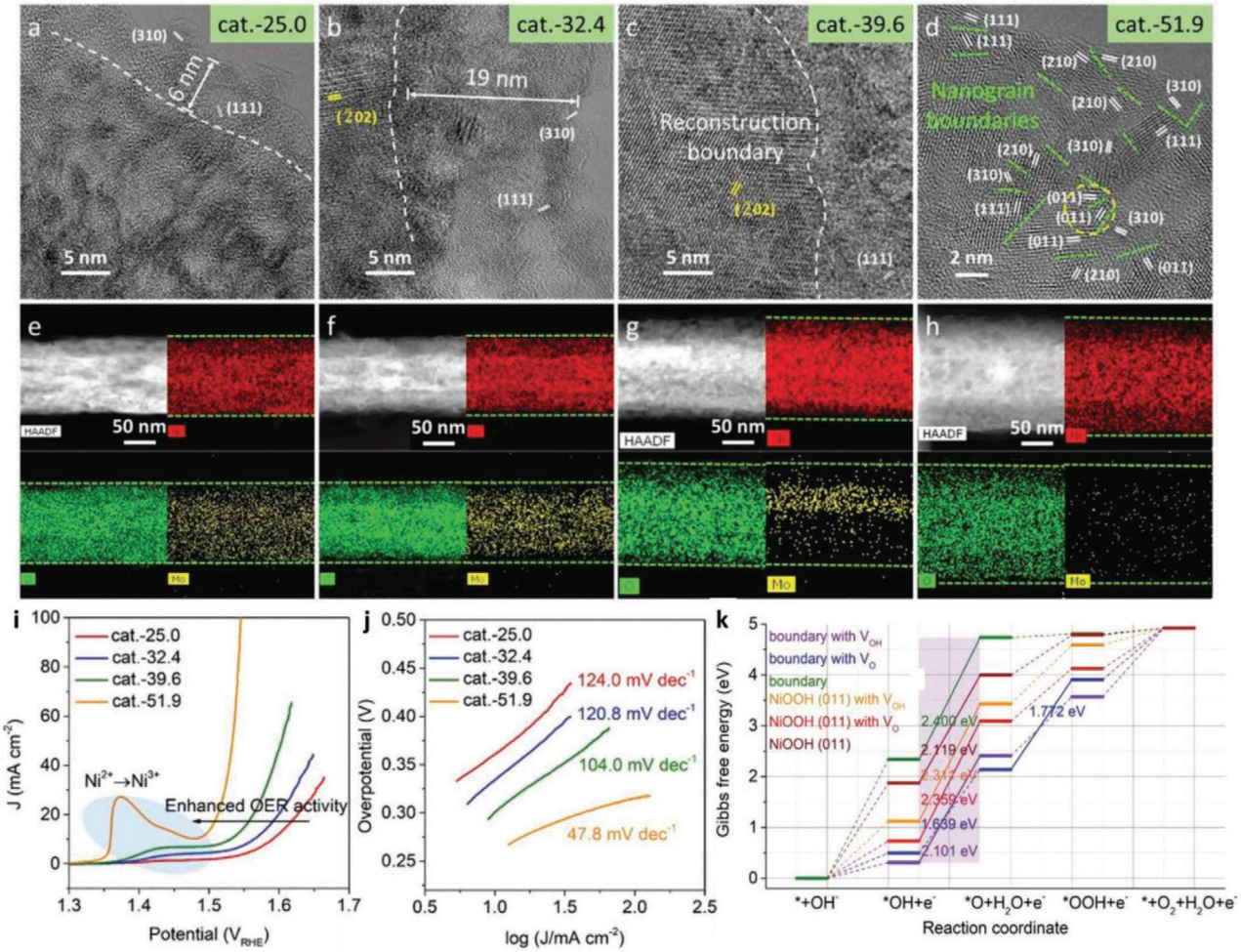

Figure 6. a–d) High-resolution TEM (HRTEM) and e–h) high-angle annular dark-field- scanning transmission electron microscopy (HAADF-STEM) images with the corresponding elemental mappings of "pre-catalysts" which were electrochemically activated at different temperatures. Note that cat.-T in this figure represents the products transformed from"pre-catalyst" at various activation temperatures, where $T = 25.0$, 32.4, 39.6, and 51.9 °C, respectively. The white lines in (a–c) represent the grain boundary formed in reconstruction time. i) LSV curves and j) Tafel slope of the corresponding products tested at 25.0 °C, respectively. k) Free energy of each reaction step on different models, considering the effects of boundary and O/OH vacancies on OER. Reproduced with permission.[104] Copyright 2020, Wiley-VCH.

group has prepared NF-supported NiGe intermetallic compounds, which rapidly and deeply transformed into OH^-/CO_3^{2-} intercalated γ-NiOOH under anodic activation along with the severe loss of Ge atoms, and thereby exhibited impressive OER activity and durability in alkaline media.[30] However, the reconstruction region for most nanostructured catalysts is normally confined at less than 10 nm range near the surface. The inner oxidation is prevented because of the dense near-surface reconstructed layer, which blocks the exposure of active sites and limits the further promotion of catalytic performance.[102,103] To this end, the deep and even complete reconstruction of "pre-catalysts" has become the necessary concern for rational catalyst design. An approach to dealing with this problem is performing an electrochemical activation process at a higher operating temperature.[104] Mai et al. employed the anode-CP method to activate the "pre-catalyst" $NiMoO_4$ on NF to be completely reconstructed into the active NiOOH species at high activation temperature of 51.9 °C. While low-degree reconstruction of the same "pre-catalyst" can be observed at the activation temperature of 25 °C. The rich grain boundaries and vacancies in the completely reconstructed NiOOH nanoparticles diminished the reaction energy barrier, accounting for the resulting excellent water splitting performance (**Figure 6**a–k).[104] The other alternative is to downsize the bulk "pre-catalysts" into ultrafine nanounits.[105] As another work of Mai et al. shows, the NiO nanosheets grown on NF (NiO/NF) was utilized as the "pre-catalyst." After breaking NiO into sub-10 nm ultrasmall nanoparticles via a lithiation treatment, the deep reconstruction of NiO into active NiOOH with abundant defects can be easily achieved through CV at anode potential. In contrast, only a 5 nm NiOOH layer was formed on the NiO "pre-catalyst" after direct electro-oxidation because of the blocked electrolyte penetration. Hence, the deep reconstructed NiOOH possessed much better OER activity, durability, and corrosion resistance in the alkaline electrolyte.[105]

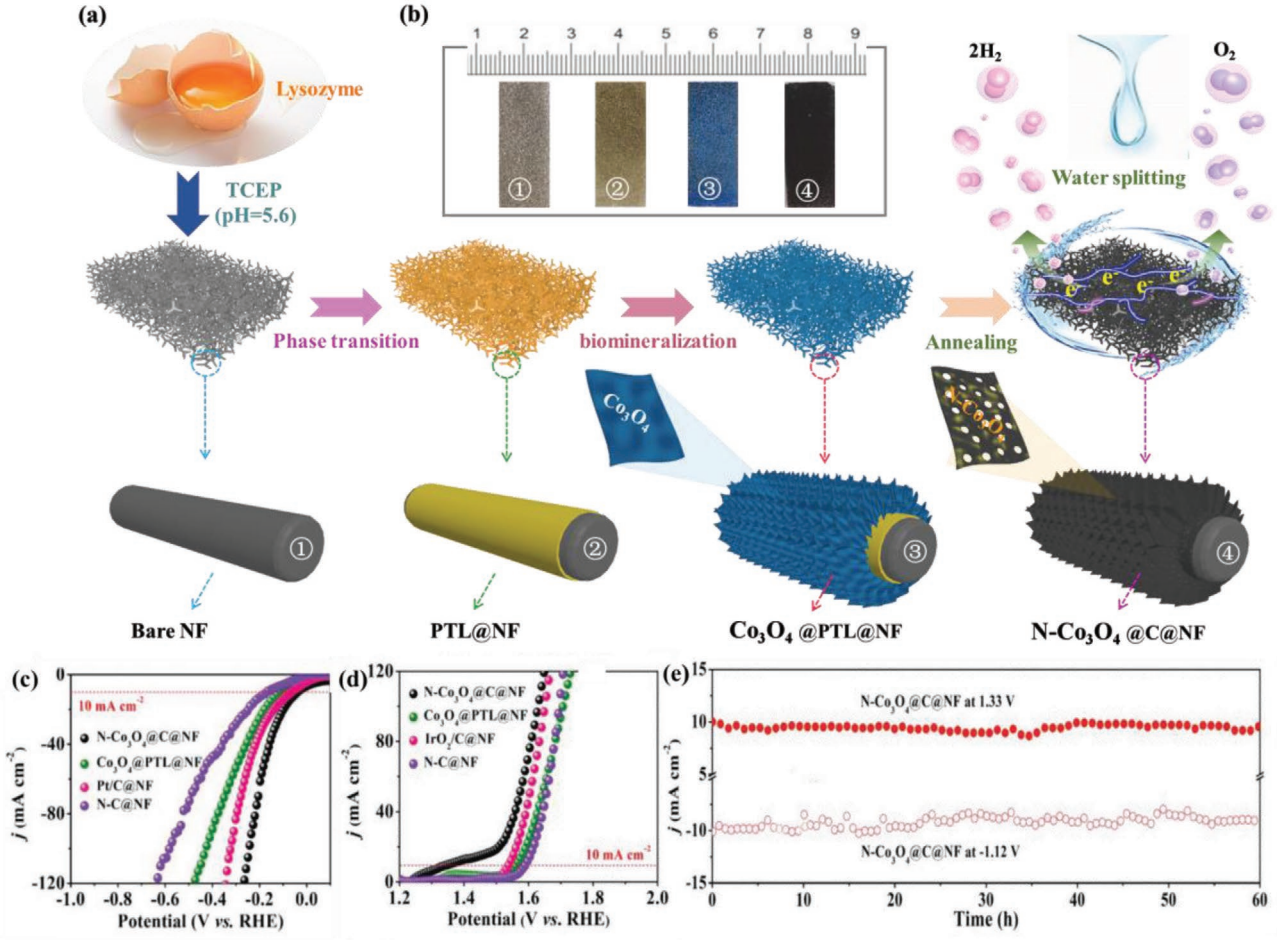

Figure 7. a) Schematic illustration of the synthesis procedure for N-Co_3O_4@C@NF. b) Photographs of bare NF, PTL@NF, Co_3O_4@PTL@NF, and N-Co_3O_4@C@NF. c) HER and d) OER polarization curves of N-Co_3O_4@C@NF, Co_3O_4@PTL@NF precursor, Pt/C@NF, and N-C@NF. e) The *i–t* curve of N-Co_3O_4@C@NF for HER and OER, respectively. Reproduced with permission.[114] Copyright 2019, Wiley-VCH.

3.2. Selection of Self-Supported Substrates

At present, most reported substrates applied in self-supported electrodes can be divided into two categories: i) Conventional conductive substrates, such as metal-based (e.g., metal foams, metal foils, and metal meshes),[106–109] carbon-based (e.g., carbon cloth, carbon paper, graphene paper),[54,67,110] and fluorine-doped tin oxide (FTO) or indium tin oxide (ITO) glass;[72,111] ii) unconventional non-conductive substrates, such as paper, textiles, and sponge.[112,113]

Conductive substrates are most widely adopted as substrates for self-supported electrodes since they can obviously elevate the conductivity of the entire electrode.[78] Among them, metal foams (especially NF and cooper foam, CF) are the most popular ones considering their characteristic 3D macroporous structure and great electrical conductivity.[34] For example, Wu et al. enabled the phase-transited lysozyme film to be adsorbed on the NF substrate (PTL@NF) through a facile immersion method. Followed by biomimetic mineralization, the 2D Co_3O_4 nanosheets were nucleated and grown on PTL@NF (Co_3O_4@PTL@NF) and finally carbonized to transform into the N-doped Co_3O_4 wrapped in carbon mesh with rich oxygen defects (N-Co_3O_4@C@NF) (**Figure 7**a,b). Because of the intimate contact between active Co_3O_4@C and NF substrate, as well as the open architecture of the self-supported electrode, the electron/ion transfer, mass transport, and the generated bubbles escape were particularly intensified. As a result, this self-supported electrocatalyst was entitled to a rapid catalytic kinetic process and long-term electrochemical reaction stability. When serving for HER and OER under alkaline conditions, it only needed 42 and 96 mV overpotentials to drive a current density of 10 mA cm^{-2}, respectively and maintained such activity for up to 60 h. (Figure 7c–e).[114] Additionally, metal foils, including nickel foil, iron foil, and titanium foils, have also received considerable attention due to their extreme accessibility and low cost.[115,116] For example, Guo et al. employed a facile and mild electroless plating method to deposit large amounts of metal borides on Ni and Ti foil with a maximum area of 10 × 10 cm^2. In particular, the Co-B deposited on Ni foil can transport 10 mA cm^{-2} at only 70 and 140 mV overpotential for HER and OER, respectively, in 1.0 M KOH. Also, it can retain a large current density up to 1000 mA cm^{-2} for 20 h without a decline in activity.[117]

Although metal-based substrates can apparently enhance the catalytic activity of the whole electrodes, their relatively poor

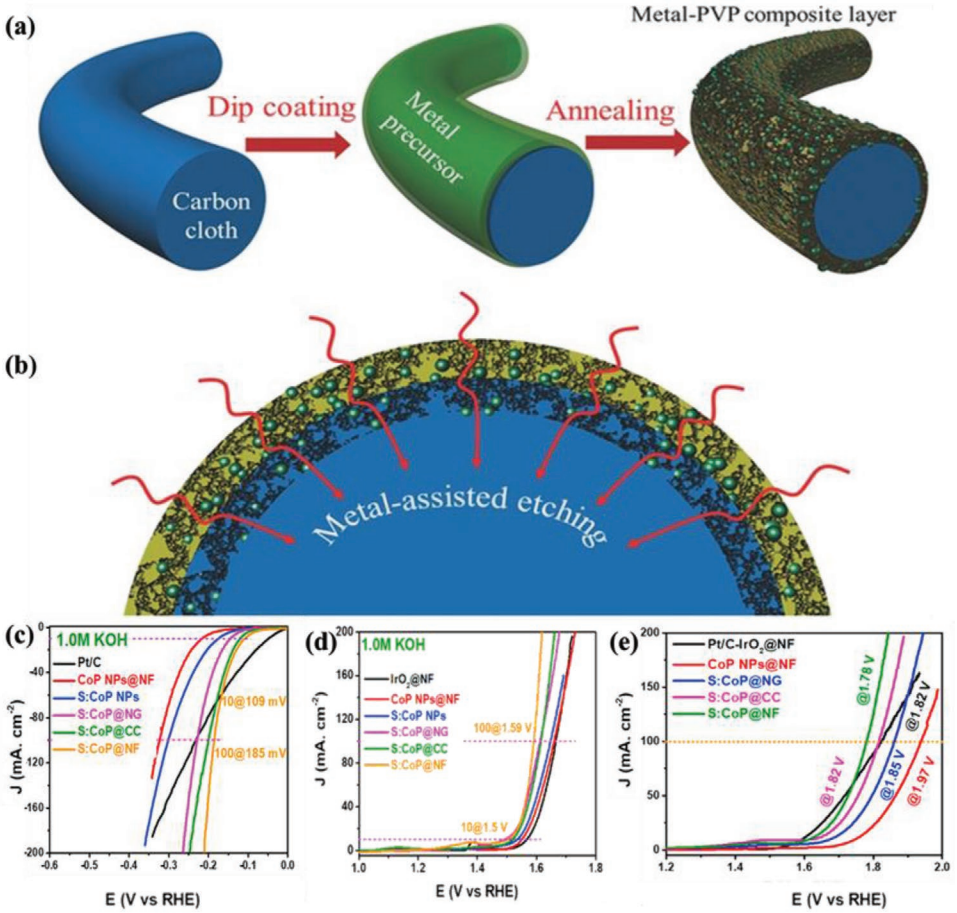

Figure 8. a) Schematic illustration of synthesis procedure for TM-based nanoparticles embedded into N doped porous carbon on CC as hybrid catalysts. b) The interaction between TM-based nanoparticles and CC. Reproduced with permission.[121] Copyright 2017, Wiley-VCH. LSV polarization curves of S:CoP@NF, S:CoP@CC and other samples for c) HER, d) OER, and e) OWS in 1.0 KOH. Reproduced with permission.[122] Copyright 2018, Elsevier.

flexibility and elasticity cause negative impacts on their fabrication and application.[118] Specifically, the most commonly utilized NF behaves too fragile as electrodes after high-temperature sample synthesis (over 400–500 °C).[119] In this regard, carbon-based substrates such as carbon cloth (CC) is highly flexible and elastic and thus considered appropriate substitutes to metal-based substrates.[71,120] Fan et al. utilized CC with strong mechanical robustness and electrolyte corrosion resistance as the substrate, which bore various TM nanoparticles embedded into N-doped carbon shell. In turn, the ultrafine metal nanoparticles etched the surface of CC, found to be highly porous (**Figure 8**a,b). With the support of a more specific surface area, rapid electron/ion transfer, and a solid bond between active catalysts and CC substrates, this self-supported electrode showed outstanding bifunctional water electrolysis activity and stability in alkaline media.[121] However, owing to the relatively lower conductivity and higher oxidation sensitivity compared with metal foams, the activity of self-supported electrocatalysts on CC is relatively inferior to that on metal foams.[113] As is observed in the paper of Lee et al., the authors deposited S doped CoP nanoparticles with the same amount on bare NF (S:CoP@NF) and bare CC substrate (S:CoP@CC), respectively. As a result, the catalytic activity of S:CoP@NF was much superior to that of S:CoP@CC for both HER and OER as well as for OWS (Figure 8c–e).[122] Hence, in accordance with different conditions of catalyst fabrication and characteristics of nanostructured catalysts, the appropriate substrates should be correspondingly selected for self-supported electrode preparation.

Apart from the common metal-based and carbon-based conductive substrates, inactive but flat FTO/ITO glass was also adopted for exploration on self-supported electrocatalysts. Although FTO/ITO bearing catalytic species shows lower work efficiency than the same species supported on more conductive metal or carbon-based substrates, they can avoid influencing catalysts characterizations and electrochemical measurements and are beneficial for direct observation of the reaction mechanism of the deposited catalysts.[123] Based on this, the investigated catalysts were usually deposited on FTO/ITO as a reference to exclude the impact of active substrates, especially metal foams, on the measured activity. In the previous works of our group, apart from comparing the catalytic performances of different materials supported on NF, the performance of the same samples on FTO/ITO was also conducted to define the trend of their intrinsic activity.[3,70,72–75,124,125]

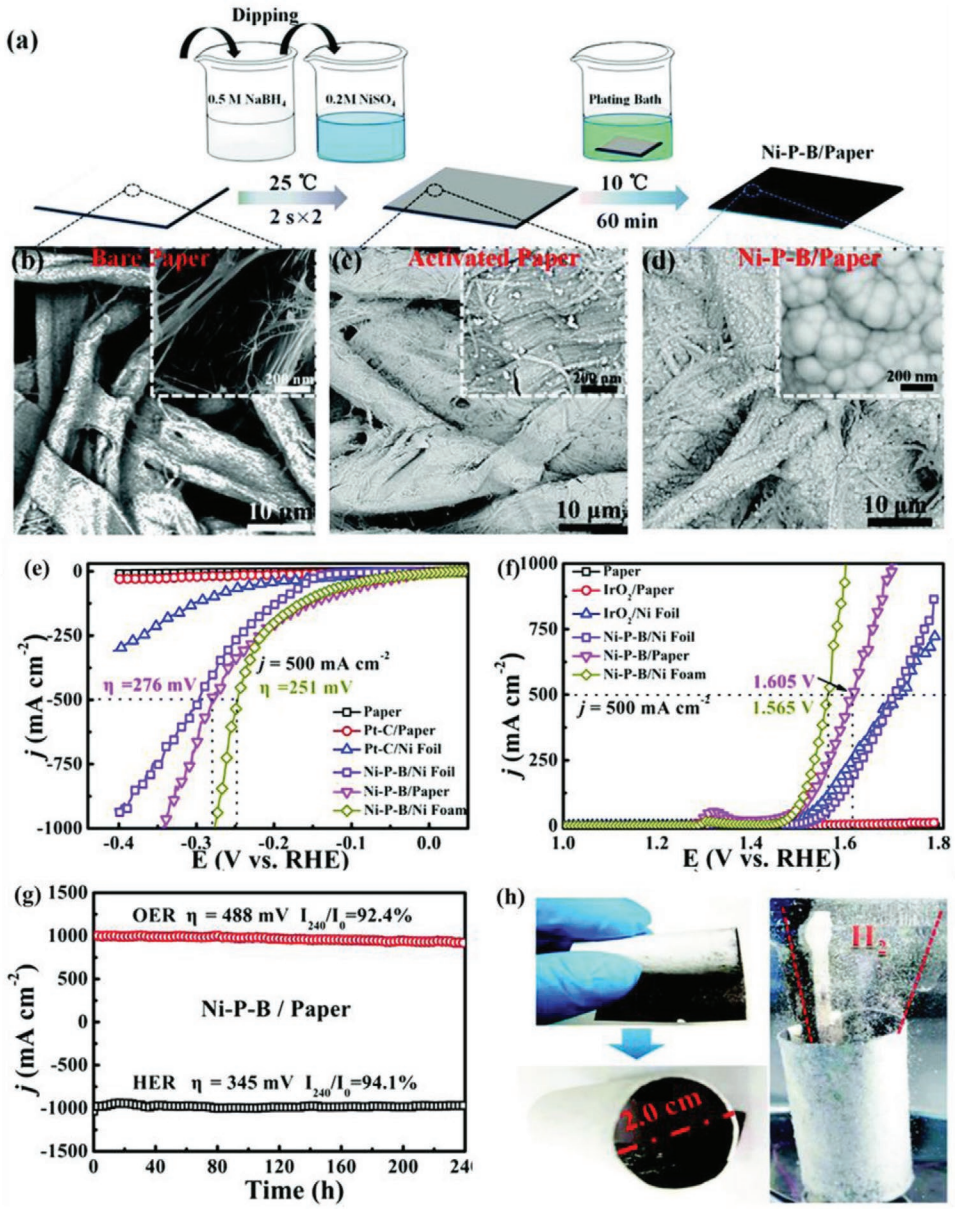

Figure 9. a) Schematic illustration of synthesis procedure for Ni-P-B/paper catalyst. SEM images of b) nonactivated paper, c) activated paper, and d) Ni-P-B/paper catalyst. LSV polarization curves of Ni-P-B/paper and other samples for e) HER and f) OER. g) *i*–*t* curves of Ni-P-B/paper at 1000 mA cm^{-2} for 240 h in 1.0 M KOH. h) Digital photograph of Ni-P-B/paper electrode when producing H_2. Reproduced with permission.[112] Copyright 2019, Royal Society of Chemistry.

Very recently, researchers have set eyes on unconventional substrates including paper, textiles, and sponges that have low-conductivities or even insulating. Such materials attained interest because of their extremely reduced cost, higher accessibility, convenience, and for being environmentally friendly.[112,113] Based on this, some researchers have pointed out that growing active catalysts with good conductivity on non-conductive but low-price substrates can not only enable the assembled self-supported electrocatalyst to display high electrochemical performance, but also fulfill the motivation of cost reduction for practical application.[112,126] Guo et al. fabricated highly active nanocatalysts on pre-activated paper, textiles, and sponges to construct a series of extremely efficient self-supported electrodes for water splitting via handy electroless plating methods (**Figure 9**a–d). Of note, the Ni-P-B catalyst deposited on the pre-activated filter paper (Ni-P-B/Paper) achieved high efficiency for both HER and OER in 1.0 M KOH. Also, they could steadily drive a large current density of 1 A cm^{-2} over 240 h (Figure 9e–g). More inspiringly, this paper-based electrode presented very light weight and great flexibility compared with the catalysts coupled with the metal-based substrate, suggesting considerable practical and environmental advantages (Figure 9h).[112]

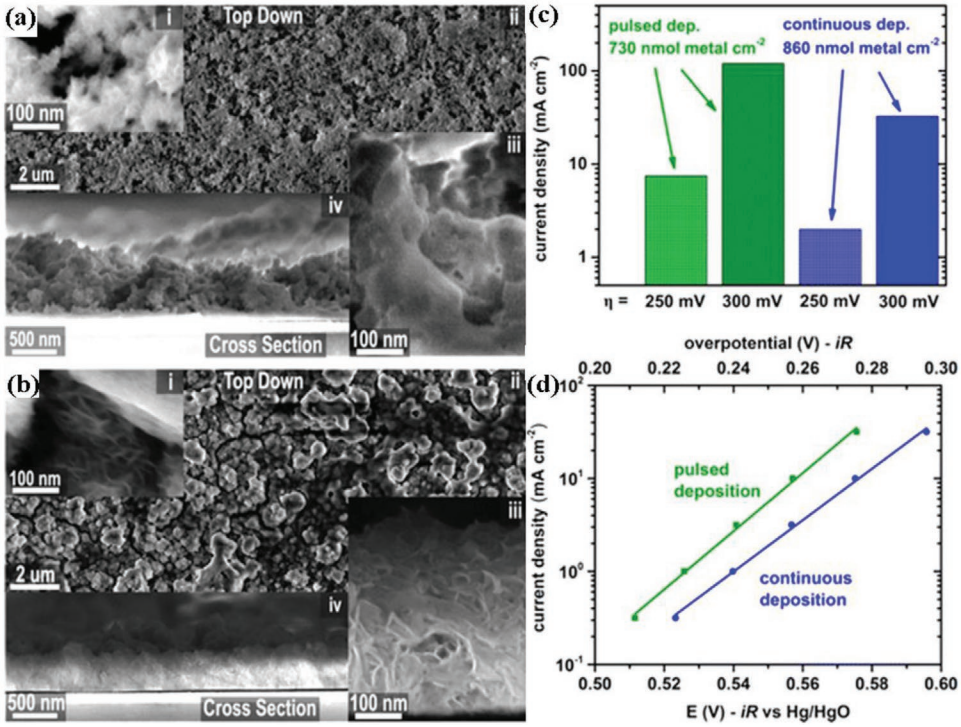

Figure 10. SEM images of a) continuous and b) pulse deposition films with both i,ii) top-down and iii,iv) cross-sectional direction. c–d) Electrocatalytic OER performance for films prepared by continuous and pulse deposition. Reproduced with permission.[133] Copyright 2015, American Chemical Society.

3.3. Fabrication Methods of Self-Supported Electrocatalysts

Various fabrication strategies have been applied to manipulate the composition, size distribution, elemental dispersion, surface morphology, and resulting catalytic activity of the nanoarrays which are supported on conductive substrates.[52,127] The majority of these methods can be classified into two types according to different synthetic procedures, that is, one-step synthetic method and multi-step synthetic method. The former refers to the in situ synthesis of well-defined TM-based catalysts on different substrates without any post-treatment, which mainly includes electrochemical deposition, hydro/solvothermal synthesis, and wet chemical methods.[71,128,129] On the other hand, the multi-step synthetic method is usually realized through the following ways. i) Precursors are deposited on the selective substrates first and then post-treated mostly in line with the composition of the targeted product (precursor-modification);[130,131] ii) The expected catalytic nanoarrays are fabricated, followed by depositing the as-obtained nanocatalysts on the conductive substrates (catalyst-deposition).[70]

The most frequently observed one-step synthetic methods are electrochemical deposition and hydro/solvothermal synthesis. Electrochemical deposition is usually conducted in a standard two or three-electrode system where the selective substrate is used as the working electrode. Under an applied electric field, CA, CP, or CV techniques are performed for the deposition of nanocatalyst on the substrate.[52] To be specific, driven by the applied electric field as well as the diffusion and convection, the solvated metal ions in the electrolyte are migrated toward the cathode which is covered with the internal Helmholtz layer and external diffusion layer. The migrated cations enter first to the diffusion layer where their solvated water molecules are aligned. Thereafter, benefiting from the high field strength of the double layer, the metal ions are liberated from the coupled water molecules, passing through the diffusion layer and reaching the internal Helmholtz layer. Finally, the free metal ions are reduced and deposited on the cathode, forming the desired TM-based nanocatalysts.[132] More importantly, electrochemical deposition exhibits a list of advantages including a short deposition period (no more than several minutes), a large range of desired chemical compounds (nearly all kinds of TM-based compounds), and a controllable loading microstructure and amount (tuned by deposition time and methodologies).[41,50] For example, Boettcher and co-workers carried out the electrochemical deposition through a two-electrode configuration, in which Au-coated glass slide or FTO were used as working electrodes to deposit Ni(Fe)OOH active catalysts by CP method at a constant cathodic current density of –10 mA cm^{-2}. The continuous deposition process without any pulse resulted in a porous microstructure of resulting Ni(Fe)OOH with large void volume, which derived from the continuously uneven precipitation of hydroxides on the surface of the growing deposited film. Nevertheless, under pulse deposition, a more densely packed structure of the deposited film was fabricated (**Figure 10**a). This can be attributed to the timely replenishment of fresh reactive electrolytes during pulse current intervals, promoting the uniform formation of hydroxides. Compared with the porous one, the denser film facilitated the superior electrical connection between the outermost part of

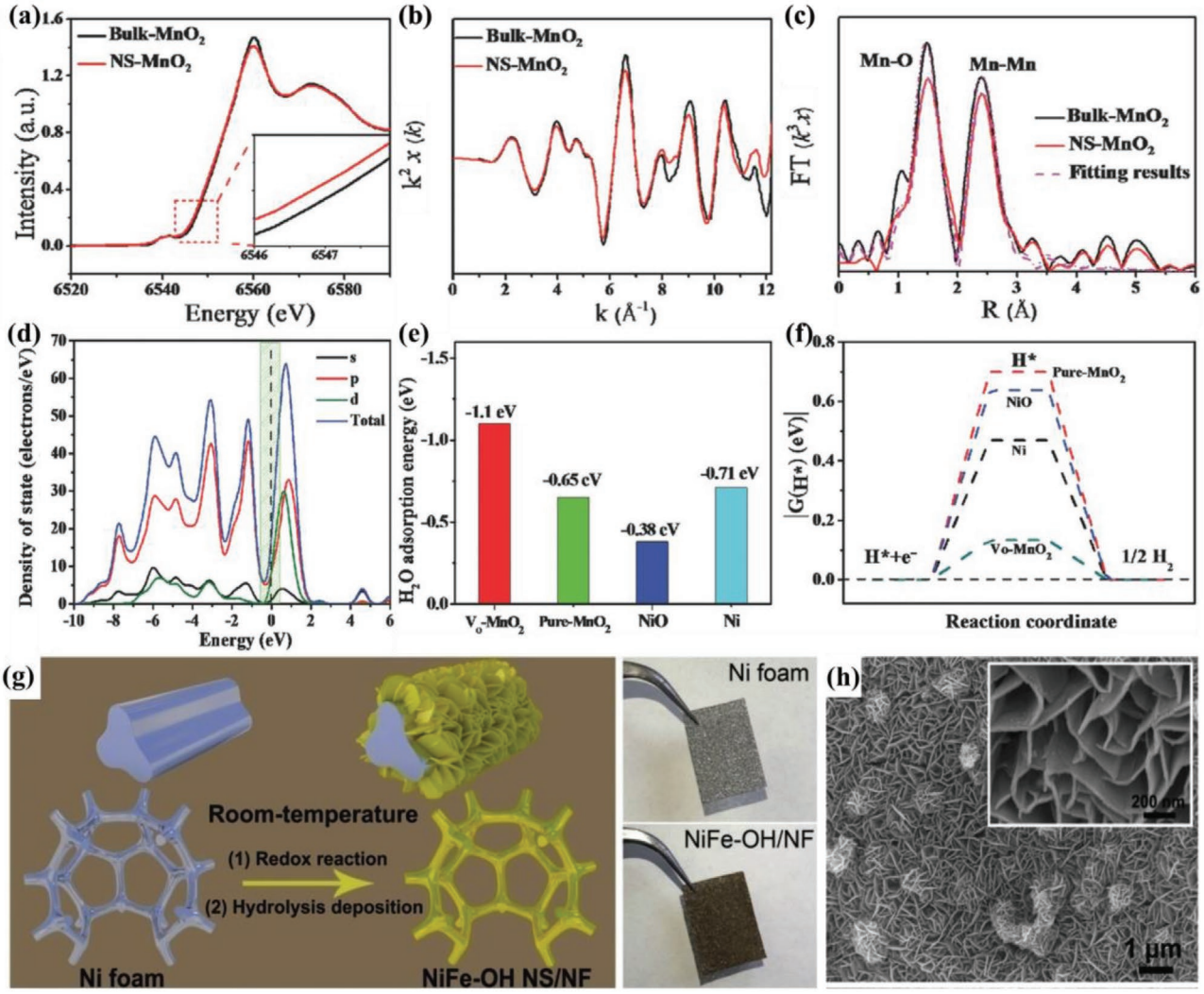

Figure 11. a) Mn K-edge X-ray absorption near edge structure (XANES) spectra, b) Mn K-edge extended X-ray absorption fine structure (EXAFS) spectra, and c) magnitude of k^2-weighted Fourier transforms of Mn K-edge EXAFS spectra for Bulk-MnO_2 and NS-MnO_2. d) Total density of states (TDOS) and partial density of states (PDOS) of V_O-MnO_2 (MnO_2 with O vacancies). The Fermi level is set at 0 eV. e) Adsorption energies of H_2O molecules and f) free-energy diagram for hydrogen evolution on the surfaces of pure-MnO_2, V_O-MnO_2, and other sample models. Reproduced with permission.[134] Copyright 2017, Wiley-VCH. g) Schematic illustration of synthetic procedure for NiFe-OH NS/NF with the digital photographs of bare NF and NiFe-OH NS/NF. h) SEM image of NiFe-OH NS/NF (inset: magnified SEM image). Reproduced with permission.[137] Copyright 2018, Elsevier.

the film and the conductive substrate, thus exhibiting better electrocatalytic activity (Figure 10b–d).[133]

Hydro/solvothermal synthesis is also a versatile approach for self-supported electrode preparation, through which various kinds of TM-based compounds can be prepared at tight pressure and moderate temperature. The crystal nucleation and conformal growth of nanocatalysts are anchored on the defects and oxyl groups on the surface of substrates, resulting in the uniform coverage and strong bond between catalytic nanoarrays and conductive supports.[52] For instance, Zhang et al. reported that by immersing a cleaned NF substrate into $KMnO_4$ solution under moderate hydrothermal conditions (at 180 °C for 3 h), the desired ultrathin manganese dioxide nanosheet arrays in situ grown on the NF (denoted as NS-MnO_2) can be fabricated. Compared with bulk MnO_2 (denoted as Bulk-MnO_2) prepared by direct calcining $KMnO_4$ at high temperature, rich O vacancies were generated on NS-MnO_2 nanosheets, facilitating the formation of exposed active Mn^{3+}, which can be verified by X-ray absorption near edge structure and extended X-ray absorption fine structure characterizations (**Figure 11**a–c). This consequently caused the enhanced conductivity, great half-metallicity feature, reduced reaction energy barrier, and thus an excellent ability of water electrolysis (Figure 11d–f).[134] Notably, under a hydro/solvothermal environment, apart from serving as substrates, the self-supported substance (especially for some metal foams and foils) can also function as the source of metal elements in the resulting active catalysts.[1,15,107–109,135] As is reported in the paper of Zou et al., the 2D Ni_3S_2 nanosheets on the surface of NF (Ni_3S_2/NF) was prepared by directly etching the bare NF with thiourea solution using solvothermal synthesis. This in situ formation also promoted the exposure of high-index faceted $\{\bar{2}10\}$, synergistically accounting for the

excellent bifunctional water slitting capacity.[135] Further, Wu et al. proposed a facile and universal one-step Na_2S-induced chemical etching method, facilitating the formation of ultrathin Fe-doped metal sulfide arrays deriving from the metal (Ni, Cu, Ti, Al) foam substrates with the presence of Fe ions. Thus, obtained optimized $Fe_{0.9}Ni_{2.1}S_2$ compound showed extremely superior bifunctional catalytic activity. When assembling as the alkaline electrolyzer, it can drive 10 mA cm^{-2} at the cell voltage of only 1.51 V.[109]

Wet chemical methods are also widely accepted as an efficient and facile technology applied in the preparation of self-supported electrocatalysts. The co-precipitation method and electroless plating that can be operated at mild temperature and pressure are particularly attractive because of the extremely simple synthesis procedure and low cost.[69,136] For example, Sun et al. proposed a one-step room temperature co-precipitation strategy, in which redox reaction took place accompanied with hydrolysis, to prepare Ni-Fe hydroxide nanosheet arrays supported on NF (NiFe-OH NS/NF) as an advanced water oxidation electrocatalyst. In detail, the pre-cleaned bare NF was immersed into 100 mM $Fe(NO_3)_3{\bullet}9H_2O$ aqueous solution for 7 h, during which, a redox reaction between NF and Fe^{3+}, as well as hydrolysis, occurred. Consequently, the generated Ni^{2+}, Fe^{2+}/Fe^{3+}, and OH^- co-precipitated to form even NiFe-OH nanosheet arrays on NF (Figure 11g,h). More impressively, the cost of manufacturing and the raw materials of this self-supported is only around \$0.0165 per cm^2 and is promising for practical application.[137] However, the products developed by the co-precipitation methods are limited to oxides or hydroxides. In fact, additional phosphorization, sulfidization and nitridization treatments are inexorable for further synthesis of the corresponding phosphides, sulfides, and nitrides.[138–140] Contrary to the co-precipitation method, electroless plating can produce efficient self-supported water electrolysis catalysts via direct deposition of phosphides and borides on all sorts of substrates, ranging from conductive metal foams, metal foils, and carbon cloth to insulated papers, textiles, and sponges.[69,71,112,117] Nevertheless, the electroless plating is usually performed using reducing agents, and therefore, the formation of active hydroxide/oxides under this process is unlikely.[141] In view of this, different synthetic methods for the construction of self-supported electrodes should be selected based on the targeted catalytic compounds.

Although one-step synthetic methods have the merits of reduced expense and a simplified fabrication process, the multi-step synthesis can more easily adjust and control the composition, morphology, crystallinity, and lattice state of catalytic materials.[52] To begin, for the precursor-modification, the methods for precursor deposition are similar to the one-step synthetic routes, such as electrochemical deposition, hydro/solvothermal synthesis, and wet chemical methods.[67,106,142,143] Deferring from the directly-used self-supported catalysts developed from the one-step synthetic method, the deposited precursors work as templates to obtain the desired morphology, chemical and crystalline state of the targeted catalysts through a series of post-treatment strategies, for example, pyrolysis treatment, electrochemical transformation, and ion-exchange method.[34,101,144] Taking the work of Jiang et al. as an example, various well-aligned metal-organic frameworks (MOFs) nanoarrays on the different conductive substrate (NF, Cu mesh, Fe mesh, and Cu foil) as precursors were grown using a pseudomorphic replication method (in which CoO nanoarrays on NF worked as the self-sacrificing templates for MOFs generation). Remarkably, among these precursors, ZIF-67 ($Co(Hmim)_2$, Hmim represents 2-methylimidazole) on NF (named as Ni@CoO@ZIF-67) nanorod arrays were pyrolyzed in N_2 atmosphere, converting into N-doped porous carbon arrays (named as Ni@CoO@CoNC) (**Figure 12**a). The resulting product preserved the array architecture of precursor with high surface area and owned enhanced bifunctional water splitting efficiency.[145] Herein, it is meaningful to mention that hybridizing the self-supported TM-based catalytic compounds with the carbonaceous materials, including the porous carbon, carbon nanotubes (CNTs), and graphene can effectively relieve the corrosion toward TM-based compounds and regulate their electronic structure, as well as increase the specific surface area, elevate the charge and mass transfer efficiency of the integrated composite system, thus improving the final electrocatalytic activity and stability.[2,8,34,145,146] For example, Chen et al. introduced the nitrogen-doped CNT arrays to encapsulate the heterostructured Ni/MoC nanoparticles, which was simultaneously supported on CC (Ni-MoC@NCNT/CC) as an advanced bifunctional water electrolysis catalyst. Such outstanding catalytic performance can be ascribed to the higher electrical conductivity and faster mass transport accelerated by the presence of the NCNT shell.[146] Indeed, the coupling of self-supported TM-based compounds/carbonaceous materials was usually realized by the pyrolysis of substrate-supported precursors, such as MOFs or pre-compounds coupled with polymeric carbon skeletons, then employed as advanced catalysts for large-scale water electrolysis.[8,34,145]

Another effective way of the multi-step synthetic method is the catalyst-deposition strategy. Compared with precursor-modification, the well-defined catalytic nanospecies which are loaded on conductive substrates without any binders can be more precisely controlled. Interestingly, the as-obtained nanostructured catalysts tend to be in the presence of ultrafine nanoparticles with highly accessible active sites.[68] Furthermore, given that the substrates will influence the surface structure of the supported nanospecies, this catalyst-first strategy can prevent the targeted deposited catalyst from confining by the corresponding substrates.[147] Taking one of our works as an instance, we converted the high-purity and well-defined molecule precursor into heterostructured nanocatalyst which was composed of $NiPt_3$ alloy coupled with amorphous NiS ($NiPt_3$@NiS) by hot-injection method (Figure 12b). The TEM, HR-TEM and selected area electron diffraction images of the as-obtained $NiPt_3$@NiS revealed that the ultrasmall crystalline $NiPt_3$ nanoparticles (diameter was around 2 nm) were homogeneously distributed into the even amorphous NiS support (Figure 12c–f). Moreover, the conversion of the single-source molecular into ultrasmall nanocatalyst enabled the exposure of numerous active sites to be controlled at the atomic level. As expected, after being electrophoretically deposited on NF, the fabricated self-supported catalyst ($NiPt_3$@NiS/NF) possessed exceptional HER activity and stability.[3]

On the other side, to avoid the over-blockage and destruction of active species, as well as unstable adhesion between active nanocatalysts and substrates, the mild but effective deposition

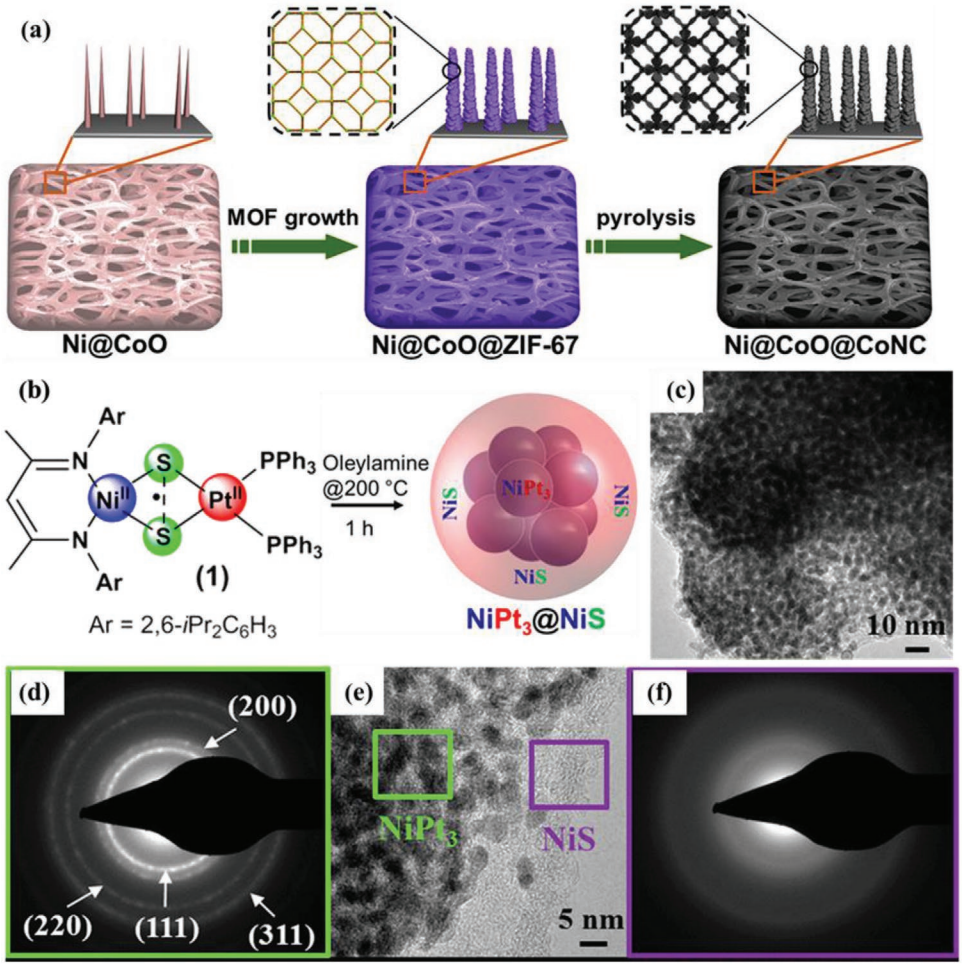

Figure 12. a) Schematic illustration of synthesis procedure for Ni@CoO@CoNC. Reproduced with permission.[145] Copyright 2017, Elsevier. b) Schematic illustration of synthesis procedure for $NiPt_3$@NiS. c) TEM image of $NiPt_3$@NiS. d) Selected area electron diffraction (SAED) pattern for crystalline $NiPt_3$ (green box) part of $NiPt_3$@NiS in (e); e) HR-TEM image of $NiPt_3$@NiS. f) SAED pattern for amorphous NiS (violet box) part of $NiPt_3$@NiS in (e). Reproduced with permission.[3] Copyright 2019, American Chemical Society.

is of significance. Currently, commonly used methods are spin coating,[148] dip coating,[121], and electrophoretic deposition.[68] In particular, electrophoretic deposition is the most promising approach that can ensure the high utilization of active sites in deposited catalytic nanoparticles, as well as the robust bond between the catalysts and substrates. More significantly, as what our previous works show, this technology is highly versatile for various TM-based compounds nanoparticles, including chalcogenides,[3,70] nitrides,[149] phosphides,[150] phosphites,[151] borophosphates,[26,27] and intermetallic compounds[28–30,72] loaded on different substrates such as metal foams, CC, and FTO. Note that the as-prepared nanocatalysts existing in the form of powder were typically dissolved in a mixture of iodine and acetone. This is because the dispersant of iodine reacts with acetone according to the keto-enol tautomerism, releasing amounts of protons, which enable the electric charge on the catalyst nanoparticles to be sufficiently positive. In this case, despite the applied electric field with low potential (at around 10 V), the particles with enough positive charges can be induced to migrate toward the cathode to electrophoretically deposit desired catalysts.[152]

Based on the above discussion, it can be found that for the design of deposited nanostructured catalysts, their component and structure should be taken into emphatic consideration since they directly regulate the resulting catalytic activity and stability. It is also worth noting that the electrochemical water splitting, especially OER, typically triggers the occurrence of surface reconstruction comprising the reorganization of surface structure and crystalline phase for the deposited catalysts. Taking more understanding and control of this unignorable phenomenon can help shed more light on the real active species and in situ reaction mechanism, as well as accelerate the reaction process. Besides, in the light of considerably optional substrates and fabrication methods with corresponding merits and limits for self-supported electrocatalysts design, the researchers are encouraged to select appropriate substrates and a suitable synthetic method to achieve the composition, structure, and application of the desired products. From this, the ultimate goal can be more approachable, that is, fabricating advanced and efficient self-supported electrocatalysts with huge application potential for massive H_2 fuel production.

4. Promising Self-Supported Electrocatalysts for Practical Application

The self-supported electrocatalysts for water splitting which are promising for practical application should show outstanding specialty in one or several of the following points, that is, i) exceptional capability in all-pH media, ii) great activity in seawater electrolyte, iii) superior performance for OWS, iv) high efficiency at large current density, and v) durable stability within long working time. In the past few years, a series of correspondingly pioneering works have been reported. The systematic review, classification, and analysis of them may pave a guiding avenue for the substantial development of H_2 fuel production.

4.1. Self-Supported Electrocatalysts in All-pH Electrolyte

The development of catalysts that can catalyze electrolysis of water efficiently in electrolytes with different pH values, that is, in acid, neutral, and alkaline solution environment (usually pH value is 0, 7, and 14, respectively, in experimental electrochemistry test), can significantly simplify the operating process and lower the cost of water electrolyzers, bringing practical application foreground for H_2 fuel production.[153–155] Whereas, such pH-universal catalysts are hard to obtain due to the complex demands for the catalysts to satisfy different thermodynamic features of water splitting in distinct electrolyte conditions.[156] In detail, the electrocatalysts working for HER tend to display superior performance in acid media to that in alkaline or neutral media. This can be ascribed to that acid electrolyte can provide sufficient protons (H^+) for the later hydrogen molecules combination, while an additional Volmer step is required for the generation of these free protons.[33] Conversely, the alkaline electrolyte is more favorable for electrocatalysts in OER with better activity and durability compared with acid, since acid solution easily leads to the dissociation and corresponding deactivation of catalysts.[157] Also, the OER performance of electrocatalysts in neutral electrolytes is poor because of the low electrical conductivity, large ohmic loss, and slow catalysis kinetics under neutral conditions.[157,158] In this case, self-supported electrocatalysts that can expedite ion/electron conduction, promote mass transport and elevate stability, have received increasing interest as a solution to wide-pH electrolyte water splitting catalysts.

In recent years, inspiring progress has been achieved in highly efficient pH-universal self-supported electrocatalysts for HER, whose performances were typically optimized by active site increments, electronic structure modulation, and reduced reaction energy barrier.[33,159–162] For example, Zhang et al. fabricated ultrathin $Ni_{0.89}Co_{0.11}Se_2$ mesoporous nanosheet arrays supported on NF (named as $Ni_{0.89}Co_{0.11}Se_2$ MNSN/NF) through hydrothermal synthesis and the post selenization and acid etching. Co doping allowed $Ni_{0.89}Co_{0.11}Se_2$ to acquire higher intrinsic conductivity and lower energy reaction barriers. Coupled with the feature of mesoporous nanosheets which can offer more exposed and accessible active sites, $Ni_{0.89}Co_{0.11}Se_2$ MNSN/NF exhibited exceptional universal HER activity in all-pH conditions, affording 10 mA cm^{-2} current density at 52, 82, and 85 mV in acid, neutral and basic media, respectively. Of note, this catalyst can maintain a large current density over 125 mA cm^{-2} over 40 h with little degradation in the acid electrolyte, implying its excellent stability.[161]

More remarkably, for all-pH applicable self-supported electrocatalysts, the specific importance was attached to the co-existence and co-operation of different active species which exhibits a preference for water dissociation (Volmer step) and hydrogen molecule formation (Heyrovsky step or Tafel step), respectively, in the same catalysts.[163,164] Note that the abovementioned two steps are considered as the rating-determining step in alkaline/neutral and acid media, respectively.[32,165] Wu et al. demonstrated that commercial carbon felt supported-$NiCo_2P_x$ nanowire arrays (denoted as $NiCo_2P_x$) showed outstanding HER activity in all-pH solution, where it only required 58, 60, and 104 mV overpotential at 10 mA cm^{-2} current density in alkaline, neutral, and acid media, respectively (**Figure 13**a–c). Figure 13d illustrates this superior pH-universal HER activity mainly originated from the cooperative effect of different active sites aiming at different reaction steps in the same catalyst. Active Ni sites in $NiCo_2P_x$ are favorable for the dissociation of the adsorbed water molecules into H^+ and OH^- (Volmer step), while the nearby Co sites are responsible for the generation and release of hydrogen molecules (Heyrovsky step or Tafel step).[164]

Compared to that for HER, the development of pH-versatile electrocatalysts for OER is more difficult accounting for the poor stability in acid media. Also, the high activity under neutral conditions is basically limited to noble metal-based catalysts, resulting in the leap of the expenses for catalyst preparation and thus an obstacle for large-scale production of hydrogen.[166,167] In view of enhancement on conductivity and durability, integrating active nanocatalysts, and conductive supports as self-supported electrocatalysts are considered as a promising approach to promoting efficient OER in the wide-pH electrolyte.[168–170] For example, Sun et al. reported a hydrophilic-treated CC supporting a hybrid catalyst which was constructed via anchoring Mo single atoms on partially oxidized surface sites of Co_9S_8 (Mo-Co_9S_8@C). The intimate contact between functionalized CC and catalytic species accelerated the electron transfer and generated bubble escape. In addition to the robust interaction between dispersive Mo atoms and support, Mo-Co_9S_8@C showed outstanding OER activity in all alkaline, neutral and acid media. More surprisingly, this self-supported electrode can catalyze OER steadily at 10 mA cm^{-2} current density in acid electrolyte for 24 h with negligible deterioration, indicating its good acid media stability.[170]

Some researchers have pointed out that defect engineering on nanostructured catalysts can induce the modulation of electronic structure, improvement of intrinsic conductivity and stability, as well as increment in the exposed active sites.[171,172] Under this circumstance, Liu et al. found that introducing defect engineering into self-supported nanostructured catalysts can further enhance the OER capability in electrolytes with entire pH values. As is shown in **Figure 14**a,b, the NF-supported 2D ultrathin $NiAl_\delta P$ nanosheet arrays exhibited porous nanostructure with dense Al vacancies. Compared with the pristine NiAlP, such surface metal vacancies tuned the coordination environment and electronic structure of neighboring unsaturated Ni and P as active sites, thus endowing

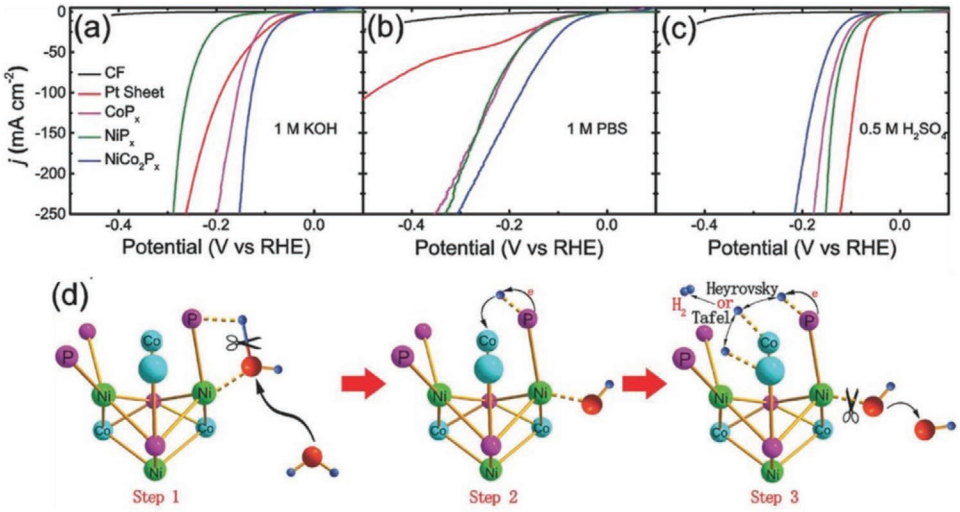

Figure 13. HER LSV polarization curves of $NiCo_2P_x$ and other samples in a) 1.0 M KOH (alkaline), b) 1.0 M phosphate-buffered saline (PBS, neutral), and c) 0.5 M H_2SO_4 (acid). d) Schematic illustration of HER reaction mechanism for $NiCo_2P_x$. Reproduced with permission.[164] Copyright 2016, Wiley-VCH.

them with the more superior ability for proton reduction and oxo-group oxidation (Figure 14c–e). Accordingly, adsorption Gibbs free energy of intermediate H* and adsorption energy of intermediate H_2O* were reduced and increased, respectively (Figure 14f). As a result, the integrated $NiAl_\delta P$ on NF had excellent bifunctional water electrolysis activity, superior to that of NiAlP on NF. Especially, for OER, $NiAl_\delta P$ can deliver 10 mA cm^{-2} current density at 256, 240, and 400 mV overpotential in acid (0.5 M H_2SO_4), alkaline (1.0 M KOH), and neutral media (1.0 M Na_2SO_4), respectively (Figure 14g–i).[163]

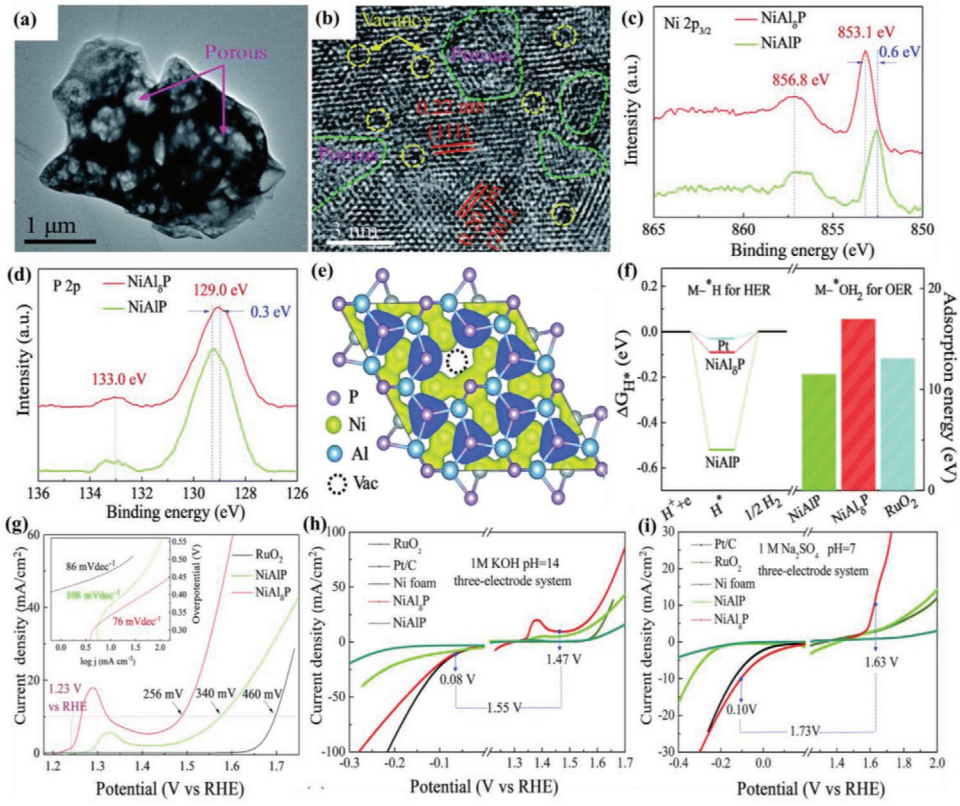

Figure 14. a) TEM image and b) HRTEM image of $NiAl_\delta P$ nanosheet. c) Ni 2p and d) P 2p X-ray photoelectron spectra (XPS) of $NiAl_\delta P$. e) Calculated charge density of $NiAl_\delta P$. f) Intermediate H adsorption Gibbs free energy and intermediate H_2O adsorption energy for NiAlP, $NiAl_\delta P$, and other reference electrodes. LSV polarization curves of NiAlP, $NiAl_\delta P$, and other samples in g) 0.5 M H_2SO_4, h) 1.0 M KOH, and i) 1.0 M Na_2SO_4. The inset of (g) is the corresponding Tafel slope. Reproduced with permission.[163] Copyright 2018, Royal Society of Chemistry.

Additionally, the self-supported catalysts with composited structure have attracted more and more attention for efficient water electrolysis because of their modified intrinsic properties, such as the optimized electronic structure, improved conductivity, and increased active sites, thus displaying huge potential for water splitting in all-pH media.[34,157,169] This can be well-demonstrated by the work of Kanatzidis et al. They proposed a novel NF-supported composited material constructed by MoS_2 nanosheets, Co_9S_8 nanosheets, and Ni_3S_2 nanorods (CoMoNiS-NF), which performed excellently in wide-pH water splitting, transporting 10 mA cm^{-2} current density in alkaline, acidic, and neutral electrolytes at the overpotentials of 113, 103, and 117 mV for HER and 166, 228, and 405 mV for OER, respectively. More impressively, the optimized CoMoNiS-NF also owned outstanding OWS activity, requiring the cell voltages of only 1.54, 1.45, and 1.80 V to afford 10 mA cm^{-2} in alkaline, acidic, and neutral media, respectively.[157]

The recently reported self-supported electrocatalysts with exceptional HER and/or OER performance in all-pH media are listed in **Table 1**, from which it is found that although considerable self-supported electrocatalysts showed satisfactory HER performance with pH-universality, pH-versatile OER catalysts were less developed, prominently limited by the poor and unstable catalytic performance.

4.2. Self-Supported Electrocatalysts in Seawater Electrolyte

The progress in the development of self-supported electrocatalysts in wide-pH media, especially in neutral media opens a door to realize the direct electrolysis of near-neutral (usually weakly alkaline) seawater and saline electrolyte, which is widely regarded as a promising way for mass H_2 fuel production.[173] In comparison to the conventional splitting of freshwater, producing H_2 via electrochemical seawater splitting is deemed to have a series of merits such as i) the utilization of abundant seawater (which occupies 96.5% of the total worldwide water supply) instead of freshwater can not only save the precious freshwater source but also serve as an effective technology for seawater desalination, bringing more interests and benefits for practical application; ii) seawater exhibits the similar ion conductivity as that of 0.5 M sodium chloride aqueous electrolyte, avoiding the addition of alkaline or acid species and thus reducing the extra cost; iii) the production of H_2 through seawater splitting can be coupled with the generation of other ocean-related renewable energy such as tidal and wind energy, elevating the overall working efficiency of the new energy system.[174,175]

However, for the current electrocatalytic seawater splitting technology, several bottlenecks still need to be solved, which can be summarized from the following points. i) The existence of dissolved ions such as Na^+, Mg^{2+}, and Ca^{2+}, as well as bacteria/microbes and small particulates in seawater, promotes the poison and corrosion of the catalysts during seawater electrolysis, contributing to the poor activity and durability;[175–177] ii) the fluctuation of local pH near electrode surface occurs, that is, the rise of pH at the cathode as well as the drop of pH at the anode, even though under moderate working current density. The local pH variation could lead to the degradation of electrocatalysts. In particular, the existing Mg^{2+} and Ca^{2+} ions in seawater will precipitate into the corresponding hydroxides along with the increase of local pH. Accordingly, the surface-active sites on electrodes will be blocked, causing the decline of catalytic activity;[178,179] iii) the complicated chemistry of chlorine species will interfere with the reaction on the electrodes. It is widely believed that several chloride electro-oxidation reactions will take place in accordance with different pH values, applied potentials, and temperatures, competing with OER, and also corrode the anode. Especially, formation of hypochlorite, which can form easily and can correspondingly block the membrane in the electrolysis cell resulting in a dramatic drop in the overall catalytic efficiency.[178,180] Meanwhile, the crossover of evolved Cl_2 or chlorides from anode will also deteriorate the stability of cathode;[181,182] iv) the development of considerable seawater splitting catalysts is still confined in the noble metal-based ones, while the inherent conductivity, activity, and corrosion-resistance of the recently emerged non-precious metal-based alternatives still need to be improved;[182,183] and most notably, (v) the seawater splitting bears almost no economical benefits in comparison to splitting purified of water, making it as an unreliable technology in the present scenario, however, expected to provide fundamental insights to the field.[184]

Benefiting from the easily-tailored electronic structure, enhanced charge conductivity, as well as optimized corrosion resistance and stability, the self-supported TM-based catalysts were regarded as promising candidates for practical seawater electrolysis. For HER in seawater electrolyte, it suffers from the influence of resolved cations in seawater most severely.[182] Such cations will produce by-products under working conditions of seawater splitting, blocking the exposed active sites, as well as poisoning and corroding the cathodes, finally weakening the durability of the catalysts (a current density loss over 50% in a short period).[185] In this case, efficient self-supported TM-based electrocatalysts with great inherent anti-corrosion properties could provide the required solutions.[186,187] For example, Ren et al. applied NF-supported heterogeneous Ni_2P-Fe_2P nanosheet arrays (Ni_2P-Fe_2P/NF) as a seawater electrolysis catalyst. This catalyst showed outstanding catalytic activity in simulated seawater (1 M KOH seawater) because the porous ultrathin sheet-like morphology provides more exposed and approachable active sites, as well as the rapid mass transport and evolved gas bubble release. More importantly, benefitting from the tight adhesion between the nanosheet arrays and NF substrate, coupled with the corrosion resistance and chemical stability of P alloying, this catalyst exhibited superior stability at a constant high large current density of 100 mA cm^{-2} over 36 h with little increase of the required overpotential.[186]

Another promising way to stabilize the active HER nanocatalysts in seawater is a combination of active nanostructure and "chainmail for catalyst." The so-called "chainmail for catalyst" refers to the protective shell, such as functional carbon shells, which can prevent the inner catalytic species destroying by the external harsh environment, while preserving the catalytic characteristics of the inner species well.[188] The implementation of porous and ultrathin carbon shell can also provide more active defect sites, larger surface area, enhanced conductivity, and modulation for the electronic structure of the encased catalysts.[2,34] Therefore, when applied in seawater electrolysis,

Table 1. Recently reported advanced self-supported non-noble metal-based electrocatalysts with promising practical application in various electrolytes.

Sample ID	Substrate	Catalyst Loading [mg cm^{-2}]	React.	Electrolyte	η [mV] @ j [mA cm^{-2}]	Tafel slope[mV dec^{-1}]	Ref.
$(Ni_{0.048}Fe_{0.952})_2P$	NF	1.0	HER	1 M KOH	103@10	76.6	[31]
			HER	1 M PBS	90@10	82.7	
			HER	0.5 M H_2SO_4	81@10	41.6	
P-CoMoS	CC	2.19	HER	1 M KOH	66@10	60.1	[153]
			HER	1 M PBS	104@10	/	
			HER	0.5 M H_2SO_4	52@10	/	
			OER	1 M KOH	260@10	70.2	
			OER	1 M PBS	345@10	/	
			OER	0.5 M H_2SO_4	369@10	/	
			OWS	1 M KOH	310@10	/	
			OWS	1 M PBS	371@10	/	
CoMoNiS-NF-3:1	NF	1.86	HER	1 M KOH	113@10	85	[157]
			HER	1 M PBS	117@10	56	
			HER	0.5 M H_2SO_4	103@10	55	
			OER	1 M KOH	166@10	58	
			OER	1 M PBS	405@10	71	
			OER	0.5 M H_2SO_4	228@10	78	
			OWS	1 M KOH	310@10	/	
			OWS	1 M PBS	570@10	/	
			OWS	0.5 M H_2SO_4	220@10	/	
Mn–Co–P	TM[a)]	5.61	HER	1 M KOH	76@10	52	[159]
			HER	1 M PBS	86@10	82	
			HER	0.5 M H_2SO_4	49@10	55	
MoP NA/CC	CC	2.5	HER	1 M KOH	80@10	83	[160]
			HER	1 M PBS	187@10	94	
			HER	0.5 M H_2SO_4	24@10	58	
$Ni_{0.89}Co_{0.11}Se_2$ MNSN	NF	2.62	HER	1 M KOH	85@10	52	[161]
			HER	1 M PBS	82@10	78	
			HER	0.5 M H_2SO_4	52@10	39	
N–Co_2P	CC	5	HER	1 M KOH	34@10	51	[162]
			HER	1 M PBS	42@10	68	
			HER	0.5 M H_2SO_4	27@10	45	
$NiAl_\delta P$	NF	/	HER	1 M KOH	80@10	/	[163]
			HER	1 M Na_2SO_4	100@10	/	
			HER	0.5 M H_2SO_4	35@10	38	
			OER	1 M KOH	242@10	/	
			OER	1 M Na_2SO_4	400@10	/	
			OER	0.5 M H_2SO_4	256@10	76	
			OWS	1 M KOH	320@10	/	
			OWS	1 M Na_2SO_4	500@10	/	
			OWS	0.5 M H_2SO_4	290@10	/	
$NiCo_2P_x$	CFe[b)]	5.9	HER	1 M KOH	58@10	34.3	[164]
			HER	1 M PBS	63@10	63.3	
			HER	0.5 M H_2SO_4	104@10	59.6	
NiCo-nitrides/$NiCo_2O_4$	GF[c)]	≈0.3	HER	1 M KOH	71@10	58	[169]
			HER	1 M PBS	418@10	78	
			HER	0.5 M H_2SO_4	432@10	68	
			OER	1 M KOH	183@10	56	
			OER	1 M PBS	673@10	183	
			OER	0.5 M H_2SO_4	460@10	73	
			OWS	1 M KOH	450@20	/	
Mo-Co_9S_8	CC	1	HER	1 M KOH	113@10	67.6	[170]
			HER	0.5 M H_2SO_4	98@10	34.6	
			OER	1 M KOH	200@10	95.6	
			OER	0.5 M H_2SO_4	370@10	90.3	
			OWS	1 M KOH	330@10	/	
			OWS	1 M Na_2SO_4	670@10	/	
			OWS	0.5 M H_2SO_4	450@10	/	

Table 1. Continued.

Sample ID	Substrate	Catalyst Loading [mg cm^{-2}]	React.	Electrolyte	η [mV] @ j [mA cm^{-2}]	Tafel slope[mV dec^{-1}]	Ref.
S-(Ni,Fe)OOH	NF	/	OER	1 м KOH	281@100	48.9	[183]
			OER	1 м KOH+0.5 м NaCl (pH ≈ 14)	278@100	/	
			OER	1 м KOH+1 м NaCl(pH ≈ 14)	275@100	/	
			OER	1 м KOH + seawater(pH ≈ 14)	300@100	/	
Mn–NiO–Ni	NF	0.25	HER	1 м PBS	200@35	121	[185]
			HER	Natural seawater (pH ≈ 8.2)	170@10	/	
Ni_2P-Fe_2P	NF	/	HER	1 м KOH	225@100	86	[186]
			HER	1 м KOH + Seawater	252@100	/	
			OER	(pH ≈ 14)	261@100	58	
			OER	1 м KOH	305@100	/	
			OWS	1 м KOH + Seawater	452@100	/	
			OWS	1 м KOH + Seawater	581@100	/	
NiCo	TFo[d]	/	HER	Natural seawater	1000@111	167	[187]
Mo_2C-MoP NPC	CFP[e]	/	HER	1 м KOH	146@10	71	[190]
			HER	0.5 м H_2SO_4	85@10	66	
			HER	Natural seawater	346@10	173	
NiMoN	NF	/	HER	1 м KOH	56@100	45.6	[191]
			HER	1 м KOH + 0.5 м NaCl (pH ≈ 14)	~80@100	/	
			HER	1 м KOH + seawater(pH ≈ 14)	82@100	/	
NiMoN@NiFeN	NF	/	OER	1 м KOH	277@100	58.6	[191]
			OER	1 м KOH + 0.5 м NaCl (pH ≈ 14)	286@100	/	
			OER	1 м KOH + seawater(pH ≈ 14)	307@100	/	
NiMoN ‖ NiMoN@NiFeN	NF	/	OWS	1 м KOH + 0.5 м NaCl (pH ≈ 14)	334@100	/	[191]
			OWS	1 м KOH + seawater(pH ≈ 14)	351@100	/	
$Na_2Co_{1-x}Fe_xP_2O_7$/C	CC	/	OER	0.1 м KOH + 0.5 м NaCl (pH ≈ 12.7)	370@100	53	[193]
Cu-W/NiCo-LDH	CM[f]	1	HER	1 м KOH	72@100	50.5	[256]
			HER	1 м PBS	443@10	/	
			HER	0.5 м H_2SO_4	112@100	79.4	
Cu NWs@WC	CF	/	HER	1 м KOH	119@10	88.7	[257]
			HER	1 м PBS	173@10	118.3	
			HER	0.5 м H_2SO_4	92@10	50.5	
CoMoOF	GFe[g]	3.79	HER	1 м KOH	79@10	43.3	[258]
			HER	0.1 м PBS	230@10	95.8	
			HER	0.5 м H_2SO_4	94@10	60.2	
FLNPC@MoP-NC/MoP-C	CC	2.42	HER	1 м KOH	69@10	52	[259]
			HER	1 м PBS	106@10	73	
			HER	0.5 м H_2SO_4	74@10	50	
CoP/Ni_5P_4/CoP	NF	/	HER	1 м KOH	140@100	58	[260]
			HER	0.5 м H_2SO_4	85@100	43	
N-CoP	CC	5	HER	1 м KOH	39@10	58	[261]
			HER	1 м PBS	74@10	69	
			HER	0.5 м H_2SO_4	25@10	49	

Table 1. Continued.

Sample ID	Substrate	Catalyst Loading [mg cm^{-2}]	React.	Electrolyte	η [mV] @ j [mA cm^{-2}]	Tafel slope[mV dec^{-1}]	Ref.
a-Ni_3S_2@NPC	CFo[h)]	/	HER	1 M KOH	60.8@10	67.5	[262]
			HER	2 M PBS	193@2	/	
			HER	0.5 M H_2SO_4	91.6@10	63.5	
CN/CNL/MoS_2	CP[i)]	/	HERHER	1 M KOH	106@10	117	[263]
			HER	1 M PBS	145@2	120	
				0.5 M H_2SO_4	112@10	77	
Mn-doped FeP/$Co_3(PO_4)_2$	CC	1.2	HER	1 M KOH	85@10	96	[264]
			HER	1 M PBS	117@10	81	
			HER	0.5 M H_2SO_4	27@10	44	
			OER	1 M KOH	166@10	49	
			OER	1 M PBS	405@10	301	
			OER	0.5 M H_2SO_4	228@10	472	
			OWS	1 M KOH	380@10	/	
			OWS	1 M PBS	590@10	/	
			OWS	0.5 M H_2SO_4	520@10	/	
HCl-c-NiFe	NFF[j)]	/	HER	1 M KOH	172@100	77/	[265]
			HER	1 M KOH + 0.5 M NaCl	175@100		
			OER	1 M KOH	178@100	27	
			OER	1 M KOH + 0.5 M NaCl	178@100	/	
			OWS	1 M KOH	≈580@100	/	
			OWS	1 M KOH + 0.5 M NaCl	580@500	/	
NiMo	NF	/	HER	1 M KOH	36.8@10	33.6	[266]
			HER	1 M KOH + 0.5 M NaCl	31.8@10	33.1	
GO@Fe@Ni–Co	NF	/	HER	1 M KOH + 0.5 M NaCl	150@10	/	[267]
			OER	1 M KOH + 0.5 M NaCl	247@50	59	
			OWS	1 M KOH + 0.5 M NaCl	360@20	/	
			OWS	1 M KOH + Seawater	710@500	/	
Se_NiFe_LDH	NFF	/	OER	1 M KOH + 1 M NaCl	220@20	37.4	[268]
Co-Se1//Co-Se4	CoFo.[k)]	Co-Se1: 4.81	OWS	1 M KOH	≈570@10	/	[269]
		Co-Se4: 33.7	OWS	Buffer solution	≈470@20	/	
			OWS	(pH = 7.4) Neutral-buffered seawater (pH = 7.09)	≈570@10.3	/	
NiCoN|Ni_xP|NiCoN	NF	1.26	HER	Natural seawater (pH ≈ 7.09)	165@10	139.2	[270]
Co-Fe LDH	TM	1.5	OER	Simulated seawater (pH = 8)	530@10	149	[271]
Ni_5P_4@ $Ni^{2+\delta}O_\delta(OH)_{2-\delta}$	CC	/	HER	1 M KOH	87@10	69	[272]
			HER	0.5 M H_2SO_4	66@10	33	
			HER	Natural seawater (pH = 7.8)	144@10	108	
B-Co_2Fe LDH	NF	1.08	OER	1 M KOH	246@100	39.2	[273]
			OER	1 M KOH + 0.5 M NaCl	≈246@100	46.5	
			OER	1 M KOH + Seawater	310@100	63.8	
Ni_3N/Ni_3S_2	NF	/	OWS	1 M KOH	≈500@10	/	[274]
			OWS	Buffer solution	570@12.4	/	

Table 1. Continued.

Sample ID	Substrate	Catalyst Loading [mg cm^{-2}]	React.	Electrolyte	η [mV] @ j [mA cm^{-2}]	Tafel slope[mV dec^{-1}]	Ref.
			OWS	Natural seawater	570@48.3	/	
Fe-Ni(OH)$_2$/Ni$_3$S$_2$	NF	/	OER	1 M KOH+0.5 M NaCl	269@10	46	[275]

[a]TM: Titanium mesh; [b]CFe: Carbon felt; [c]GF: Graphite fiber; [d]TFo.: Titanium foil; [e]CFP: Carbon fiber paper; [f]CM: Copper mesh; [g]GFe.: Graphite felt; [h]CFo: Copper foil; [i]CP: Carbon paper; [j]NFF: Nickel iron foam; [k]CoFo: Cobalt foil.

the outer coupled carbon species enable the catalyst to be highly active and robust.[189] For example, Hu et al. embedded carbon paper-supported Mo_2C/MoP hetero-nanoparticle into N, P co-doped carbon nanofibers as a seawater HER catalyst. The carbon substance owned abundant sites for anchoring the catalytic nanoparticles, protecting them from being corroded and poisoned. Consequently, apart from great HER activity in seawater, this hybrid self-supported catalyst can retain over 10 mA cm^{-2} current density over 16 h without obvious decrease, displaying outstanding seawater splitting durability.[190]

As for OER at the anode, the major problem is the competitive chloride electro-oxidation reactions, that is generation of chlorine-related products (e.g., chlorine, hypochlorous acid, and hypochlorite) along with the change of applied potential and local pH of the electrolyte during the OER process.[178,182] However, according to the Pourbaix diagram of the aqueous saline water proposed by Strasser et al., in the alkaline environment, OER dominates the whole working process within the maximum overpotential of 480 mV without the interference from chloride electro-oxidation (**Figure 15**a,b).[178] Adopting this criterion for the guidance of Cl-free anode oxidation catalysts, some self-supported electrocatalysts which can afford large current density under low overpotential (lower than 480 mV) have been reported.[191–193] For instance, Ren et al. fabricated NiMoN nanorods which were decorated with NiFeN nanoparticles and supported on NF (denoted as NiMoN@NiFeN) as highly efficient seawater electrocatalysts. Taking advantage of the 3D core-shell hybrid structure of NiMoN@NiFeN with high-level porosity, this catalyst exhibited features including numerous active sites, fast charge transfer, and swift gas bubbles escape (Figure 15c–e). Thus, this catalyst shows high catalytic efficiency, especially for OER in both 1 M KOH + 0.5 M NaCl and 1 M KOH + natural seawater at room temperature. In Figure 15f, at 100 and 500 mA cm^{-2}, NiMoN@NiFeN catalyst just required an overpotential of 286 and 347 mV in 1 M KOH + 0.5 M NaCl, as well as 307 and 369 mV in 1 M KOH + natural seawater, respectively. Because of the ultralow overpotential, no chloride electro-oxidation reactions competed with the OER, ensuring high reaction selectivity. When assembled with NiMoN as a two-electrode alkaline electrolyzer (where NiMoN@NiFeN serves as the anode and NiMoN serves as the cathode), this electrolyzer can preserve the robust overall seawater splitting activity with little degradation over 100 h at a constant current density of 100 and 500 mA cm^{-2} in the abovementioned electrolytes (Figure 15g).[191]

In the past years, considerable efforts have been dedicated to the design and fabrication of efficient self-supported electrocatalysts for seawater splitting with some impressive achievements (Table 1) in laboratory conditions. Nevertheless, most of these works were still operated in the simulated seawater media or in the seawater with the addition of extra buffer solutions. In order to realize more environmental, economic, and energy desires, further breakthroughs are required for direct electrolysis of natural seawater with a more complicated chemical and physical environment which presently seems to be impractical.

4.3. Self-Supported Electrocatalysts for Overall Water Splitting

At present, although great progress has been achieved in the development of advanced electrocatalysts for half-reaction of water splitting (such as chalcogenides, nitrides, and phosphides displayed outstanding HER performance, while hydroxides/oxides and perovskites are investigated as efficient OER catalysts), only a few of them show outstanding bifunctional catalytic performance, capable of catalyzing HER and OER simultaneously at an integrated OWS cell (where the catalysts serve as both cathode and anode) in the same media.[34,194] This can be ascribed to the mismatched activity and durability of these catalysts in wide pH ranges., for example, the acid electrolyte is favorable for HER, while OER is typically sluggish and unstable in the same acid media.[195] However, stimulated by the facile applicability, simplified fabrication process, and reduced manufacturing cost for a full water splitting system, it is of utmost importance to explore excellent bifunctional electrocatalysts for the realization of H_2 production practically and sustainably.[196,197]

Conventionally, the powder bifunctional catalysts are deposited on the substrates with the assistance of polymeric binders for being integrated into the OWS cell. The presence of these binders will induce the increment of charge transfer resistance, reduction of the exposed active sites, and obstruction of electrolyte penetration. Accordingly, such assembled electrolyzers usually need a high cell voltage over 1.6 V at 10 mA cm^{-2}, let alone at a larger current density, which is far from satisfactory for economically viable and scalable generation of H_2 through water splitting.[198–200] Given this condition, the efficient and low-cost self-supported TM-based electrocatalysts without any binders or additives required during the preparation process can ensure the intimate contact between nanocatalysts and substrates, and thus possess superior catalytic activity and durability for OWS.

Among self-supported TM-based compounds catalysts, oxides/hydroxides-based ones are particularly considered to be suitable for full water splitting. On one hand, compared with other self-supported compound catalysts, they typically have better OER activity, endowing them to be suitable anodes directly in the OWS system. Also, most of the other TM-based compounds will partially or completely transform into the

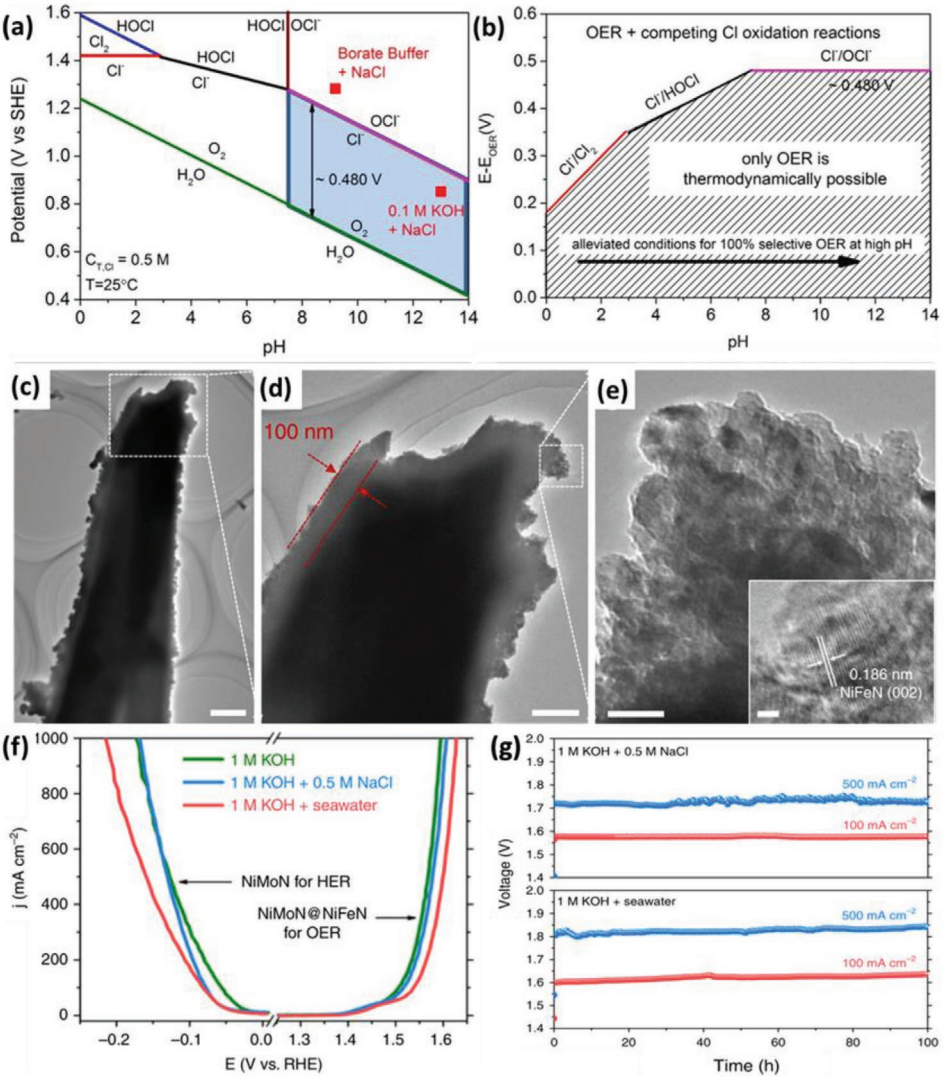

Figure 15. a) Pourbaix diagram of the aqueous saline water and b) corresponding prediction diagram originating from the Pourbaix diagram in (a) to reflect the maximum kinetic overpotentials as a function of pH for absolute OER on the anode. Reproduced with permission.[178] Copyright 2016, Wiley-VCH. c,d) TEM images and e) HRTEM image of NiMoN@NiFeN. f) OER and HER polarization curves of NiMoN@NiFeN and other samples in different media. g) CP tests of the electrolyzer at a constant current density of 100 and 500 mA cm^{-2} in different media at 25 °C. Reproduced with permission.[191] Copyright 2019, NPG.

corresponding (oxy)hydroxides (which are widely regarded as the real active species) shortly after OER takes place.[124,200,201] On the other hand, the electronic structure of oxides/hydroxides are easily tuned to be beneficial to the reduction of the reaction energy barrier for HER, thus they can function as efficient cathodes in full water splitting electrolyzers.[35,202,203] Taking the work of Yu et al. for illustration, they fabricated structurally disordered sulfur-doped S-CoO_x supported on NF (denoted as S-CoO_x/NF) through a facile room-temperature ion-exchange method. After the incorporation of electronegative sulfur, the crystalline state of the original CoO_x precursor was destroyed, resulting in an enormous amount of active defect sites and the corresponding low oxygen coordination. Apart from the increment of additional active sites, the electronic structure of the oxide was easily regulated which was favorable for the adsorption of intermediates of both HER and OER. As a result, such S-CoO_x/NF showed outstanding bifunctional catalytic activity, delivering 100 and 170 mA cm^{-2} current density with a cell voltage of only 1.85 and 1.93 V, both significantly lower than that of benchmark noble metal-based alkaline electrolyzer for full water splitting at the same current density.[144]

Compared with other TM-based oxides/hydroxides, layered double hydroxides (LDHs) have achieved increasing attention for electrocatalysis, which can be described in a general formula of $[M^{2+}_{1-x}M^{3+}_{x}(OH)_2]^{x+}[A^{n-}_{x/n}]^{x-}\cdot mH_2O$, where M^{2+} and M^{3+} refer to the metal ions with +2 and +3 valence, respectively, and A^{n-} represents the charge-balancing anions.[204] Considering LDHs exhibit the characteristics of a 2D ultrathin nanostructure, amounts of exposed active sites, variable composition, and easily-modulated electronic structure, self-supported LDHs or their derived oxides electrocatalysts were extensively investigated for OWS.[34,205–207] For example, Li et al. reported the NF-supported

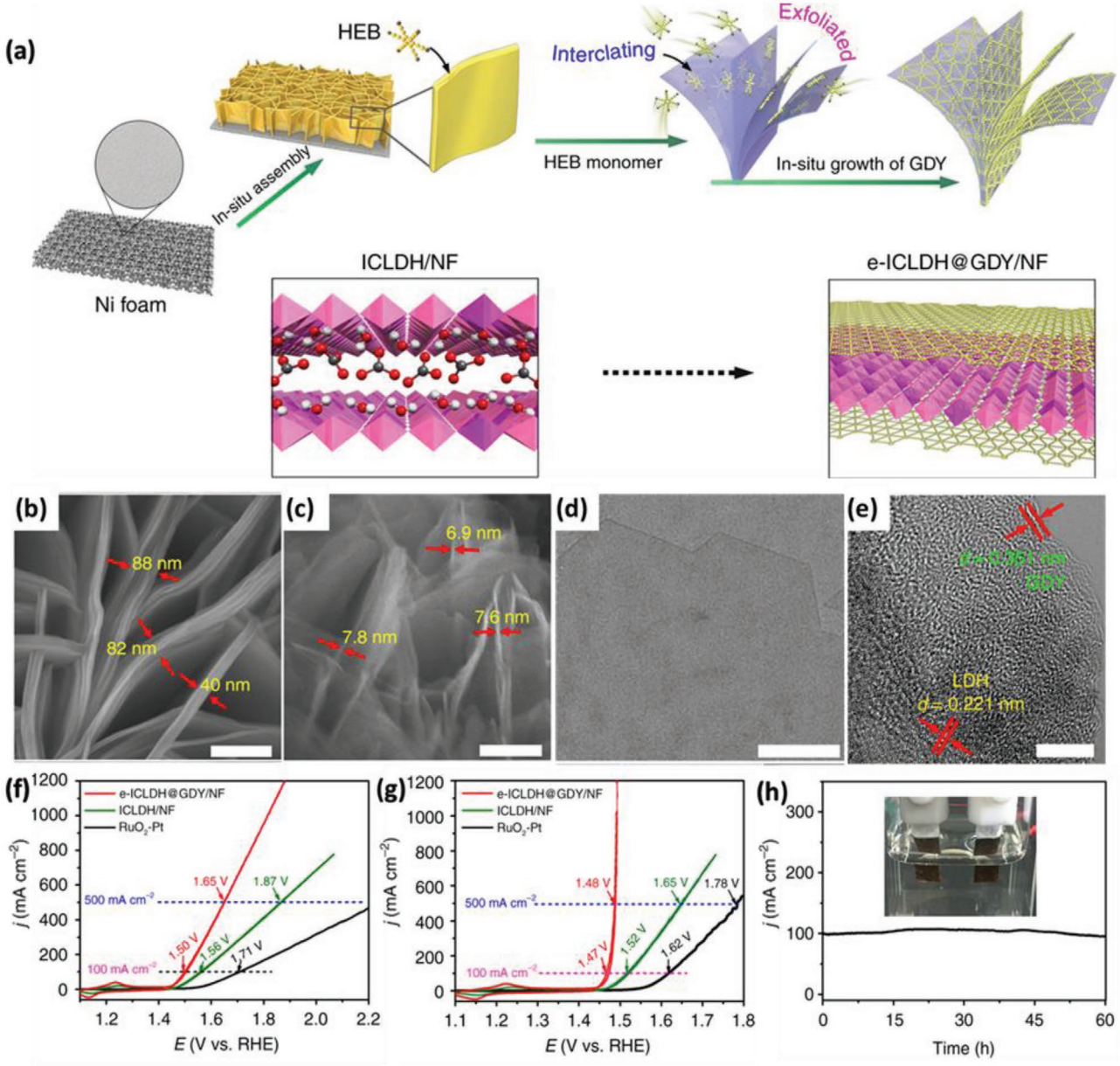

Figure 16. a) Schematic illustration of synthesis procedure for e-ICLDH@GDY/NF. SEM images of b) pristine ICLDH/NF and c) e-ICLDH@GDY/NF. Note that scale bars in (b) and (c) are both 200 nm. d) TEM and e) HRTEM image of e-ICLDH@GDY nanosheet. Note that scale bars in (d) and (e) are 100 and 5 nm, respectively. LSV polarization curves of e-ICLDH@GDY/NF and other samples f) without and g) with iR-correction. h) CA test of e-ICLDH@GDY/NF electrolyzer at a constant cell voltage of 1.56 V with inset of the photograph for this electrolyzer. Reproduced with permission.[208] Copyright 2018, NPG.

sandwich-like nanoarchitecture where both sides of exfoliated iron-cobalt LDHs (e-ICLDHs) were clamped by the all-carbon material graphdiyne (GDY) as a highly efficient bifunctional electrocatalyst (e-ICLDH@GDY/NF). The fabrication process of this hybrid nanostructure was illustrated in **Figure 16**a, in which hexaethynylbenzene monomers were intercalated the interlayer spacing of ICLDHs, followed by the in situ formation of GDY layers through the coupling of the alkynyl units. The stress/deformation of the intimate contact between LDH and GDY enlarged the interlayer distance of LHDs, finally leading to the complete exfoliation of ICLDHs and the formation of e-ICLDH@GDY/NF catalyst. The thinner and more wrinkled e-ICLDH compared with the pristine bulk ICLDH (b-ICLDH) can be more favorable for mass transport, gas release, and active site utilization (Figure 16b,c). Additionally, the successful coupling of GDY not only enhanced the electrical conductivity but also elevated the anti-corrosion ability (Figure 16d,e). Integrated with all the above merits, e-ICLDH@GDY/NF had excellent catalytic activity and stability in alkaline media. As shown in Figure 16f,g, when served as both cathode and anode for OWS, ICLDH@GDY/NF can drive 10, 100, and 1000 mA cm^{-2} at only 1.43, 1.46, and 1.49 V cell voltage under iR-correction, respectively. More

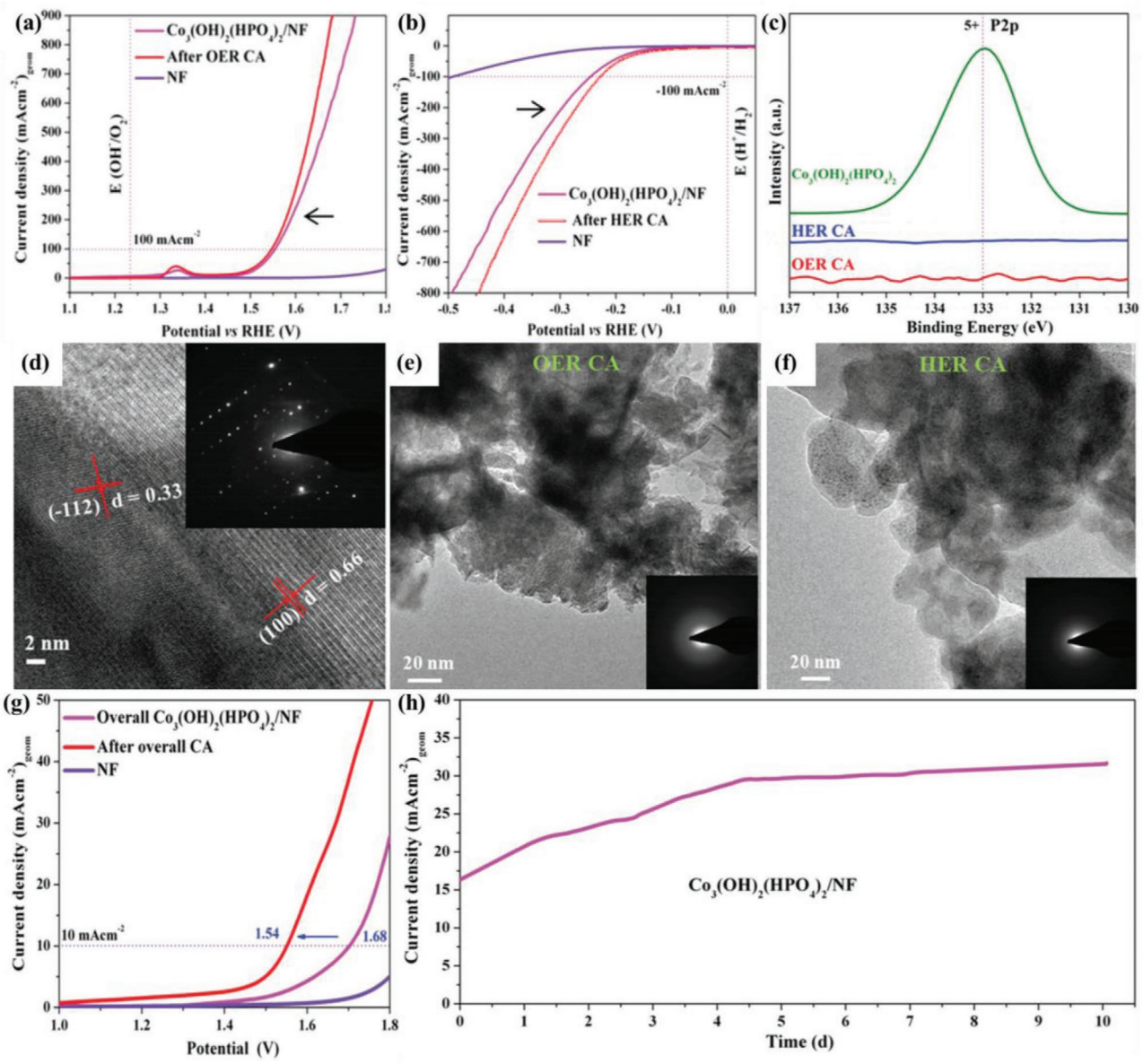

Figure 17. LSV polarization curves of $Co_3(OH)_2(HPO_4)_2$/NF before and after CA test for a) OER and b) HER. c) P 2p XPS spectra of $Co_3(OH)_2(HPO_4)_2$, as well as, the $Co_3(OH)_2(HPO_4)_2$ after OER and HER. HRTEM images of d) $Co_3(OH)_2(HPO_4)_2$, e) $Co_3(OH)_2(HPO_4)_2$ after OER CA, and f) $Co_3(OH)_2(HPO_4)_2$ after HER CA. g) LSV polarization curves of the electrolyzer where $Co_3(OH)_2(HPO_4)_2$/NF worked as both anode and cathode before and after CA test, as well as, bare NF. h) CA test of $Co_3(OH)_2(HPO_4)_2$/NF electrolyzer at a constant cell voltage of 1.7 V. Reproduced with permission.[213] Copyright 2019, WILEY-VCH.

encouragingly, this two-electrode alkaline electrolyzer can maintain a current density of 100 mA cm^{-2} without decline, indicating huge potential for practical application (Figure 16h).[208] Finally, it is worth mentioning that the intrinsic conductivity of TM-based oxides/hydroxides and LDHs are usually poor, as demonstrated by Wu and his co-workers, where the large inherent resistance of NiCo LDHs was determined by the four-point probe.[78] However, the integration of TM-based oxides/hydroxides and LDHs nanocatalysts with the conductive substrates into the assembled self-supported electrodes can distinctly facilitate the charge transfer ability, thus endowing them with tremendously enhanced electrochemical performance.[34,78]

Besides, self-supported oxides/hydroxides-based catalysts, other TM-based compounds, including chalcogenides,[21,209] phosphides,[210,211] nitrides,[212] phosphate,[213] borides,[71] alloys,[28] etc. were also developed for integration of highly efficient OWS electrolyzers. This can be attributed to their relatively high electrical conductivity and robust corrosion resistance in a harsh environment with strong acid or alkaline solutions.[214] On the other hand, when utilized as the anodes for OER, the in situ transform of these TM-based compounds into the corresponding vacancy and defect-rich (oxy)hydroxides was triggered with the leaching of the original elements, and such formed (oxy)hydroxides can further boost the water

oxidation reaction.[200,215] Some of our previous work uncovered this phenomenon in detail.[23,213] Taking one of them as an example, we employed a facile and mild hydrothermal synthetic method to obtain the crystalline Lazulite cobalt phosphate ($Co_3(OH)_2(HPO_4)_2$), which was then electrophoretically deposited on nickel foam, constructing the self-supported catalyst $Co_3(OH)_2(HPO_4)_2$/NF. Notably, after a long-term OER CA test, the post-OER $Co_3(OH)_2(HPO_4)_2$/NF significantly exhibited enhanced OER catalytic with a comparison with the pre-OER one (**Figure 17**a). The same trend can also be observed for HER, manifesting the improved bifunctional catalytic activity after electrochemical reactions (Figure 17b). This can be accounted for the leaching of P in pristine $Co_3(OH)_2(HPO_4)_2$ during CA for both OER and HER, resulting in the conversion of highly crystalline cobalt phosphate into porous amorphous Co-rich $CoO_x(OH)$ phases with abundant defect and vacancies, which served as the more active species for water splitting (Figure 17c–f). Similarly, when $Co_3(OH)_2(HPO_4)_2$/NF was used as both anode and cathode in an OWS electrolyzer, it showed continuously improved curve in CA test, as well as the lowered cell voltage at the same current density after OWS CA, demonstrating the enhancement effect caused by self-reconstruction of TM-based compounds for full water splitting (Figure 17g,h). As a result, the activated $Co_3(OH)_2(HPO_4)_2$/NF just required 1.54 V cell voltage to drive 10 mA cm^{-2} current density, showing highly efficient OWS capability.[213]

Although numerous promising works have been developed for OWS (as is depicted in **Table 2**), most of these self-supported electrocatalysts displayed exceptional activity only in alkaline media. More importance should be dedicated to developing efficient OWS electrolyzers in wide and even entire pH electrolytes, which will provide more applicability and scalability from the economic perspective.

4.4. Self-Supported Electrocatalysts under Large Current Density

Driving large current density efficiently and robustly is vital for industrial application, including AWE (200–400 mA cm^{-2} current density) and PEM (600–2000 mA cm^{-2} current density) water electrolysis.[63] To construct such an advanced electrocatalyst with satisfactory large-current-density activity for water splitting, efficient electron, and mass transfer should be guaranteed. However, conventional catalysts which are prepared as powders demand polymer binders and/or carbon-based additives to be deposited on the substrates. In this case, the charge transfer channels will be clogged and the escape of evolved gas bubbles will be stinted. Furthermore, the increasing generation of violent bubbles under large current density may enable the deposited powder catalysts to be peeled off, distinctly depraving the finally catalytic activity and stability. Meanwhile, the oxidation or corrosion of carbon-based additives easily occurs under the sharp reaction of large current density, damaging the nanostructure of the catalyst.[32,50,216] On the contrary, the self-supported configuration where the catalysts are chemically bonded with the substrate ensures their tight affinity, beneficial for the transport of charge/mass conductivity, optimization of electrochemically active sites as well as stability under a harsh working environment. Favored with these strong points, several highly efficient self-supported electrocatalysts have been emerged for large-current-density water splitting and being considered promising candidates for enormous H_2 fuel preparation.[78,117,186,217] More details of the self-supported electrocatalysts with excellent performance for high-current-density water splitting can be seen in **Table 3**.

For those reported advanced catalysts, two aspects are particularly taken into consideration to achieve the outstanding activity, especially under large current density, that is, structure and surface morphology design and electronic state modulation. First of all, controlling various structure and surface morphology, including downsizing the catalyst into ultrasmall nanoparticles, building multidimensional architecture, creating porous and rough nanostructure, can accelerate electron transfer and mass diffusion, promote the utilization and exposure of active sites, improve reaction kinetics, and mechanical stability, thus helping the catalysts work efficiently under large current density.[218–220] For example, Fan et al. coupled ultrafine amorphous NiFe oxyhydroxides nanoparticles (<5 nm) with the crystalline NiFe alloys core on NF (denoted as Ni_xFe_{1-x}–AHNAs) as efficient water splitting catalyst using a facile one-step wet-chemical deposition with the assistance of external magnetic field (**Figure 18**a). As is displayed in Figure 18b–d, HRTEM images verified that the inner crystalline NiFe alloy was encased by an ultrathin layer (1–5 nm) consisting of amorphous nanodomains. Compared with other oxyhydroxides fabricated through conventional electrodeposition, hydro/solvothermal, or wet-chemical methods, this amorphous NiFe oxyhydroxides nanodomains was much smaller, thus more conducive to the reduction of electron transfer resistance and increment of surface area and active catalytic sites. Therefore, this self-supported hybrid catalyst exhibited outstanding activity, especially under large current density (Figure 18e,f). At the optimized atomic ratio of Ni: Fe (0.8: 0.2), $Ni_{0.8}Fe_{0.2}$–AHNAs can drive 500 and 1000 mA cm^{-2} current density at the ultralow overpotentials of 248 and 258 mV, respectively, in 1.0 M KOH for OER. Also, when $Ni_{0.8}Fe_{0.2}$–AHNAs was employed as the anode to assemble the alkaline OWS cell with bare Ni nanowire (without Fe content) cathode, this electrolyzer only demanded low cell voltages of 1.55, 1.7, and 1.76 V at large current densities of 100, 500, and 1000 mA cm^{-2}, respectively. The acquired cell voltages, in this case, were distinctly lower than those of standard Ni and stainless-steel (the electrode pair in the industrial cell) electrolyzer at the same current densities. More importantly, combining the faradaic efficiency (FE) of this $Ni_{0.8}Fe_{0.2}$–AHNAs electrolyzer for generating O_2 and H_2 (both around 100%, Figure 18g), with Equation (23) (the details are given below) for the amount of charge (Q) required when 1 kg H_2 was generated, the authors calculated the required amount of electricity (W) for 1 kg H_2 production under the common current density of industrial electrolyzer, 500 mA cm^{-2} via Equation (24). According to cell voltages (U) measured in Figure 18f, $Ni_{0.8}Fe_{0.2}$–AHNAs assembling electrolyzer can save 11.16 kWh electricity compared with the simulated industrial one, intuitively manifesting its huge commercial practice prospect.[221]

$$Q = \left(1000\text{g} \times N_A \times 2e\right)/\left(M_{H2} \times FE\right) \quad (23)$$

$$W = Q \times U \quad (24)$$

Table 2. Recently reported advanced self-supported non-noble metal-based electrocatalysts with promising overall-water splitting activity.

Sample ID	Substrate	Catalyst loading [mg cm^{-2}]	Electrolyte	Cell voltage [V] @ j [mA cm^{-2}]	Ref.
LiMnBPO	NF	1.3	1 M KOH	1.48@10	[26]
LiCoBPO	NF	≈3	1 M KOH	1.53@10	[27]
$FeSn_2$	NF	≈1.6 ± 0.1	1 M KOH	1.53@10	[28]
$Ni_{0.82}Co_{0.18}O$@C	NF	/	1 M KOH	1.42@10	[34]
Co@N-CS/N-HCP	CC	≈3.2	1 M KOH	1.545@10	[67]
Ni–W–B	CC	5.6	1 M KOH	1.524@25	[71]
CoFeCo PBA	CC	/	1 M KOH	1.58@20	[100]
$Fe_{0.9}Ni_{2.1}S_2$	NF	/	1 M KOH	1.51@10	[109]
Ni–P–B	Paper	6.15	1 M KOH	1.661@50	[112]
N-Co_3O_4@C	NF	/	1 M KOH	1.4@10	[114]
Co-B	NFo[a)]	/	1 M KOH	1.41@10	[117]
Cu_3N-CuO	NF	≈3	1 M KOH	1.62@10	[124]
FeP	NF	≈1	1 M KOH	1.59@10	[150]
$Ni_{11}(HPO_3)_8(OH)_6$	NF	≈3	1 M KOH	1.6@10	[151]
$CoSn_2$	NF	≈3	1 M KOH	1.55@10	[152]
P-CoMoS	CC	2.19	1 M KOH 1 M PBS	1.54@10 1.601@10	[153]
CoMoNiS-NF-3:1	NF	1.86	1 M KOH 0.5 M H_2SO_4	1.54@10 1.45@10	[157]
$NiAl_\delta P$	NF	/	1 M KOH 0.5 M H_2SO_4	1.55@10 1.52@10	[163]
Mo-Co_9S_8	CC	1	1 M KOH 0.5 M H_2SO_4	1.56@10 1.68@10	[170]
$NiFeO_x$	CFP	≈1.6	1 M KOH	1.51@10	[196]
e-ICLDH@GDY	NF	/	1 M KOH	1.46@100 1.49@1000	[208]
$Ni_xCo_{2-x}P$@NC NA	NF	/	1 M KOH	1.56@20	[210]
Ni_2P	NF	≈3	1 M KOH	1.58@10	[211]
Activated $Co_3(OH)_2(HPO_4)_2$	NF	≈2	1 M KOH	1.54@10	[213]
Mn-doped FeP/Co_3 $(PO_4)_2$	CC	1.2	0.5 M H_2SO_4	1.75@10	[264]
NMNAs	NF	7.33	1 M KOH	1.423@10	[276]
Ni-ZIF/Ni-B	NF	/	1 M KOH	1.54@10	[277]
CoFe-PBA NS	NF	/	1 M KOH	1.545@10	[278]
NiFeMo alloy inverse-opals	NF	12	1 M KOH	1.47@10	[279]
V-CoP@ a-CeO_2	CC	/	1 M KOH	1.71@100	[280]
(Ni,Fe)OOH	NF	4	1 M KOH	1.586@500 1.657@1000	[281]
Cu@CoS_x	CF	/	1 M KOH	1.5@10	[282]
MoS_2–Ni_3S_2	NF	13	1 M KOH	1.5@10	[283]
B-FeNi	HS[b)]	/	1 M KOH	1.456@10	[284]
Karst NF	NF	/	1 M PBS	2@30 2.2@100	[285]
S-$NiFe_2O_4$	NF	/	1 M PBS	1.95@10	[286]
CoO/$CoSe_2$	TM	2	0.5 M PBS	2.18@10	[287]

[a)]NFo: Nickel foil; [b)]HS: Hydrophilic sponge.

In the above two equations, N_A represents the Avogadro constant, e represents an electron charge and M_{H2} represents the relative molecular mass of a hydrogen molecule.[221]

In addition, building a self-supported with porous/rough nanostructure can also enhance the water splitting activity in large-current-density working conditions. High porosity and

Table 3. Recently reported advanced self-supported non-noble metal-based electrocatalysts with outstanding large-current-density activity.

Sample ID	Substrate	Catalyst Loading [mg cm^{-2}]	React.	Electrolyte	η [mV] @ j [mA cm^{-2}]	Tafel slope [mV dec^{-1}]	Ref.
$CoMoS_x$	NF	/	HER	1 M KOH	269@500	94	[47]
			OER	1 M KOH	442@500	/	
			OWS	1 M KOH	660@500	/	
A-NiCo LDH	NF	3.15	HER	1 M KOH	286@500 381@1000	57	[78]
Ni–P–B	Paper	6.15	HER	1 M KOH	276@500	39.2	[112]
			OER	1 M KOH	375@500	70.6	
NiMoN	NF	/	HER	1 M KOH	127@500	45.6	[191]
			HER	1 M KOH + Seawater	160@500 218@1000	/	
NiMoN@NiFeN	NF	/	OER	1 M KOH	337@500	58.6	[191]
			OER	1 M KOH + 0.5 M NaCl	347@500	/	
			OER	1 M KOH + Seawater	369@500 398@1000	/	
NiMoN || NiMoN@NiFeN	NF	/	OWS	1 M KOH + 0.5 M NaCl	505@500 614@1000	/	[191]
			OWS	1 M KOH+ Seawater	544@500 671@1000	/	
$Ni_{2(1-x)}Mo_{2x}P$	NF	7.4	HER	1 M KOH	240@500 294@1000	46.4	[217]
Fe-CoP	NF	4.2	OER	1 M KOH	295@500 428@1000	36	[219]
Fe^0–Ni_xS_y	NF	/	OER	1 M KOH	345@1000 372@1500	92	[220]
$Ni_{0.8}Fe_{0.2}$ AHNA	NF	2.5/	OER	1 M KOH	248@500 258@1000	34.7	[221]
$Ni_{0.8}Fe_{0.2}$ AHNA //Ni nanowire			OWS	1 M KOH	470@500 530@1000	/	
$NiFe/NiCo_2O_4$	NF	/	OER	1 M KOH	340@1200	38.8	[223]
MoS_2/Mo_2C	TFo	/	HER	1 M KOH	191@500 220@1000	43	[225]
			HER	0.5 H_2SO_4	227@1000	~55	
(Ni,Fe)SO(OH)	NF	2.84	OER	1 M KOH	260@1000	/	[228]
Fe_2P-Co_2P	CoFa)	3	HER	1 M KOH	208@500 254@1000	56	[231]
			OER	1 M KOH	291@500 317@1000	51	
			OWS	1 M KOH	640@500	/	
NiFe/Ni/Ni	NMb)	1.4	OER	1 M KOH	300@500	108.1	[239]
			OWS	1 M KOH	730@500	/	
Cu-W/NiCo-LDH	CM	1	HER	1 M KOH	139@500 190@1000	50.5	[256]
			HER	0.5 M H_2SO_4	246@1000	79.4	
(Ni,Fe)OOH (Ni,Fe)OOH// $MoNi_4$	NF	4	OER	1 M KOH	259@500 289@1000	/	[281]
			OWS	1 M KOH	356@500 427@1000	/	
Fe_x–Ni/C	NF	3.9 ± 0.3	HER	1 M KOH	183@1000	26	[288]
			OER	1 M KOH	300@1000	52	
			OWS	1 M KOH	430@500	/	
P-Fe_3O_4 NiFe LDH || P-Fe_3O_4	FF[c)]	/	HER	1 M KOH	≈240@1000	41.9	[289]
			OWS	1 M KOH	350@500	/	
$F_{0.25}C_1CH$	NF	/	HER	1 M KOH	246@500 256@1000	99	[290]
			OER	1 M KOH	270@500 308@1000	42	
			OWS	1 M KOH	290@500	/	
FeP/Ni_2P	NF	8	HER	1 M KOH	≈260@1000	24.2	[291]
			OER	1 M KOH	281@690	22.7	
			OWS	1 M KOH	490@500 550@1000	/	
Ni_2P Ni_2P||Ni–Fe LDH	NF	/	HER	1 M KOH	306@1000 ≈770@1000	76	[292]
			OWS	1 M KOH			

Table 3. Continued.

Sample ID	Substrate	Catalyst Loading [mg cm^{-2}]	React.	Electrolyte	η [mV] @ j [mA cm^{-2}]	Tafel slope [mV dec^{-1}]	Ref.
FeS	FF	/	HER	1 M KOH	336@1000	77	[293]
$Ni_3Fe_{1-x}V_x$	CFP	/	OER	1 M KOH	291@500	39	[294]
$NiFe_2O_4$/NiFe LDH	NF	2.8	HER	1 M KOH	297@500 314@750	67.1	[295]
			OER	1 M KOH	242@500 265@1000	28.2	
			OWS	1 M KOH	702@500	/	
$FeCoNiP_xS_y$	TFo.	/	HER	1 M KOH	264@1000360@1000	99	[296]
			OER	1 M KOH		80	
Co–P	CoF	/	HER	1 M KOH	290@1000	78	[297]
			HER	0.5 M H_2SO_4	≈300@900	/	
			OER	1 M KOH	380@1000	37	
			OWS	1 M KOH	750@1000	/	
$Ni_{60}Fe_{30}Mn_{10}O_x$	NF	/	OER	1 M KOH	360@1000	62	[298]
Fe_2O_3@Ni_2P/ $Ni(PO_3)_2$	NF	/	OER	1 M KOH	340@500 370@1000	48.2	[299]
(Ni–MoO2)@C	NF	20.5	HER	1 M KOH	260@1000 304@2000	50	[300]
			OER	1 M KOH	365@1000 400@2000	62	

[a]CoF: Cobalt foam; [b]NM: Nickel mesh; [c]FF: Iron foam.

roughness can bestow the catalysts to possess a larger surface area with more electrochemical active sites.[222–224] For example, Qiu et al. coupled mesoporous NiFe-LDH nanosheets with a 3D MXene frame scaffolded on NF, which can efficiently drive a large current density of 500 mA cm^{-2} at a low cell voltage of 1.75 V in 1.0 M KOH.[224] Also, modifying porosity and roughness is considered to be key points for the control of the surface wettability of electrodes.[48,255] The surface with superhydrophilicity (when the liquid contact angle of a droplet on a solid surface is less than 5 or 10° in the air) can significantly promote the permeability of electrolyte, ensuring the majority of active sites can be accessed.[32] On the other side, the underwater gas-bubble contact angle over 150° means that the self-supported electrocatalyst is superaerophobic, so that the evolved bubbles can depart from the electrode more smoothly.[226] Because of the interfacial energy balance, an electrocatalyst featuring superhydrophilicity will inherently exhibit superaerophobicity.[227] As a result, under the condition of large current density, the superhydrophilic/superaerophobic electrocatalyst will avoid the severe accumulation of generated gas bubbles and promote the utilization of active sites, thus displaying excellent catalytic activity and stability.[47] For instance, Ding et al. reported a porous nanocatalyst, NiFe (sulfur)oxyhydroxide nanoclusters supported on NF (denoted as (Ni,Fe)SO(OH)/NF), via the simple one-step wet-chemical method. The porous and rough outer layer enabled this catalyst to have both superhydrophilicity and superaerophobicity (**Figure 19**a,b). Therefore, (Ni,Fe)SO(OH)/NF possessed better electrolyte permeability, more exposed and accessible active catalytic sites, and stronger ability of bubbles release, affording an OER current density of 1 A cm^{-2} at 260 mV overpotential in 1 M KOH.[228]

Another strategy to further boost high-current-density catalytic capability for self-supported electrocatalysts is the rational modulation of electronic state, which can improve their intrinsic conductivity and favor the formation of intermediates during water splitting reaction.[217,221] The most common electronic regulation methods are by incorporation of foreign atoms/small groups and other components.[218,219,223] For instance, Zou et al. fabricated Ni-doped Co_3S_4 nanoparticles which was coupled with Ni_3S_2 nanosheets on NF. Density functional theory calculations revealed that the Ni doping obviously diminished the adsorption free energy of intermediate H*, accounting for the exceptional activity for HER under large current density.[218] In fact, theoretical calculations have been widely applied to analyze the electronic regulation as well as the corresponding effects on thermokinetics for water splitting. In this regard, Luo et al. reported that after the successful substitution of S by incorporating N into CoS_2, more electrons transfer from Co to N was observed to Co to S (Figure 19c,d). Thus, active Co sites in N-doped CoS_2 with more positive charges were favorable for the adsorption of polarity water molecules (Figure 19e,f). The optimized electronic state can further lower the Gibbs free adsorption energy of intermediate *H (ΔG_{*H}) for N-doped CoS_2 compared with the pristine CoS_2 (Figure 19g,h), enabling NF-supported N-doped CoS_2 to drive large current density efficiently for both HER and OER.[229]

Even though tremendous efforts have been devoted, most of the self-supported electrocatalysts exhibited extraordinary large-current-density activity only in alkaline media. When extended to other electrolytes, such as acid electrolyte which is applied in commercial in PEM water electrolysis, the exciting breakthroughs are still missing because of the poor activity of TM-based electrocatalysts,[230] thus more particular attention should be paid to this area.

4.5. Self-Supported Electrocatalysts with Long-Term Stability

Exceedingly robust stability is essential to the commercialization and industrialization of H_2 production via water electrolysis

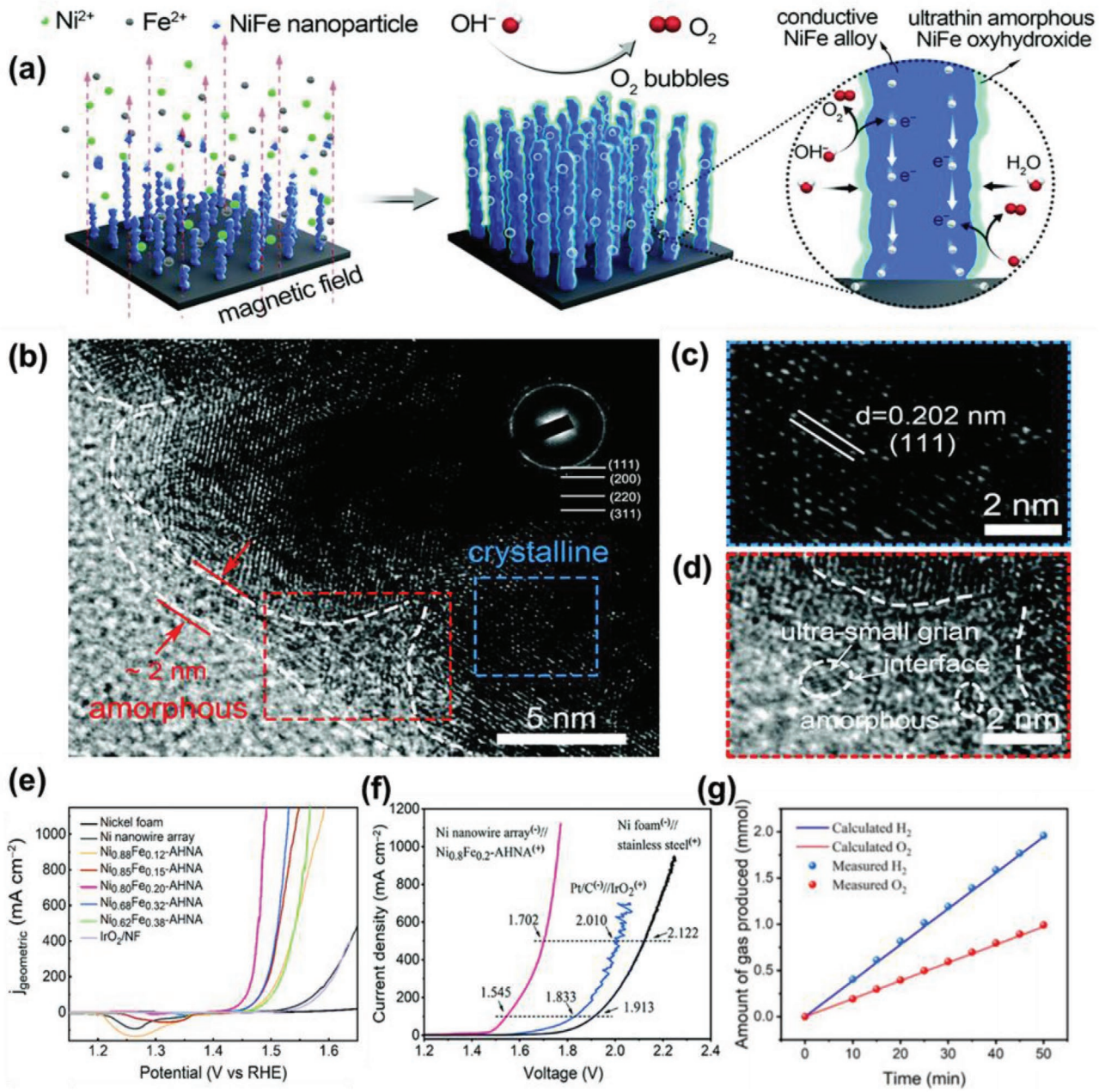

Figure 18. a) Schematic illustration of synthesis procedure for Ni_xFe_{1-x}–AHNAs. HRTEM images of b) Ni_xFe_{1-x}–AHNAs, c) crystalline NiFe alloy region, and d) amorphous NiFe oxyhydroxide region. e) OER LSV polarization curves of Ni_xFe_{1-x}–AHNAs with different atomic ratios of Ni/Fe, as well as, other comparison samples. f) LSV polarization curves of the electrolyzers assembled by pairs of $Ni_{0.8}Fe_{0.2}$–AHNAs and Ni nanowire array, stainless steel and NF, and other reference samples. g) Experimentally and theoretically measured gas amounts generated by the $Ni_{0.8}Fe_{0.2}$–AHNAs and Ni nanowire array electrolyzer at a constant current density of 500 mA cm^{-2}. Reproduced with permission.[221] Copyright 2020, Royal Society of Chemistry.

technology. Currently, the thousands-of-hour durability requirement is the main gap between laboratory research and practical application.[50] Most electrocatalysts developed in the laboratory can just maintain a small current density for a period of dozens of hours at mild electrolytes and temperatures.[231] This can be ascribed to the unavoidable shedding and deactivation of catalytic species during long-time operation (for at least hundreds of hours) or/and under harsh working environment (more corrosive electrolyte, higher perform temperature, or larger current density), especially for those powder catalysts which are deposited on collectors using binders or additives.[52,232] In this respect, integrating active catalysts and substrates as self-supported electrodes without any external additions can assure the long-term durability of water splitting catalysts from both mechanical and chemical aspects,[45] further advancing the progress of practical water electrolysis.

Benefiting from the reasonable design, a series of novel and advanced self-supported electrocatalysts have shown

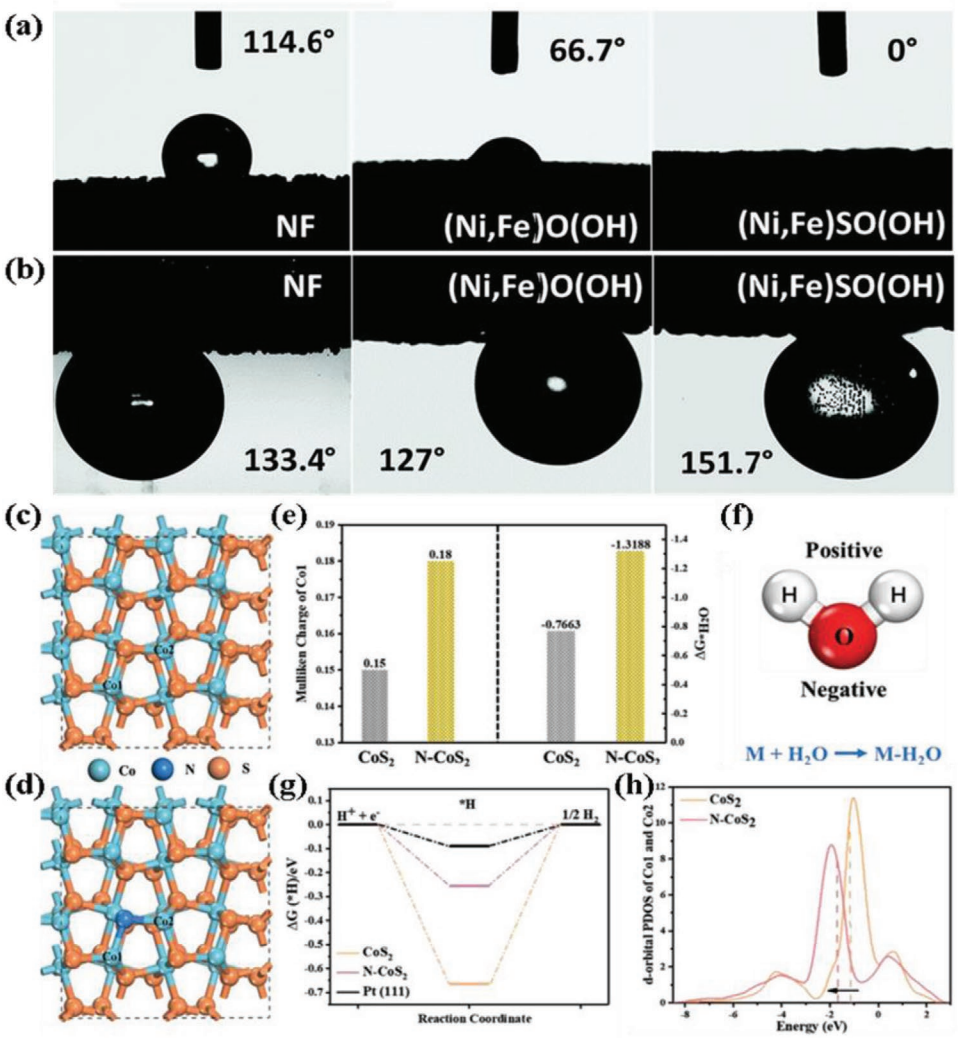

Figure 19. Comparison of a) hydrophilicity and b) underwater aerophobicity of (Ni,Fe)SO(OH) and other samples. Reproduced with permission.[228] Copyright 2019, Royal Society of Chemistry. Calculation model structures of c) CoS_2 with possible catalytic sites Co1 and Co2 on (001) plane and d) N-CoS_2 with possible catalytic sites Co1 and Co2 on (001) plane. e) The Mülliken charge analysis of catalytic sites Co1 on CoS_2 (001) plane and N-CoS_2 (001) plane, respectively (left); The water adsorption free energies on catalytic sites Co1 of CoS_2 (001) plane and N-CoS_2 (001) plane, respectively (right). f) The illustration of polarity H_2O molecule and the H_2O adsorption equation for HER. g) The calculated free-energy diagram for HER on N-CoS_2 (001) and other models. h) The d-orbital partial density of states (d-PDOS) of Co1 and Co2 sites for CoS_2 (001) plane and N-CoS_2 (001) plane. Reproduced with permission.[229] Copyright 2019, WILEY-VCH.

outstanding stability for water splitting.[140,231,233–235] For example, Xiao et al. prepared a NF-supported $FeNi_3N$ OER catalyst by a facile precipitation-calcination method. When served as both cathode and anode, this $FeNi_3N$/NF || $FeNi_3N$/NF alkaline electrolyzer keeps high working efficiency at a constant current density of 10 mA cm^{-2} for over 400 h in 1.0 M KOH.[140] Similarly, Yu et al. constructed NF-supported Ni nanoparticles coupling V-doped NiFe LDH nanosheets with abundant Ni and O vacancies (denoted as P-V-NiFe LDH NSA) through hydrothermal synthesis-H_2 plasma reduction. This self-supported electrode showed robust durability when assembled as an OWS cell, withstanding 10 mA cm^{-2} current density for an ultra-long running time of 1000 h in 1.0 M KOH.[234] However, such long-term catalytic robustness for alkaline water electrolysis are majorly performed under a moderate laboratory environment, that is, mild electrolyte and room temperature. As for the current industrial application, the harsher operation conditions have to be satisfied (temperature is 70–80 °C, KOH is in 25–30 wt%).[236] Some impressive works on self-supported electrocatalysts meeting such conditions have been reported.[104,232,237–239] For example, Mai et al. prepared MoO_2-Ni arrays on the NF, which can work stably at simulated industrial application temperature of 51.9 °C for 115 h as HER cathode. When paired with $NiMoO_4$/NF which was completely activated by anodic potential, the assembled alkaline electrolyzer can work at the unchanging 10 mA cm^{-2} current density for 220 h at 51.9 °C without obvious decline.[104] More notably, the direct corrosion method of metal substrates can endow the prepared self-electrocatalysts with excellent stability, which can be illustrated by the report of Zou and his co-workers. They

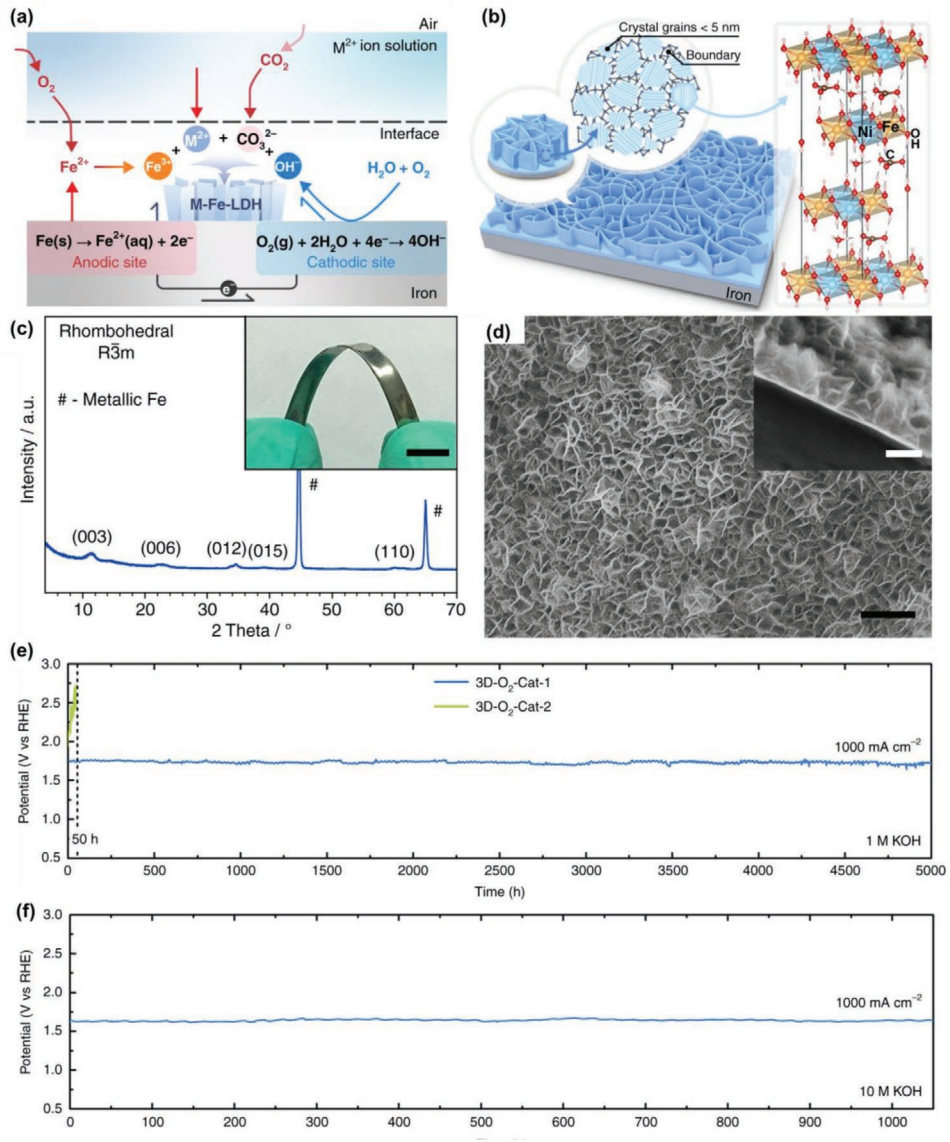

Figure 20. a,b) Schematic illustration of corrosive reaction for the formation of Fe-based LDH. c) Powder X-ray diffraction (XRD) pattern and d) SEM image of as-obtained Fe-based LDH on Fe substrate with a scale bar of 400 nm. Inset of (c) is the corresponding digital image, and the inset of (d) is a cross-section SEM image with a scale bar of 200 nm. CP curves of e) 3D-O_2-Cat-1 in1.0 M KOH compared with 3D-O_2-Cat-2, and f) 3D-O_2-Cat-1 in 10.0 M KOH at a constant current density of 1000 mA cm^{-2}. Reproduced with permission.[237] Copyright 2018, NPG.

immersed iron substrates, which served as both support and Fe source, into an aqueous corrosive solution with amounts of divalent cations in the air. The introduction of divalent cations promoted the formation of Fe-based LDH nanosheets with rich grain boundaries on the Fe substrates (**Figure 20**a,b). The optimized self-supported electrode was FeNi LDH nanosheets supported on Fe foam (Figure 20c,d), which was denoted as 3D-O_2-Cat-1, and the comparison sample was the same LDH on Fe plate, O_2-Cat-2. Because of the strong affinity of LDH with the Fe foam support and highly active LDH architecture, 3D-O_2-Cat-1 can retain a constant large current density of 1000 mA cm^{-2} for over 6000 h in 1.0 M KOH for OER. Afterward, when applied in a practical AWE electrolyte of 10.0 M KOH solution, this catalyst can also keep the similar extraordinary durability (Figure 20e,f), showing huge potential for commercial application.[237]

Apart from attention to the industrial conditions for the design and fabrication of highly stable self-supported electrocatalysts, the inherent features of the nanostructured catalysts themselves should be also taken into consideration, especially the reconstruction conversion of anodic catalysts which are responsible for OER. As discussed above, on one hand, the in situ transformation of self-supported TM-based catalysts into the corresponding (oxy)hydroxides is nearly inevitable with subsequent electrocatalytic water oxidation.[23,101,200,213,215] On the other hand, the deep or even complete transformation will lead to more efficient and robust OER performance.[104,105] Mai and co-workers found the in situ formed porous (oxy)hydroxides

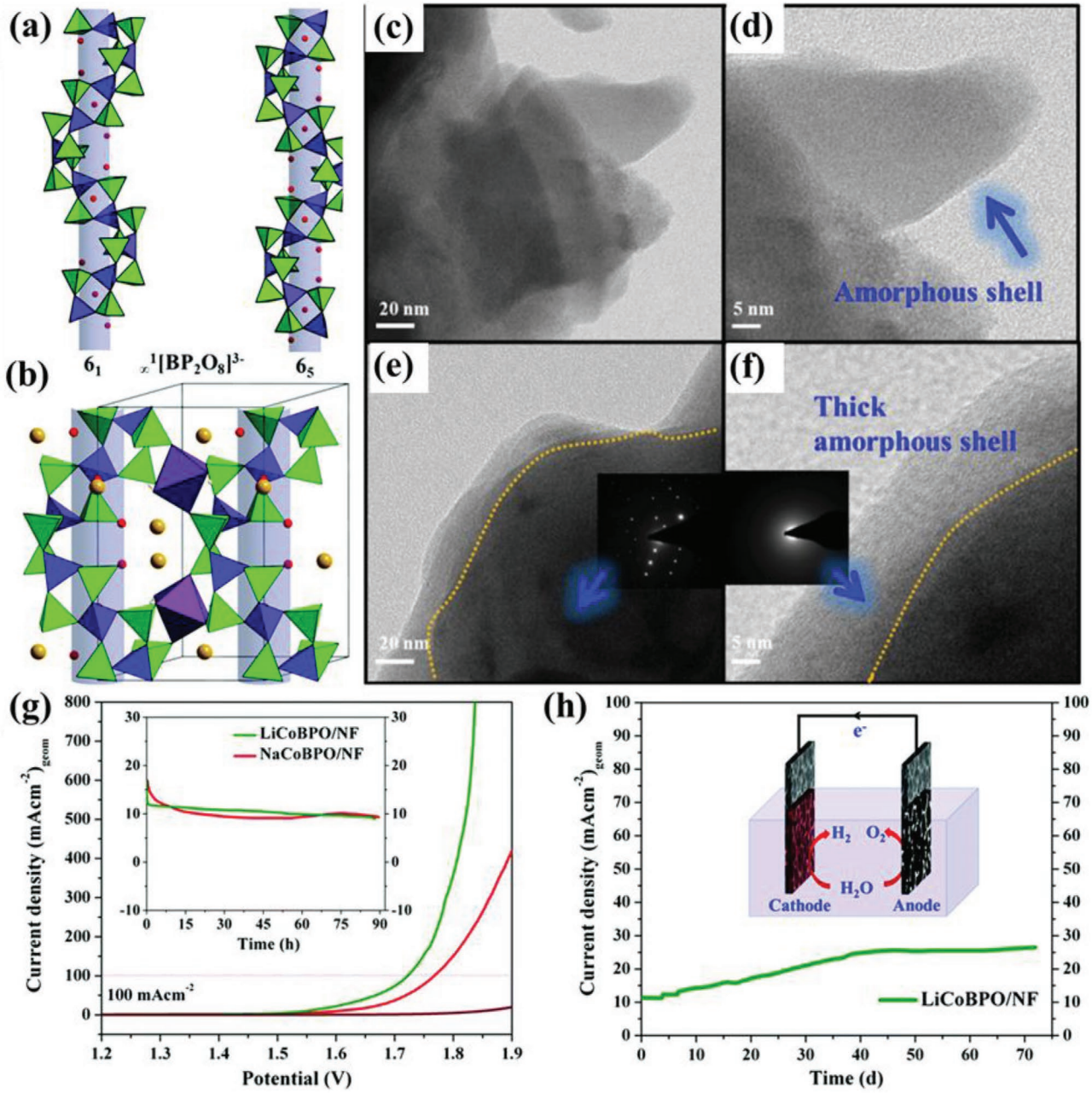

Figure 21. a) The partial anionic structure of helical borophosphates, where violet tetrahedra represent BO_4 and green tetrahedra represents PO_4. b) The helices running along [001] are interconnected via the $CoO_4(OH_2)_2$ (fuchsia) coordination octahedra. Yellow spheres represent Li or Na ions occupying the free threads of helices. Red spheres represent hydrate water in the helical channels. c) TEM image with a scale bar of 20 nm and d) HRTEM image scale bar of 20 nm for LiCoBPO after OER CV. e) TEM image with a scale bar of 20 nm and f) HRTEM image scale bar of 20 nm for LiCoBPO after OER CA for 24 h. The corresponding SAED images were depicted in the insets. g) LSV polarization curves of the LiCoBPO/NF || LiCoBPO/NF electrolyzer and other comparison samples for OWS in 1.0 M KOH. The inset displayed CA curves of LiCoBPO/NF || LiCoBPO/NF electrolyzer and other comparison samples for 90 h. h) CA curve of LiCoBPO/NF || LiCoBPO/NF electrolyzer (which was illustrated in the inset) for around 73 days at a constant cell voltage of 1.53 V in 1.0 M KOH. Reproduced with permission.[27] Copyright 2019, Royal Society of Chemistry.

with great gas release ability were thermally stable under high operation temperature, enabling this catalyst with outstanding stability.[104] Based on this, constructing self-supported electrocatalysts which are flexible for maximum reconstruction during water oxidation can further boost and maintain the OER activity, thus exhibiting a durable OWS performance.[27,213]

Our group has fabricated two desired helical cobalt-based borophosphates, LiCoBPO ($LiCo(H_2O)_2[BP_2O_8]H_2O$) and NaCoBPO ($NaCo(H_2O)_2[BP_2O_8]H_2O$), both supported NF for water splitting. As is shown in **Figure 21**a, the structure of prepared BPOs featured infinite loop-branched helical main chains constructed by alternating borate and phosphate tetrahedra which

are connected by sharing the common corners. The helical DNA-like chains along the [001] are interrelated through the coordination octahedra $CoO_4(OH_2)_2$, whose free threads accommodate the Li or Na ions irregularly surrounding the O atoms (Figure 21b). Benefiting from this fascinating structure, BPOs can easily transform into amorphous (oxy)hydroxides with rich vacancies and defects because of the leaching of Li or Na, as well as P and B during OER. Of note, after a short-time OER CV, an ultrathin amorphous shell appeared on the surface of LiCoBPO (Figure 21c,d), while a much thicker amorphous phase corresponding to (oxy)hydroxides can be observed in Figure 21e,f for LiCoBPO after 24 h OER CA, demonstrating the deeper reconstruction conversion along with the increase of OER time. Most importantly, coupled with its good catalytic performance for HER, LiCoBPO on NF (LiCoBPO/NF) showed more impressing OWS activity in 1.0 M KOH, and when the durability of LiCoBPO/NF AWE was estimated by CA, an unceasingly growing time-current density curve can be found from 10 mA cm^{-2} in the initial 40 days (Figure 21g,h). Consequently, such a curve was stabilized and withstood for up to two and a half months (Figure 21h). This phenomenon was caused by the gradual and continuous structure reconstruction of LiCoBPO on the anode into Co-rich (oxy)hydroxide phase, which continuously accelerated the overall water electrolysis and steadily dominated the water splitting after the maximized phase transform. Thus, LiCoBPO/NF is considered as a promising self-supported electrode for commercial water electrolysis.[27] Inspired by the excellent durability of cobalt-based BPOs for water splitting in an alkaline environment, we recently further developed the novel manganese-based BPOs (LiMnBPO and NaMnBPO) which still crystallized in the same chiral space groups. As expected, such catalysts easily transformed into active amorphous MnO_x phase under anodic potential. Notably, after depositing on NF, the self-supported LiMnBPO presented highly robust and unceasing OWS activity for over 160 days, confirming the commercialization potential of this class of emerging materials.[26]

Despite a series of self-supported electrocatalysts with remarkable stability for water splitting, some challenges still demand effective solutions. The first challenge, as **Table 4** demonstrates, most of the currently reported self-supported electrodes show working stability within a duration of hundreds of hours, which cannot fulfill the requirements of present industrial use. The other challenge is that all of these highly robust self-supported electrocatalysts are almost performed in alkaline media. Best to our knowledge, very few of the stable self-supported non-noble metal-based catalysts are developed for enduring operation in acid media, which is the required electrolyte for PEM water electrolysis. This limits the scalability of the self-supported catalysts.

Finally, for those as-prepared TM-based self-supported electrocatalysts, many factors should be taken into the consideration, especially their performance validation, cell design, energy efficiency, degradation mechanism, and performance optimization. However, achieving all these parameters with a single electrocatalyst is highly challenging. As discussed above, nearly all of these points can be exemplified by a series of a novel but efficient TM-based borophosphates (LiCoBPO, NaCoBPO, LiMnBPO, and NaMnBPO) developed in our group.[26,27] To validate their outstanding water electrolysis performance, a half-cell composed of three electrodes and a two-electrode alkaline electrolyzer was designed and established, where 1 M KOH was used as an electrolyte, while the self-supported BPO on FTO and NF directly served as both cathode and anode. (In the case of Mn-based BPO, it was coupled with a Pt/C cathode). In agreement with what was reflected in half-cell measurements, all these BPO exhibited exceptional OWS where Li-containing BPO with the same composition outperformed its Na-analogues and the catalytic efficiency also varied depending on the supports used (NF-or FTO). The optimization for such electrodes in a durable alkaline electrolyzer led to high energetic efficiency, reaching over 75% (80 and 78% for LiCoBPO and NaCoBPO, respectively) on the basis of minimal electrical potential difference for water splitting, as well as exceeding 90% based on the electrical potential difference for heating value of H_2 gas (97% and 94% for LiCoBPO and NaCoBPO, respectively). Remarkably, in the case of LiMnBPO, the energetic efficiency even surpassed the 80% level on the basis of minimal electrical potential difference for water splitting and reached 100% based on the higher heating value. When it comes to the degradation mechanisms of these four BPO catalysts, all catalysts transformed under harsh alkaline conditions and it can be observed that FTO supporting ones displayed much less catalytic performance than ones loaded on NF.[26,27] The suitability and the better performance of NF can be ascribed to its great electric conductivity and synergistic effect on water splitting reaction.[240] The better stabilizing effect of NF substrates under a long-term working environment has been demonstrated in other previous works,[28,29] indicating the substrates of self-supported electrodes can extremely influence the activity maintaining because of their inherent property and binding strength toward the deposited nanocatalysts. This implies that the shortened or declined catalysis stability of many self-supported catalysts arises from the poor charge transfer ability of substrates during catalysis and their weak adhesion toward the deposited nanocatalysts. More significantly, because of the above concerns, the NF substrates have been strongly considered one of the best support for the integration of self-supported electrodes, endowing the electrodes with improved activity. Moreover, the selection of easy-leaching alkali metals can also facilitate the rapid and thorough reconstruction of the BPO catalysts (especially in the water oxidation process), thus optimizing their catalytic activity.[26,27,240] Similarly, recently prepared self-supported oxide/hydroxides ($NiFeO_x$), intermetallic compounds (such as FeSi, $FeSn_2$, and $CoSn_2$) or alloys (NiMo, NiFe, FeIr) have shown exceptional catalytic performance which was indeed validated at high-current densities and industrial level conditions displaying excellent energetic efficiencies. The degradation mechanism of such electrodes was systematically studied to understand the crucial parameters that are required for stabilizing the active sites on the surface of the electrodes.[28,42,152,221,241–243]

One of the important factors worth highlighting is the degradation mechanism of most TM-based self-supported electrocatalysts during the water electrolysis process, particularly under the anodic water oxidation reaction where usually the severe reconstruction occurs. In this regard, the aggregation of reconstructed nanostructures and bury of active sites, as well as the (partial or complete) dissolution of components easily

Table 4. Recently reported advanced self-supported non-noble metal-based electrocatalysts with outstanding long-term stability.

Sample ID	Substrate	Catalyst Loading [mg cm^{-2}]	WorkingTem. [°C]	React.	Electrolyte	StabilityCA: E(V)@t [h][a]CP: j [mA cm^{-2}]@t [h]	Ref.
LiMnBPO	NF	1.48	/	OWS	1 M KOH	CA: 1.7@1100 1.48@3850	[26]
LiCoBPO	NF	≈3	RT	OWS	1 M KOH	CA: 1.53@≈1752*	[27]
MoO_2-Nicat.-51.9	NF	/	51.9	HER	1 M KOH	CP: 10@115	[104]
cat.-51.9//MoO_2-Ni	NF		25	OER	1 M KOH	CP: 10@275	
			51.9	OER	1 M KOH	CP: 10@250	
			51.9	OWS	1 M KOH	CP: 10@220	
$FeNi_3N$	NF	/	RT	OWS	1 M KOH	CP: 10@>400	[157]
$NiFeO_x$	CFP	≈1.6	/	OWS	1 M KOH	CP: 500@200	[196]
Activated $Co_3(OH)_2(HPO_4)_2$	NF	≈2	RT	OWS	1 M KOH	CA: 1.7@240*	[213]
Fe_2P-Co_2P	CoF	3	/	HER	1 M KOH	CP: 10–1000@300	[231]
			/	OER	1 M KOH	CP: 10–1000@300	
			25	OWS	1 M KOH	CP: 10–500@300	
			65	OWS	1 M KOH	CP: 10–1000@120	
Porous sintered iron	FS[b]	7.5	25	OER	5.35 M KOH	CP: 10@1000	[232]
Co_3O_4-T	CFo	2.2	/	OER	1 M KOH	CP: 100@300	[233]
P-V-NiFe LDH NSA	NF	/	/	OWS	1 M KOH	CA: 1.43@1000* CA: 2.01@1000*	[234]
$W_{0.5}Co_{0.4}Fe_{0.1}$	NF	/	RT	OER	1 M KOH	CP: 20@>500	[235]
FeNi LDH	FF	/	/	OER	1 M KOH +10 M KOH	CP: 1000@1000 + 1000@1050	[237]
NSI-FeS-200	FS*	7.5	25	OER	5.35 M KOH	CP: 10@1500	[238]
NiFe/Ni/Ni	NM	1.4	RT	OWS	6 M KOH	CP: 500@200	[239]
NiFe LDH	FF	/	20	OWS	1 M KOH	CP: 1000@1000	[289]
‖ P-Fe_3O_4			60	OWS	6 M KOH	CP: 10000@≈7	
Co–P	CoF	/	/	HER	1 M KOH	CP: 1000@3000	[297]
				OER	1 M KOH	CP: 1000@3000	
				OWS	1 M KOH	CP: 1000@4000	
NCN	CC	2	/	OWS	1 M KOH	CP: 10@250	[301]
				OWS	0.5 M H_2SO_4	CP: 10@100	
CoP NWs	CoF	/	RT	OWS	1 M KOH	CP: 20@1000	[302]
				OWS	1 M KOH	CP: 100@1000	
NiFeP-MoO_2	NF	/	/	HER	1 M KOH	CP: 300@>100	[303]
				OER	1 M KOH	CP: 300@100	
				OWS	1 M KOH	CP: 300@>500	
Co/CoO/$Co(OH)_2$	NF	≈7.6	/	OER	1 M KOH	CP: 20@200	[304]
				OER	1 M KOH	CP: 500@200	
SCFP	NF	/	/	OWS	1 M KOH	CP: 10@650	[305]
Co_3Se_4	CoF	2.6	RT	OWS	1 M KOH	CP: 10@>3500	[306]
				OWS	1 M KOH	CP: 100@≈2000	

[a]For CA applied in OWS, the constant E refers to the whole cell voltage; [b]FS: Iron substrate.

occurs, leading to the obvious deterioration of catalytic performance.[244] However, such phenomenon was often ignored in the previously reported literature but now gaining noteworthy attention. Aiming at this, Yang et al. proposed a novel NiO-based OER catalyst, which was stabilized by the chemically stable CeO_2 and supported on CC. The introduction of CeO_2 effectively suppressed the leaching of active composition and promoted the homogenous distribution of reconstructed catalytic NiOOH nanodomains without aggregation, thus endowing such heterostructured nanocatalysts with tremendously better OER stability compared with the bare NiO supported on CC.[244]

5. Conclusions and Perspectives

Due to several remarkable traits, that is, a large amount of deposited catalytic species, rapid delivery of charge and mass, intimate coupling of active catalysts and substrates, and

easy-adjusted wettability of electrode surface, considerable efficient and low-cost self-supported TM-based electrocatalysts have been developed in the past few years. In this review, we firstly provide a comprehensive overview of the design and fabrication strategies for these catalysts from the perspectives of deposited nanocatalysts, preparation methods, and selection of supported substrates. Through a one-step or multi-step synthetic method, all sorts of nanocatalysts with various components, nanostructure, and surface morphology were deposited on appropriate substrates, integrating as the self-supported electrodes. Moreover, the reconstruction of nanostructure and crystalline phase during the electrochemical anodic reaction was also highlighted for the understanding of the reaction mechanism and further guidance to the preparation of active and robust electrocatalysts. When used in water electrolysis, including HER, OER, and OWS, these self-supported catalysts exhibited encouraging potentials for practical application, elaborately reviewed from the aspects of catalytic performance in pH-universal media, seawater media, full water splitting, large current density, and enduring working time, respectively. Our elaboration of design strategies and summarization of underlying influences for catalytic ability may propose a reference for the later research, propelling the development of self-supported water splitting electrocatalysts into practically commercial utilization and thus realize massive H_2 production in an efficient, inexpensive, and environmentally friendly way. Nevertheless, to better exploit advanced self-supported catalysts for practical water electrolysis, some urgent issues as follows should be rationally handled.

i) The majority of currently explored self-supported TM-based catalysts displayed outstanding performance only for alkaline water electrolysis under the strict conditions of practical application. In other words, in acid or neutral media, such efficient catalysts were rarely reported, especially for full water splitting, at large current density, and within an ultralong working period. This may be mainly attributed to the poor OER activity, unstable chemical and structural properties of electrocatalysts in the acid environment, as well as low solution conductivity of the neutral electrolyte.[120,245,246] To deal with it, some points are suggested to be considered. First, some compositions with relatively great inherent corrosion resistance in acid media should be favorably selected to synthesize electrocatalysts, such as nitrides, phosphides, alloys, and intermetallics.[28–30,214,247,248] Second, the "anti-corrosion coating," which will simultaneously keep or even boost the activity of inner catalytic species in an acid environment can be utilized, for example, carbon-based materials.[188,249,250] Third, for low-conductive neutral electrolytes, the emphasis should be given to the improvement of intrinsic conductivity and increment of electrochemically active sites of the electrocatalysts themselves.

ii) Most of the investigated self-supported electrodes catalyzed the splitting of the simulated seawater solution with well-defined composition, concentration, and pH value, instead of real seawater. The environment of seawater is much more complicated with abundant non-innocent ions, bacteria/microbes, and small particulates, as well as unstable local pH regions.[182,251] Thus, it is of tremendous importance to achieve a breakthrough on direct electrolysis of real seawater catalyzed by advanced self-supported electrodes with high activity and selectivity, although no great advantages are expected in the near future with respect to cost-effectiveness and technical reliability.

iii) Presently, for self-supported electrocatalysts, the most common substrates are 3D macroporous metal foams, especially NF, CF, and FF. Although these substrates are relatively well conductive, their mechanical strength is not able to satisfy the real long-term application at large current density and under high temperature. Furthermore, as abovementioned, these metal foams may become extremely fragile when they are subject to a high-temperature environment (over 400–500 °C), while in many cases of fabrication of self-supported electrocatalysts, such temperatures are required for the pyrolysis of precursors supported on the metal foams. Correspondingly, the selection of synthesis strategy for self-supported electrocatalysts narrows down. On the other hand, the alternatives to metal foams are usually CC with excellent mechanical flexibility and elasticity, as well as high-temperature stability. Whereas, their conductivity is visibly inferior to that of metal foams, negatively influencing the final catalytic capability of self-supported electrodes.[122] Also, a pre-treatment in nitric acid (HNO_3) is often required for the originally commercial CC to remove the residual organic species and endow CC with strong affinity with deposited species, leading to additional energy and cost consumption.[168,252] However, most of the current attention is focused on the design and modification of deposited nanostructured catalysts, but the research on substrates is rare. Thus, more efforts should be dedicated to developing advanced substrates which can not only contribute to the great catalytic activity of the self-supported electrodes but also robustly and stably work for a long period in practical application.

iv) Most of the currently developed catalysts are "pre-catalysts," which partially or completely transform into real catalytically active structures under different conditions of HER, OER, or working electrolytes. Paying deeper insight into the real active species, morphological and electronic changes, surface/bulk structure and substrate-catalyst relation under in situ states for self-supported electrocatalysts can help researchers fully understand the self-supported system and accordingly design the self-supported catalysts which are more in line with expectation. However, the primary methods employed to investigate the real active structures for self-catalysts are ex situ ones, which cannot manage to obtain enough and accurate information under a real working environment. In view of this, advanced in situ or operando techniques, including spectroscopic techniques (such as X-ray absorption (XAS), XPS, Raman, Fourier-transform infrared spectroscopy, Mössbauer, nuclear resonant inelastic X-ray scattering, electrochemical impedance spectroscopy and XRD)[253] as well as microscopic techniques (such as atomic force microscopy and TEM)[254,255] should be more applied to get better real-time observation and consequently receive guidance for the design and fabrication of self-supported electrocatalysts for water splitting with high activity, stability, and selectivity.

Acknowledgements

The authors gratefully acknowledge the funding from Deutsche Forschungsgemeinschaft (DFG, German Research Foundation) under

Germany's Excellence Strategy—EXC 2008/1—390540038—UniSysCat. H.Y. is indebted to China Scholarship Council (CSC) for the financial support.

Open access funding enabled and organized by Projekt DEAL.

Conflict of Interest

The authors declare no conflict of interest.

Keywords

electrocatalysts, hydrogen fuel, practical application, self-supported, water electrolysis

Received: July 7, 2021
Revised: August 11, 2021
Published online: September 1, 2021

[1] P. Chen, T. Zhou, M. Zhang, Y. Tong, C. Zhong, N. Zhang, L. Zhang, C. Wu, Y. Xie, *Adv. Mater.* **2017**, *29*, 1701584.
[2] J. Lu, S. Yin, P. K. Shen, *Electrochem. Energy Rev.* **2019**, *2*, 105.
[3] C. Panda, P. W. Menezes, S. Yao, J. Schmidt, C. Walter, J. N. Hausmann, M. Driess, *J. Am. Chem. Soc.* **2019**, *141*, 13306.
[4] Z. Chen, M. Chen, X. Yan, H. Jia, B. Fei, Y. Ha, H. Qing, H. Yang, M. Liu, R. Wu, *ACS Nano* **2020**, *14*, 6968.
[5] H. Wu, C. Feng, L. Zhang, J. Zhang, D. P. Wilkinson, *Electrochem. Energy Rev.* **2021**, https://doi.org/10.1007/s41918-020-00086-z.
[6] X. Li, Z. Cheng, X. Wang, *Electrochem. Energy Rev.* **2021**, *4*, 136.
[7] S. Jiao, X. Fu, S. Wang, Y. Zhao, *Energy Environ. Sci.* **2021**, *14*, 1722.
[8] Z. Chen, H. Qing, K. Zhou, D. Sun, R. Wu, *Prog. Mater. Sci.* **2020**, *108*, 100618.
[9] International Energy Agency (IEA), The Future of Hydrogen: Seizing today's opportunities, OECD, Paris Cedex 16 **2019**, https://doi.org/10.1787/1e0514c4-en.
[10] Y. Yao, S. Hu, W. Chen, Z. Huang, W. Wei, T. Yao, R. Liu, K. Zang, X. Wang, G. Wu, W. Yuan, T. Yuan, B. Zhu, W. Liu, Z. Li, D. He, Z. Xue, Y. Wang, X. Zheng, J. Dong, C. Chang, Y. Chen, X. Hong, J. Luo, S. Wei, W. Li, P. Strasser, Y. Wu, Y. Li, *Nat. Catal.* **2019**, *2*, 304.
[11] A. Indra, R. Beltrán-Suito, M. Müller, R. P. Sivasankaran, M. Schwarze, A. Acharjya, B. Pradhan, J. Hofkens, A. Brückner, A. Thomas, P. W. Menezes, M. Driess, *ChemSusChem* **2021**, *14*, 306.
[12] A. Indra, A. Acharjya, P. W. Menezes, C. Merschjann, D. Hollmann, M. Schwarze, M. Aktas, A. Friedrich, S. Lochbrunner, A. Thomas, M. Driess, *Angew. Chem., Int. Ed.* **2017**, *56*, 1653.
[13] B. Chakraborty, A. Indra, P. V. Menezes, M. Driess, P. W. Menezes, *Mater. Today Chem.* **2020**, *15*, 100226.
[14] S. Anantharaj, S. Noda, V. R. Jothi, S. Yi, M. Driess, P. W. Menezes, *Angew. Chem.* **2021**, *133*, 2.
[15] J. Zhang, Z. Zhang, Y. Ji, J. Yang, K. Fan, X. Ma, C. Wang, R. Shu, Y. Chen, *Appl. Catal., B* **2021**, *282*, 119609.
[16] Y. Jiao, Y. Zheng, M. Jaroniec, S. Z. Qiao, *Chem. Soc. Rev.* **2015**, *44*, 2060.
[17] J. Xu, D. Aili, Q. Li, E. Christensen, J. O. Jensen, W. Zhang, M. K. Hansen, G. Liu, X. Wang, N. J. Bjerrum, *Energy Environ. Sci.* **2014**, *7*, 820.
[18] C. Niether, S. Faure, A. Bordet, J. Deseure, M. Chatenet, J. Carrey, B. Chaudret, A. Rouet, *Nat. Energy* **2018**, *3*, 476.
[19] Z. Chen, Y. Ha, Y. Liu, H. Wang, H. Yang, H. Xu, Y. Li, R. Wu, *ACS Appl. Mater. Interfaces* **2018**, *10*, 7134.
[20] J. Yu, Y. Zhong, X. Wu, J. Sunarso, M. Ni, W. Zhou, Z. Shao, *Adv. Sci.* **2018**, *5*, 1800514.
[21] B. Chakraborty, R. Beltrán-Suito, V. Hlukhyy, J. Schmidt, P. W. Menezes, M. Driess, *ChemSusChem* **2020**, *13*, 3222.
[22] Y. Surendranath, M. W. Kanan, D. G. Nocera, *J. Am. Chem. Soc.* **2010**, *132*, 16501.
[23] A. Indra, P. W. Menezes, I. Zaharieva, H. Dau, M. Driess, *J. Mater. Chem. A* **2020**, *8*, 2637.
[24] C. Lu, D. Tranca, J. Zhang, F. R. Hernández, Y. Su, X. Zhuang, F. Zhang, G. Seifert, X. Feng, *ACS Nano* **2017**, *11*, 3933.
[25] J. Masa, I. Sinev, H. Mistry, E. Ventosa, M. de la Mata, J. Arbiol, M. Muhler, B. R. Cuenya, W. Schuhmann, *Adv. Energy Mater.* **2017**, *7*, 1700381.
[26] P. W. Menezes, C. Walter, B. Chakraborty, J. N. Hausmann, I. Zaharieva, A. Frick, E. von Hau, H. Dau, M. Driess, *Adv. Mater.* **2021**, *33*, 2004098.
[27] P. W. Menezes, A. Indra, I. Zaharieva, C. Walter, S. Loos, S. Hoffmann, R. Schlögl, H. Dau, M. Driess, *Energy Environ. Sci.* **2019**, *12*, 988.
[28] B. Chakraborty, R. Beltrán-Suito, J. N. Hausmann, S. Garai, M. Driess, P. W. Menezes, *Adv. Energy Mater.* **2020**, *10*, 2001377.
[29] J. N. Hausmann, R. A. Khalaniya, C. Das, I. Remy-Speckmann, S. Berendts, A. V. Shevelkov, M. Driess, P. W. Menezes, *Chem. Commun.* **2021**, *57*, 2184.
[30] P. W. Menezes, S. Yao, R. Beltrn-Suito, J. N. Hausmann, P. V. Menezes, M. Driess, *Angew. Chem., Int. Ed.* **2021**, *60*, 4640.
[31] W. Zhang, Y. Zou, H. Liu, S. Chen, X. Wang, H. Zhang, X. She, D. Yang, *Nano Energy* **2019**, *56*, 813.
[32] Y. Xu, C. Wang, Y. Huang, J. Fu, *Nano Energy* **2021**, *80*, 105545.
[33] H. Jin, X. Liu, A. Vasileff, Y. Jiao, Y. Zhao, Y. Zheng, S. Qiao, *ACS Nano* **2018**, *12*, 12761.
[34] H. Yang, Z. Chen, W. Hao, H. Xu, Y. Guo, R. Wu, *Appl. Catal., B* **2019**, *252*, 214.
[35] C. Hu, L. Zhang, Z. Zhao, A. Li, X. Chang, J. Gong, *Adv. Mater.* **2018**, *30*, 1705538.
[36] C. G. Morales-Guio, L. A. Stern, X. Hu, *Chem. Soc. Rev.* **2014**, *43*, 6555.
[37] Y. Chen, G. Yu, W. Chen, Y. Liu, G. D. Li, P. Zhu, Q. Tao, Q. Li, J. Liu, X. Shen, H. Li, X. Huang, D. Wang, T. Asefa, X. Zou, *J. Am. Chem. Soc.* **2017**, *139*, 12370.
[38] C. Xia, Q. Jiang, C. Zhao, M. N. Hedhili, H. N. Alshareef, *Adv. Mater.* **2016**, *28*, 77.
[39] R. Ye, P. Del Angel-Vicente, Y. Liu, M. J. Arellano-Jimenez, Z. Peng, T. Wang, Y. Li, B. I. Yakobson, S. H. Wei, M. J. Yacaman, J. M. Tour, *Adv. Mater.* **2016**, *28*, 1427.
[40] I. Katsounaros, S. Cherevko, A. R. Zeradjanin, K. J. Mayrhofer, *Angew. Chem., Int. Ed.* **2014**, *53*, 102.
[41] Z. Yan, H. Sun, X. Chen, H. Liu, Y. Zhao, H. Li, W. Xie, F. Cheng, J. Chen, *Nat. Commun.* **2018**, *9*, 2373.
[42] J. Kwon, H. Han, S. Choi, K. Park, S. Jo, U. Paik, T. Song, *ChemCatChem* **2019**, *11*, 5898.
[43] Y. Wang, Q. Cao, C. Guan, C. Cheng, *Small* **2020**, *16*, 2002902.
[44] P. Wang, T. Jia, B. Wang, *J. Power Sources* **2020**, *474*, 228621.
[45] T. Ma, S. Dai, S. Qiao, *Mater. Today* **2016**, *19*, 265.
[46] J. Jiang, Y. Li, J. Liu, X. Huang, C. Yuan, X. Lou, *Adv. Mater.* **2012**, *24*, 5166.
[47] X. Shan, J. Liu, H. Mu, Y. Xiao, B. Mei, W. Liu, G. Lin, Z. Jiang, L. Wen, L. Jiang, *Angew. Chem., Int. Ed.* **2020**, *59*, 1659.
[48] W. Xu, Z. Lu, X. Sun, L. Jiang, X. Duan, *Acc. Chem. Res.* **2018**, *51*, 1590.
[49] G. Chen, T. Ma, Z. Liu, N. Li, Y. Su, K. Davey, S. Qiao, *Adv. Funct. Mater.* **2016**, *26*, 3314.
[50] H. Sun, Z. Yan, F. Liu, W. Xu, F. Cheng, J. Chen, *Adv. Mater.* **2020**, *32*, 1806326.
[51] S. Verma, S. Sinha-Ray, S. Sinha-Ray, *Polymers* **2020**, *12*, 238.

[52] J. Liu, D. Zhu, Y. Zheng, A. Vasileff, S. Qiao, *ACS Catal.* **2018**, *8*, 6707.
[53] J. Zhang, C. Si, T. Kou, J. Wang, Z. Zhang, *Sustainable Energy Fuels* **2020**, *4*, 2625.
[54] Y. Zhang, J. Xiao, Q. Lv, S. Wang, *Front. Chem. Sci. Eng.* **2018**, *12*, 494.
[55] H. Wang, C. Tsai, D. Kong, K. Chan, F. Abild-Pedersen, J. K. Nørskov, Y. Cui, *Nano Res.* **2015**, *8*, 566.
[56] E. Skúlason, V. Tripkovic, M. E. Björketun, S. Gudmundsdóttir, G. Karlberg, J. Rossmeisl, T. Bligaard, H. Jónsson, J. K. Nørskov, *J. Phys. Chem. C* **2010**, *114*, 18182.
[57] P. Li, R. Zhao, H. Chen, H. Wang, P. Wei, H. Huang, Q. Liu, T. Li, X. Shi, Y. Zhang, M. Liu, X. Sun, *Small* **2019**, *15*, 1805103.
[58] L. Lv, Z. Yang, K. Chen, C. Wang, Y. Xiong, *Adv. Energy Mater.* **2019**, *9*, 1803358.
[59] I. C. Man, H. Su, F. Calle-Vallejo, H. A. Hansen, J. I. Martínez, N. G. Inoglu, J. Kitchin, T. F. Jaramillo, J. K. Nørskov, J. Rossmeisl, *ChemCatChem* **2011**, *3*, 1159.
[60] J. Lu, S. Yin, P. Shen, *Electrochem. Energy Rev.* **2019**, *2*, 105.
[61] S. Anantharaj, S. Noda, M. Driess, P. W. Menezes, *ACS Energy Lett.* **2021**, *6*, 1607.
[62] C. Wei, Z. J. Xu, *Small Methods* **2018**, *2*, 1800168.
[63] M. Carmo, D. L. Fritz, J. Mergel, D. Stolten, *Int. J. Hydrogen Energy* **2013**, *38*, 4901.
[64] K. Xu, H. Ding, H. Lv, S. Tao, P. Chen, X. Wu, W. Chu, C. Wu, Y. Xie, *ACS Catal.* **2017**, *7*, 310.
[65] A. Dutta, N. Pradhan, *J. Phys. Chem. Lett.* **2017**, *8*, 144.
[66] X. Shang, K. Yan, Z. Liu, S. Lu, B. Dong, J. Chi, X. Li, Y. Liu, Y. Chai, C. Liu, *Appl. Surf. Sci.* **2017**, *402*, 120.
[67] Z. Chen, Y. Ha, H. Jia, X. Yan, M. Chen, M. Liu, R. Wu, *Adv. Energy Mater.* **2019**, *9*, 1803918.
[68] C. Panda, P. W. Menezes, M. Driess, *Angew. Chem., Int. Ed.* **2018**, *57*, 11130.
[69] W. Hao, H. Huang, Z. Chen, L. Wang, X. Ma, M. Huang, X. Ou, Y. Guo, *Electrochim. Acta* **2020**, *354*, 136645.
[70] C. Panda, P. W. Menezes, C. Walter, S. Yao, M. E. Miehlich, V. Gutkin, K. Meyer, M. Driess, *Angew. Chem., Int. Ed.* **2017**, *56*, 10506.
[71] W. Hao, R. Wu, H. Yang, Y. Guo, *J. Mater. Chem. A* **2019**, *7*, 12440.
[72] P. W. Menezes, C. Walter, J. N. Hausmann, R. Beltrán-Suito, C. Schlesiger, S. Praetz, V. Y. Verchenko, A. V. Shevelkov, M. Driess, *Angew. Chem., Int. Ed.* **2019**, *58*, 16569.
[73] B. Chakraborty, S. Kalra, R. Beltrán-Suito, C. Das, T. Hellmann, P. W. Menezes, M. Driess, *Chem. - Asian J.* **2020**, *15*, 852.
[74] P. W. Menezes, A. Indra, V. Gutkin, M. Driess, *Chem. Commun.* **2017**, *53*, 8018.
[75] J. N. Hausmann, E. M. Heppke, R. Beltrán-Suito, J. Schmidt, M. Mühlbauer, M. Lerch, P. W. Menezes, M. Driess, *ChemCatChem* **2020**, *12*, 1161.
[76] M. Kim, M. A. R. Anjum, M. Lee, B. J. Lee, J. S. Lee, *Adv. Funct. Mater.* **2019**, *29*, 1809151.
[77] Y. Chen, Z. Ren, H. Fu, X. Zhang, G. Tian, H. Fu, *Small* **2018**, *14*, 1800763.
[78] H. Yang, Z. Chen, P. Guo, B. Fei, R. Wu, *Appl. Catal., B* **2020**, *261*, 118240.
[79] G. Zhang, B. Wang, J. Bi, D. Fang, S. Yang, *J. Mater. Chem. A* **2019**, *7*, 5769.
[80] G. Cao, H. Wu, X. Wen, X. Liu, W. Zang, Z. Hong, J. Ding, P. Yuan, S. J. Pennycook, J. Wang, *Nano Energy* **2018**, *48*, 73.
[81] J. Song, C. Wei, Z. Huang, C. Liu, L. Zeng, X. Wang, Z. Xu, *Chem. Soc. Rev.* **2020**, *49*, 2196.
[82] C. L. Bentley, M. Kang, P. R. Unwin, *J. Am. Chem. Soc.* **2019**, *141*, 2179.
[83] C. Jiao, M. Hassan, X. Bo, M. Zhou, *J. Alloys Compd.* **2018**, *764*, 88.
[84] A. Vasileff, S. Chen, S. Qiao, *Nanoscale Horiz.* **2016**, *1*, 41.
[85] M. Yao, H. Hu, B. Sun, N. Wang, W. Hu, S. Komarneni, *Small* **2019**, *15*, 1905201.
[86] Y. Wang, S. Zhao, Y. Zhu, R. Qiu, T. Gengenbach, Y. Liu, L. Zu, H. Mao, H. Wang, J. Tang, D. Zhao, C. Selomulya, *iScience* **2020**, *23*, 100761.
[87] C. Tang, N. Cheng, Z. Pu, W. Xing, X. Sun, *Angew. Chem., Int. Ed.* **2015**, *54*, 9351.
[88] B. Liu, Y. Wang, H. Peng, R. Yang, Z. Jiang, X. Zhou, C. Lee, H. Zhao, W. Zhang, *Adv. Mater.* **2018**, *30*, 1803144.
[89] Y. Yin, J. Xu, W. Guo, Z. Wang, X. Du, C. Chen, Z. Zheng, D. Liu, D. Qu, Z. Xie, H. Tang, J. Li, *Electrochim. Acta* **2019**, *307*, 451.
[90] Y. Jiang, Y. Lu, J. Lin, X. Wang, Z. Shen, *Small Methods* **2018**, *2*, 1700369.
[91] A. Kumar, S. Bhattacharyya, *ACS Appl. Mater. Interfaces* **2017**, *9*, 41906.
[92] G. Han, X. Li, Y. Liu, B. Dong, W. Hu, X. Shang, X. Zhao, Y. Chai, Y. Liu, C. Liu, *RSC Adv.* **2016**, *6*, 52761.
[93] L. Jin, H. Xu, C. Wang, Y. Wang, H. Shang, Y. Du, *Nanoscale* **2020**, *12*, 21850.
[94] L. Yu, X. Yu, X. Lou, *Adv. Mater.* **2018**, *30*, 1800939.
[95] J. Nai, X. Lou, *Adv. Mater.* **2018**, *30*, 1706825.
[96] J. Tian, N. Cheng, Q. Liu, X. Sun, Y. He, A. M. Asiri, *J. Mater. Chem. A* **2015**, *3*, 20056.
[97] Y. Tan, H. Wang, P. Liu, Y. Shen, C. Cheng, A. Hirata, T. Fujita, Z. Tang, M. Chen, *Energy Environ. Sci.* **2016**, *9*, 2257.
[98] P. W. Menezes, A. Indra, A. Bergmann, P. Chernev, C. Walter, H. Dau, P. Strasser, M. Driess, *J. Mater. Chem. A* **2016**, *4*, 10014.
[99] N. C. S. Selvam, L. Du, B. Xia, P. J. Yoo, B. You, *Adv. Funct. Mater.* **2021**, *31*, 2008190.
[100] B. Singh, O. Prakash, P. Maiti, P. W. Menezes, A. Indra, *Chem. Commun.* **2020**, *56*, 15036.
[101] J. N. Hausmann, S. Mebs, K. Laun, I. Zebger, H. Dau, P. W. Menezes, M. Driess, *Energy Environ. Sci.* **2020**, *13*, 3607.
[102] L. A. Stern, L. Feng, F. Song, X. Hu, *Energy Environ. Sci.* **2015**, *8*, 2347.
[103] T. Wu, S. Sun, J. Song, S. Xi, Y. Du, B. Chen, W. A. Sasangka, H. Liao, C. Gan, G. G. Scherer, L. Zeng, H. Wang, H. Li, A. Grimaud, Z. Xu, *Nat. Catal.* **2019**, *2*, 763.
[104] X. Liu, R. Guo, K. Ni, F. Xia, C. Niu, B. Wen, J. Meng, P. Wu, J. Wu, X. Wu, L. Mai, *Adv. Mater.* **2020**, *32*, 2001136.
[105] X. Liu, K. Ni, B. Wen, R. Guo, C. Niu, J. Meng, Q. Li, P. Wu, Y. Zhu, X. Wu, L. Mai, *ACS Energy Lett.* **2019**, *4*, 2585.
[106] H. Yang, J. Liu, Z. Chen, R. Wang, B. Fei, H. Liu, Y. Guo, R. Wu, *Chem. Eng. J.* **2021**, *420*, 127671.
[107] L. Yu, H. Zhou, J. Sun, F. Qin, F. Yu, J. Bao, Y. Yu, S. Chen, Z. Ren, *Energy Environ. Sci.* **2017**, *10*, 1820.
[108] Z. Wang, S. Wang, L. Ma, Y. Guo, J. Sun, N. Zhang, R. Jiang, *Small* **2021**, *17*, 2006770.
[109] B. Fei, Z. Chen, J. Liu, H. Xu, X. Yan, H. Qing, M. Chen, R. Wu, *Adv. Energy Mater.* **2020**, *10*, 2001963.
[110] J. Wang, H. Zhong, Z. Wang, F. Meng, X. Zhang, *ACS Nano* **2016**, *10*, 2342.
[111] M. Amiri, M. Fallahi, A. Bezaatpour, R. Jijie, M. Nozari-asbmarz, M. Rouhi, R. Boukherroub, S. Szunerits, *J. Phys. Chem. C* **2018**, *122*, 16510.
[112] W. Hao, R. Wu, H. Huang, X. Ou, L. Wang, D. Sun, X. Ma, Y. Guo, *Energy Environ. Sci.* **2020**, *13*, 102.
[113] A. Sahasrabudhe, H. Dixit, R. Majee, S. Bhattacharyya, *Nat. Commun.* **2018**, *9*, 2014.
[114] Y. Ha, L. Shi, Z. Chen, R. Wu, *Adv. Sci.* **2019**, *6*, 1900272.
[115] B. C. M. Martindale, E. Reisner, *Adv. Energy Mater.* **2016**, *6*, 1502095.
[116] S. Kim, M. Cho, Y. Lee, *J. Electrochem. Soc.* **2017**, *164*, 3029.
[117] W. Hao, R. Wu, R. Zhang, Y. Ha, Z. Chen, L. Wang, Y. Yang, X. Ma, D. Sun, F. Fang, Y. Guo, *Adv. Energy Mater.* **2018**, *8*, 1801372.

[118] C. Du, M. Shang, J. Mao, W. Song, *J. Mater. Chem. A* **2017**, *5*, 15940.
[119] F. Ming, H. Liang, H. Shi, X. Xu, G. Mei, Z. Wang, *J. Mater. Chem. A* **2016**, *4*, 15148.
[120] Z. Pu, Y. Xue, W. Li, I. S. Amiinu, S. Mu, *New J. Chem.* **2017**, *41*, 2154.
[121] Y. Zhang, X. Xia, X. Cao, B. Zhang, N. H. Tiep, H. He, S. Chen, Y. Huang, H. Fan, *Adv. Energy Mater.* **2017**, *7*, 1700220.
[122] M. A. R. Anjuma, M. S. Okyay, M. Kim, M. Lee, N. Park, J. Lee, *Nano Energy* **2018**, *53*, 286.
[123] Q. Daniel, R. B. Ambre, B. Zhang, B. Philippe, H. Chen, F. Li, K. Fan, S. Ahmadi, H. Rensmo, L. Sun, *ACS Catal.* **2017**, *7*, 1143.
[124] C. Panda, P. W. Menezes, M. Zheng, S. Orthmann, M. Driess, *ACS Energy Lett.* **2019**, *4*, 747.
[125] A. Indra, P. W. Menezes, C. Das, C. Göbel, M. Tallarida, D. Schmeißer, M. Driess, *J. Mater. Chem. A* **2017**, *5*, 5171.
[126] L. Zhang, P. Zhu, F. Zhou, W. Zeng, H. Su, G. Li, J. Gao, R. Sun, C. Wong, *ACS Nano* **2016**, *10*, 1273.
[127] C. G. Morales-Guio, L. Liardet, X. Hu, *J. Am. Chem. Soc.* **2016**, *138*, 8946.
[128] Y. Pi, Q. Shao, P. Wang, F. Lv, S. Guo, J. Gu, X. Huang, *Angew. Chem., Int. Ed.* **2017**, *56*, 4502.
[129] Y. Sun, C. Liu, D. C. Grauer, J. Yano, J. Long, P. Yang, C. Chang, *J. Am. Chem. Soc.* **2013**, *135*, 17699.
[130] C. Lv, Z. Peng, Y. Zhao, Z. Huang, C. Zhang, *J. Mater. Chem. A* **2016**, *4*, 1454.
[131] F. Wang, Y. Li, T. Shifa, K. Liu, F. Wang, Z. Wang, P. Xu, Q. Wang, J. He, *Angew. Chem., Int. Ed.* **2016**, *55*, 6919.
[132] C. R. K. Rao, D. C. Trivedi, *Coord. Chem. Rev.* **2005**, *249*, 613.
[133] A. S. Batchellor, S. W. Boettcher, *ACS Catal.* **2015**, *5*, 6680.
[134] Y. Zhao, C. Chang, F. Teng, Y. Zhao, G. Chen, R. Shi, G. I. N. Waterhouse, W. Huang, T. Zhang, *Adv. Energy Mater.* **2017**, *7*, 1700005.
[135] L. Feng, G. Yu, Y. Wu, G. Li, H. Li, Y. Sun, T. Asefa, W. Chen, X. Zou, *J. Am. Chem. Soc.* **2015**, *137*, 14023.
[136] W. Zhang, X. Wen, S. Yang, Y. Berta, Z. Wang, *Adv. Mater.* **2003**, *15*, 822.
[137] W. Zhu, T. Zhang, Y. Zhang, Z. Yue, Y. Li, R. Wang, Y. Ji, X. Sun, J. Wang, *Appl. Catal., B* **2019**, *244*, 844.
[138] W. Li, S. Zhang, Q. Fan, F. Zhang, S. Xu, *Nanoscale* **2017**, *9*, 5677.
[139] Z. Zheng, L. Lin, S. Mo, D. Ou, J. Tao, R. Qin, X. Fang, N. Zheng, *Small* **2018**, *14*, 1800759.
[140] B. Zhang, C. Xiao, S. Xie, J. Liang, X. Chen, Y. Tang, *Chem. Mater.* **2016**, *28*, 6934.
[141] X. Gan, Y. Wu, L. Liu, B. Shen, W. Hu, *Surf. Coat. Technol.* **2007**, *201*, 7018.
[142] Y. Li, H. Zhang, M. Jiang, Q. Zhang, P. He, X. Sun, *Adv. Funct. Mater.* **2017**, *27*, 1702513.
[143] F. Song, W. Li, J. Yang, G. Han, P. Liao, Y. Sun, *Nat. Commun.* **2018**, *9*, 4531.
[144] X. Yu, Z. Yu, X. Zhang, P. Li, B. Sun, X. Gao, K. Yan, H. Liu, Y. Duan, M. Gao, G. Wang, S. Yu, *Nano Energy* **2020**, *71*, 104652.
[145] G. Cai, W. Zhang, L. Jiao, S. Yu, H. Jiang, *Chem* **2017**, *2*, 791.
[146] B. Geng, F. Yan, L. Liu, C. Zhu, B. Li, Y. Chen, *Chem. Eng. J.* **2021**, *406*, 126815.
[147] S. Zou, M. S. Burke, M. G. Kast, J. Fan, N. Danilovic, S. W. Boettcher, *Chem. Mater.* **2015**, *27*, 8011.
[148] T. Reier, Z. Pawolek, S. Cherevko, M. Bruns, T. Jones, D. Teschner, S. Selve, A. Bergmann, H. N. Nong, R. Schlogl, K. J. J. Mayrhofer, P. Strasser, *J. Am. Chem. Soc.* **2015**, *137*, 13031.
[149] C. Walter, P. W. Menezes, S. Orthmann, J. Schuch, P. Connor, B. Kaiser, M. Lerch, M. Driess, *Angew. Chem., Int. Ed.* **2018**, *57*, 698.
[150] S. Yao, V. Forstner, P. W. Menezes, C. Panda, S. Mebs, E. M. Zolnhofer, M. E. Miehlich, T. Szilvasi, N. A. Kumar, M. Haumann, K. Meyer, H. Grützmacher, M. Driess, *Chem. Sci.* **2018**, *9*, 8590.
[151] P. W. Menezes, C. Panda, S. Loos, F. Bunschei-Bruns, C. Walter, M. Schwarze, X. Deng, H. Dau, M. Driess, *Energy Environ. Sci.* **2018**, *11*, 1287.
[152] P. W. Menezes, C. Panda, S. Garai, C. Walter, A. Guiet, M. Driess, *Angew. Chem., Int. Ed.* **2018**, *57*, 15237.
[153] C. Ray, S. C. Lee, K. V. Sankar, B. Jin, J. Lee, J. H. Park, S. C. Jun, *ACS Appl. Mater. Interfaces* **2017**, *9*, 37739.
[154] C. Yang, H. Lei, W. Zhou, J. Zeng, Q. Zhang, Y. Hua, C. Xu, *J. Mater. Chem. A* **2018**, *6*, 14281.
[155] P. Kuang, T. Tong, K. Fan, J. Yu, *ACS Catal.* **2017**, *7*, 6179.
[156] J. Zhang, R. Cui, X. Li, X. Liu, W. Huang, *J. Mater. Chem. A* **2017**, *5*, 23536.
[157] Y. Yang, H. Yao, Z. Yu, S. M. Islam, H. He, M. Yuan, Y. Yue, K. Xu, W. Hao, G. Sun, H. Li, S. Ma, P. Zapol, M. G. Kanatzidis, *J. Am. Chem. Soc.* **2019**, *141*, 10417.
[158] X. Zou, X. Huang, A. Goswami, R. Silva, B. R. Sathe, E. Mikmekov, T. Asefa, *Angew. Chem., Int. Ed.* **2014**, *53*, 4372.
[159] T. Liu, X. Ma, D. Liu, S. Hao, G. Du, Y. Ma, A. M. Asiri, X. Sun, L. Chen, *ACS Catal.* **2017**, *7*, 98.
[160] Z. Pu, S. Wei, Z. Chen, S. Mu, *Appl. Catal., B* **2016**, *196*, 193.
[161] B. Liu, Y. Zhao, H. Peng, Z. Zhang, C. Sit, M. Yuen, T. Zhang, C. Lee, W. Zhang, *Adv. Mater.* **2017**, *29*, 1606521.
[162] Y. Men, P. Li, J. Zhou, G. Cheng, S. Chen, W. Luo, *ACS Catal.* **2019**, *9*, 3744.
[163] W. Cheng, H. Zhang, X. Zhao, H. Su, F. Tang, J. Tian, Q. Liu, *J. Mater. Chem. A* **2018**, *6*, 9420.
[164] R. Zhang, X. Wang, S. Yu, T. Wen, X. Zhu, F. Yang, X. Sun, X. Wang, W. Hu, *Adv. Mater.* **2017**, *29*, 1605502.
[165] X. Zou, Y. Zhang, *Chem. Soc. Rev.* **2015**, *44*, 5148.
[166] K. Sun, I. A. Moreno-Hernandez, W. C. SchmidtJr., X. Zhou, J. C. Crompton, R. Liu, F. H. Saadi, Y. Chen, K. M. Papadantonakis, N. S. Lewis, *Energy Environ. Sci.* **2017**, *10*, 987.
[167] L. C. Seitz, C. F. Dickens, K. Nishio, Y. Hikita, J. Montoya, A. Doyle, C. Kirk, A. Vojvodic, H. Y. Hwang, J. K. Norskov, T. F. Jaramillo, *Science* **2016**, *353*, 1011.
[168] C. Ray, S. Lee, K. V. Sankar, B. Jin, J. Lee, J. Park, S. Jun, *ACS Appl. Mater. Interfaces* **2017**, *9*, 37739.
[169] Z. Liu, H. Tan, D. Liu, X. Liu, J. Xin, J. Xie, M. Zhao, L. Song, L. Dai, H. Liu, *Adv. Sci.* **2019**, *6*, 1801829.
[170] L. Wang, X. Duan, X. Liu, J. Gu, R. Si, Y. Qiu, Y. Qiu, D. Shi, F. Chen, X. Sun, J. Lin, J. Sun, *Adv. Energy Mater.* **2020**, *10*, 1903137.
[171] B. Fei, Z. Chen, Y. Ha, R. Wang, H. Yang, H. Xu, R. Wu, *Chem. Eng. J.* **2020**, *394*, 124926.
[172] G. Ye, Y. Gong, J. Lin, B. Li, Y. He, S. T. Pantelides, W. Zhou, R. Vajtai, P. M. Ajayan, *Nano Lett.* **2016**, *16*, 1097.
[173] C. Dinh, A. Jain, F. P. G. de Arquer, P. D. Luna, J. Li, N. Wang, X. Zheng, J. Cai, B. Z. Gregory, O. Voznyy, B. Zhang, M. Liu, D. Sinton, E. J. Crumlin, E. H. Sargent, *Nat. Energy* **2019**, *4*, 107.
[174] Y. Kuang, M. J. Kenney, Y. Meng, W. Hung, Y. Liu, J. Huang, R. Prasanna, P. Li, Y. Li, L. Wang, M. Lin, M. D. McGehee, X. Sun, H. Dai, *Proc. Natl. Acad. Sci. U. S. A.* **2019**, *116*, 6624.
[175] S. Dresp, F. Dionigi, M. Klingenhof, P. Strasser, *ACS Energy Lett.* **2019**, *4*, 933.
[176] B. S. Oh, S. G. Oh, Y. Hwang, H. Yu, J. Kang, I. S. Kim, *Sci. Total Environ.* **2010**, *408*, 5958.
[177] H. K. Abdel-Aal, I. A. Hussein, *Int. J. Hydrogen Energy* **1993**, *18*, 485.
[178] F. Dionigi, T. Reier, Z. Pawolek, M. Gliech, P. Strasser, *ChemSusChem* **2016**, *9*, 962.
[179] D. W. Kirk, A. E. Ledas, *Int. J. Hydrogen Energy* **1982**, *7*, 925.
[180] J. E. Bennett, *Int. J. Hydrogen Energy* **1980**, *5*, 401.
[181] M. Schalenbach, T. Hoefner, P. Paciok, M. Carmo, W. Lueke, D. Stolten, *J. Phys. Chem. C* **2015**, *119*, 25145.

[182] W. Tong, M. Forster, F. Dionigi, S. Dresp, R. S. Erami, P. Strasser, A. J. Cowan, P. Farràs, *Nat. Energy* **2020**, *5*, 367.
[183] L. Yu, L. Wu, B. McElhenny, S. Song, D. Luo, F. Zhang, Y. Yu, S. Chen, Z. Ren, *Energy Environ. Sci.* **2020**, *13*, 3439.
[184] J. N. Hausmann, R. Schlögl, P. W. Menezes, M. Driess, *Energy Environ. Sci.* **2021**, *14*, 3679.
[185] X. Lu, J. Pan, E. Lovell, T. Tan, Y. H. Ng, R. Amal, *Energy Environ. Sci.* **2018**, *11*, 1898.
[186] L. Wu, L. Yu, F. Zhang, B. McElhenny, D. Luo, A. Karim, S. Chen, Z. Ren, *Adv. Funct. Mater.* **2021**, *31*, 2006484.
[187] Y. Zhang, P. Li, X. Yang, W. Fa, S. Ge, *J. Alloys Compd.* **2018**, *732*, 248.
[188] J. Deng, D. Deng, X. Bao, *Adv. Mater.* **2017**, *29*, 1606967.
[189] Y. Ma, C. Wu, X. Feng, H. Tan, L. Yan, Y. Liu, Z. Kang, E. Wang, Y. Li, *Energy Environ. Sci.* **2017**, *10*, 788.
[190] T. Liu, H. Liu, X. Wu, Y. Niu, B. Feng, W. Li, W. Hu, C. Li, *Electrochim. Acta* **2018**, *281*, 710.
[191] L. Yu, Q. Zhu, S. Song, B. McElhenny, D. Wang, C. Wu, Z. Qin, J. Bao, Y. Yu, S. Chen, Z. Ren, *Nat. Commun.* **2019**, *10*, 5106.
[192] Y. Surendranath, M. Dinca, *J. Am. Chem. Soc.* **2009**, *131*, 2615.
[193] H. J. Song, H. Yoon, B. Ju, D. Y. Lee, D. W. Kim, *ACS Catal.* **2020**, *10*, 702.
[194] Y. Jia, L. Zhang, G. Gao, H. Chen, B. Wang, J. Zhou, M. T. Soo, M. Hong, X. Yan, G. Qian, J. Zou, A. Du, X. Yao, *Adv. Mater.* **2017**, *29*, 1700017.
[195] J. Zhang, Y. Wang, C. Zhang, H. Gao, L. Lv, L. Han, Z. Zhang, *ACS Sustainable Chem. Eng.* **2018**, *6*, 2231.
[196] H. Wang, H.-W. Lee, Y. Deng, Z. Lu, P.-C. Hsu, Y. Liu, D. Lin, Y. Cui, *Nat. Commun.* **2015**, *6*, 7261.
[197] Y. Yan, B. Xia, B. Zhao, X. Wang, *J. Mater. Chem. A* **2016**, *4*, 17587.
[198] Z. Chen, H. Xu, Y. Ha, X. Li, M. Liu, R. Wu, *Appl. Catal., B* **2019**, *250*, 213.
[199] P. Liu, S. Yang, B. Zhang, H. Yang, *ACS Appl. Mater. Interfaces* **2016**, *8*, 34474.
[200] B. Cao, Y. Cheng, M. Hu, P. Jing, Z. Ma, B. Liu, R. Gao, J. Zhang, *Adv. Funct. Mater.* **2019**, *29*, 1906316.
[201] H. Xu, J. Wei, K. Zhang, M. Zhang, C. Liu, J. Guo, Y. Du, *J. Mater. Chem. A* **2018**, *6*, 22697.
[202] D. Yan, R. Chen, Z. Xiao, S. Wang, *Electrochim. Acta* **2019**, *303*, 316.
[203] Y. Liu, F. Wang, T. A. Shifa, J. Li, J. Tai, Y. Zhang, J. Chu, X. Zhan, C. Shan, J. He, *Nanoscale* **2019**, *11*, 11736.
[204] R. Ma, Z. Liu, L. Li, N. Iyi, T. Sasaki, *J. Mater. Chem.* **2006**, *16*, 3809.
[205] H. Yin, Z. Tang, *Chem. Soc. Rev.* **2016**, *45*, 4873.
[206] W. Ye, X. Fang, X. Chen, D. Yan, *Nanoscale* **2018**, *10*, 19484.
[207] R. Yang, Y. Zhou, Y. Xing, D. Li, D. Jiang, M. Chen, W. Shi, S. Yuan, *Appl. Catal., B* **2019**, *253*, 131.
[208] L. Hui, Y. Xue, B. Huan, H. Yu, C. Zhang, D. Zhang, D. Jia, Y. Zhao, Y. Li, H. Liu, Y. Li, *Nat. Commun.* **2018**, *9*, 5309.
[209] C. Panda, P. W. Menezes, C. Walter, S. Yao, M. E. Miehlich, V. Gutkin, K. Meyer, M. Driess, *Angew. Chem., Int. Ed.* **2017**, *56*, 10506.
[210] J. Liu, Y. Gao, X. Tang, K. Zhan, B. Zhao, B. Y. Xia, Y. Yan, *J. Mater. Chem. A* **2020**, *8*, 19254.
[211] P. W. Menezes, A. Indra, C. Das, C. Walter, C. Göbel, V. Gutkin, D. Schmeiber, M. Driess, *ACS Catal.* **2017**, *7*, 103.
[212] Y. Wang, D. Liu, Z. Liu, C. Xie, J. Huo, S. Wang, *Chem. Commun.* **2016**, *52*, 12614.
[213] P. W. Menezes, C. Panda, C. Walter, M. Schwarze, M. Driess, *Adv. Funct. Mater.* **2019**, *29*, 1808632.
[214] R. Beltrán-Suito, V. Forstner, J. N. Hausmann, S. Mebs, J. Schmidt, I. Zaharieva, K. Laun, I. Zebger, H. Dau, P. W. Menezes, M. Driess, *Chem. Sci.* **2020**, *11*, 11834.
[215] S. Duttaa, A. Indra, Y. Feng, H. Han, T. Song, *Appl. Catal., B* **2019**, *241*, 521.
[216] I. Katsounaros, S. Cherevko, A. R. Zeradjanin, K. J. J. Mayrhofer, *Angew. Chem., Int. Ed.* **2014**, *53*, 102.
[217] L. Yu, I. K. Mishra, Y. Xie, H. Zhou, J. Sun, J. Zhou, Y. Ni, D. Luo, F. Yu, Y. Yu, S. Chen, Z. Ren, *Nano Energy* **2018**, *53*, 492.
[218] Y. Wu, Y. Liu, G. Li, X. Zou, X. Lian, D. Wang, L. Sun, T. Asefab, X. Zou, *Nano Energy* **2017**, *35*, 161.
[219] L. Cao, Y. Hu, S. Tang, A. Iljin, J. Wang, Z. Zhang, T. Lu, *Adv. Sci.* **2018**, *5*, 1800949.
[220] X. Cheng, C. Lei, J. Yang, B. Yang, Z. Li, J. Lu, X. Zhang, L. Lei, Y. Hou, K. Ostrikov, *ChemElectroChem* **2018**, *5*, 3866.
[221] C. Liang, P. Zou, A. Nairan, Y. Zhang, J. Liu, K. Liu, S. Hu, F. Kang, H. Fan, C. Yang, *Energy Environ. Sci.* **2020**, *13*, 86.
[222] Y. Wang, C. Xie, D. Liu, X. Huang, J. Huo, S. Wang, *ACS Appl. Mater. Interfaces* **2016**, *8*, 18652.
[223] C. Xiao, Y. Li, X. Lu, C. Zhao, *Adv. Funct. Mater.* **2016**, *26*, 3515.
[224] M. Yu, Z. Wang, J. Liu, F. Sun, P. Yang, J. Qiu, *Nano Energy* **2019**, *63*, 103880.
[225] Y. Luo, L. Tang, U. Khan, Q. Yu, H. Cheng, X. Zou, B. Liu, *Nat. Commun.* **2019**, *10*, 269.
[226] J. Hao, W. Yang, Z. Huang, C. Zhang, *Adv. Mater. Interfaces* **2016**, *3*, 1600236.
[227] J. E. George, S. Chidangil, S. D. George, *Adv. Mater. Interfaces* **2017**, *4*, 1601088.
[228] Y. Wang, Y. Li, L. Ding, Z. Chen, A. Ong, W. Lu, T. S. Herng, X. Li, J. Ding, *J. Mater. Chem. A* **2019**, *7*, 18816.
[229] N. Yao, P. Li, Z. Zhou, R. Meng, G. Cheng, W. Luo, *Small* **2019**, *15*, 1901993.
[230] N. Han, K. R. Yang, Z. Lu, Y. Li, W. Xu, T. Gao, Z. Cai, Y. Zhang, V. S. Batista, W. Liu, X. Sun, *Nat. Commun.* **2018**, *9*, 924.
[231] X. Liu, Y. Yao, H. Zhang, L. Pan, C. Shi, X. Zhang, Z. Huang, J. Zou, *ACS Sustainable Chem. Eng.* **2020**, *8*, 17828.
[232] D. Mitra, P. Trinh, S. Malkhandi, M. Mecklenburg, S. M. Heald, M. Balasubramanian, S. R. Narayanan, *J. Electrochem. Soc.* **2018**, *165*, 392.
[233] G. Cheng, T. Kou, J. Zhang, C. Si, H. Gao, Z. Zhang, *Nano Energy* **2017**, *38*, 155.
[234] Y. Tang, Q. Liu, L. Dong, H. Wu, X. Yu, *Appl. Catal., B* **2020**, *266*, 118627.
[235] Y. Pi, Q. Shao, P. Wang, F. Lv, S. Guo, J. Guo, X. Huang, *Angew. Chem., Int. Ed.* **2017**, *56*, 4502.
[236] M. E. C. Pascuzzi, A. J. W. Man, A. Goryachev, J. P. Hofmann, E. J. M. Hensen, *Catal. Sci. Technol.* **2020**, *10*, 5593.
[237] Y. Liu, X. Liang, L. Gu, Y. Zhang, G. Li, X. Zou, J. Chen, *Nat. Commun.* **2018**, *9*, 2609.
[238] D. Mitra, S. R. Narayanan, *Top. Catal.* **2018**, *61*, 591.
[239] P. Wang, L. Wan, Y. Lin, B. Wang, *ChemSusChem* **2019**, *12*, 4038.
[240] J. Kwon, H. Han, S. Jo, S. Choi, K. Y. Chung, G. Ali, K. Park, U. Paik, T. Song, *Adv. Energy Mater.* **2021**, *11*, 2100624.
[241] J. N. Hausmann, R. Beltrán-Suito, S. Mebs, V. Hlukhyy, T. F. Fässler, H. Dau, M. Driess, P. W. Menezes, *Adv. Mater.* **2021**, *33*, 2008823.
[242] D. Wang, Q. Li, C. Han, Q. Lu, Z. Xing, X. Yang, *Nat. Commun.* **2019**, *10*, 3899.
[243] J. Chen, Y. Wang, G. Qian, T. Yu, Z. Wang, L. Luo, F. Shen, S. Yin, *Chem. Eng. J.* **2021**, *421*, 129892.
[244] H. Yang, G. Dai, Z. Chen, J. Wu, H. Huang, Y. Liu, M. Shao, Z. Kang, *Small* **2021**, *17*, 2101727.
[245] L. Fu, X. Hu, Y. Li, G. Cheng, W. Luo, *Nanoscale* **2019**, *11*, 8898.
[246] J. R. Kish, M. B. Ives, J. R. Rodda, *J. Electrochem. Soc.* **2000**, *147*, 3637.
[247] N. T. Suen, S. F. Hung, Q. Quan, N. Zhang, Y. J. Xu, H. M. Chen, *Chem. Soc. Rev.* **2017**, *46*, 337.
[248] C. Walter, P. W. Menezes, M. Driess, *Chem. Sci.* **2021**, *12*, 8603.
[249] J. Youn, S. Jeong, H. Kang, M. Kovendhan, C. Park, K. Jeon, *Int. J. Hydrogen Energy* **2019**, *44*, 20641.

[250] S. Sarawutanukul, N. Phattharasupakun, M. Sawangphruk, *Carbon* **2019**, *151*, 109.
[251] B. S. Oh, S. G. Oh, Y. Y. Hwang, H. Yu, J. Kang, I. S. Kim, *Sci. Total Environ.* **2010**, *408*, 5958.
[252] Y. Tang, H. Zhu, L. Dong, A. Zhang, S. Li, J. Liu, Y. Lan, *Appl. Catal., B* **2019**, *245*, 528.
[253] X. Li, H. Wang, H. Yang, W. Cai, S. Liu, B. Liu, *Small Methods* **2018**, *2*, 1700395.
[254] S. Hwang, X. Chen, G. Zhou, D. Su, *Adv. Energy Mater.* **2020**, *10*, 1902105.
[255] J. H. J. Wijten, L. D. B. Mandemaker, T. C. van Eeden, J. E. Dubbeld, B. M. Weckhuysen, *ChemSusChem* **2020**, *13*, 3172.
[256] S. Parvin, A. Kumar, A. Ghosh, S. Bhattacharyya, *Chem. Sci.* **2020**, *11*, 3893.
[257] M. Yao, B. Wang, B. Sun, L. Luo, Y. Chen, J. Wang, N. Wang, S. Komarneni, X. Niua, W. Hu, *Appl. Catal., B* **2021**, *280*, 119451.
[258] L. Lei, D. Huang, Y. Chen, S. Chen, R. Deng, *J. Mater. Chem. A* **2021**, *9*, 8730.
[259] B. Liu, H. Li, B. Cao, J. Jiang, R. Gao, J. Zhang, *Adv. Funct. Mater.* **2018**, *28*, 1801527.
[260] I. K. Mishra, H. Zhou, J. Sun, K. Dahal, S. Chen, Z. Ren, *Energy Environ. Sci.* **2018**, *11*, 2246.
[261] Y. Men, P. Li, F. Yang, G. Cheng, S. Chen, W. Luo, *Appl. Catal., B* **2019**, *253*, 21.
[262] C. Yang, M. Y. Gao, Q. B. Zhang, J. R. Zeng, X. T. Li, A. P. Abbott, *Nano Energy* **2017**, *36*, 85.
[263] J. Dong, X. Zhang, J. Huang, J. Hu, Z. Che, Y. Lai, *Chem. Eng. J.* **2021**, *412*, 128556.
[264] H. Liu, X. Peng, X. Liu, G. Qi, J. Luo, *ChemSusChem* **2019**, *12*, 1334.
[265] S. Duan, Z. Liu, H. Zhuo, T. Wang, J. Liu, L. Wang, J. Liang, J. Han, Y. Huang, Q. Li, *Nanoscale* **2020**, *12*, 21743.
[266] W. Yuan, Z. Cui, S. Zhu, Z. Li, S. Wu, Y. Liang, *Electrochim. Acta* **2021**, *365*, 137366.
[267] A. R. Jadhav, A. Kumar, J. Lee, T. Yang, S. Na, J. Lee, Y. Luo, X. Liu, Y. Hwang, Y. Liu, H. Lee, *J. Mater. Chem. A* **2020**, *8*, 24501.
[268] W. Hung, B Xue, T. Lin, S. Lu, I. Tsao, *Mater. Today Energy* **2021**, *19*, 100575.
[269] Y. Zhao, B. Jin, Y. Zheng, H. Jin, Y. Jiao, S. Qiao, *Adv. Energy Mater.* **2018**, *8*, 1801926.
[270] L. Yu, L. Wu, S. Song, B. McElhenny, F. Zhang, S. Chen, Z. Ren, *ACS Energy Lett.* **2020**, *5*, 2681.
[271] F. Cheng, X. Feng, X. Chen, W. Lin, J. Rong, W. Yang, *Electrochim. Acta* **2017**, *251*, 336.
[272] Y. Huang, L. Hu, R. Liu, Y. Hu, T. Xiong, W. Qiu, M. S. Baloguna, A. Pan, Y. Tong, *Appl. Catal., B* **2019**, *251*, 181.
[273] L. Wu, L. Yu, Q. Zhu, B. McElhenny, F. Zhang, C. Wu, X. Xing, J. Bao, S. Chen, Z. Ren, *Nano Energy* **2021**, *83*, 105838.
[274] Y. Zhao, B. Jin, A. Vasileffa, Y. Jiao, S. Qiao, *J. Mater. Chem. A* **2019**, *7*, 8117.
[275] B. Cui, Z. Hu, C. Liu, S. Liu, F. Chen, S. Hu, J. Zhang, W. Zhou, Y. Deng, Z. Qin, Z. Wu, Y. Chen, L. Cui, W. Hu, *Nano Res.* **2021**, *14*, 1149.
[276] J. Zhang, S. Guo, B. Xiao, Z. Lin, L. Yan, D. Du, S. Shen, *Chem. Eng. J.* **2021**, *416*, 129127.
[277] H. Xu, B. Fei, G. Cai, Y. Ha, J. Liu, H. Jia, J. Zhang, M. Liu, R. Wu, *Adv. Energy Mater.* **2020**, *10*, 1902714.
[278] Z. Chen, B. Fei, M. Hou, X. Yan, M. Chen, H. Qing, R. Wu, *Nano Energy* **2020**, *68*, 104371.
[279] C. Hsieh, C. Huang, Y. Chen, S. Lu, *Appl. Catal., B* **2020**, *267*, 118376.
[280] L. Yang, R. Liu, L. Jiao, *Adv. Funct. Mater.* **2020**, *30*, 1909618.
[281] H. Zhou, F. Yu, Q. Zhu, J. Sun, F. Qin, L. Yu, J. Bao, Y. Yu, S. Chen, Z. Ren, *Energy Environ. Sci.* **2018**, *11*, 2858.
[282] Y. Liu, Q. Li, R. Si, G. Li, W. Li, D. Liu, D. Wang, L. Sun, Y. Zhang, X. Zou, *Adv. Mater.* **2017**, *29*, 1606200.
[283] Y. Yang, K. Zhang, H. Lin, X. Li, H. Chan, L. Yang, Q. Gao, *ACS Catal.* **2017**, *7*, 2357.
[284] W. Hao, D. Yao, Q. Xu, R. Wang, C. Zhang, Y. Guo, R. Sun, M. Huang, Z. Chen, *Appl. Catal., B* **2021**, *292*, 120188.
[285] X. Gao, Y. Chen, T. Sun, J. Huang, W. Zhang, Q. Wang, R. Cao, *Energy Environ. Sci.* **2020**, *13*, 174.
[286] J. Liu, D. Zhu, T. Ling, A. Vasileffa, S. Qiao, *Nano Energy* **2017**, *40*, 264.
[287] K. Li, J. Zhang, R. Wu, Y. Yu, B. Zhang, *Adv. Sci.* **2016**, *3*, 1500426.
[288] H. Sun, Y. Min, W. Yang, Y. Lian, L. Lin, K. Feng, Z. Deng, M. Chen, J. Zhong, L. Xu, Y. Peng, *ACS Catal.* **2019**, *9*, 8882.
[289] J. Zhang, X. Shang, H. Ren, J. Chi, H. Fu, B. Dong, C. Liu, Y. Chai, *Adv. Mater.* **2019**, *31*, 1905107.
[290] L. Hui, Y. Xue, D. Jia, H. Yu, C. Zhang, Y. Li, *Adv. Energy Mater.* **2018**, *8*, 1800175.
[291] F. Yu, H. Zhou, Y. Huang, J. Sun, F. Qin, J. Bao, W. A. Goddard, S. Chen, Z. Ren, *Nat. Commun.* **2018**, *9*, 2551.
[292] X. Yu, Z. Y. Yu, X. L. Zhang, Y. R. Zheng, Y. Duan, Q. Gao, R. Wu, B. Sun, M. R. Gao, G. Wang, S. H. Yu, *J. Am. Chem. Soc.* **2019**, *141*, 7537.
[293] X. Zou, Y. Wu, Y. Liu, D. Liu, W. Li, L. Gu, H. Liu, P. Wang, L. Sun, Y. Zhang, *Chem* **2018**, *4*, 1139.
[294] J. Jiang, F. Sun, S. Zhou, W. Hu, H. Zhang, J. Dong, Z. Jiang, J. Zhao, J. Li, W. Yan, M. Wang, *Nat. Commun.* **2018**, *9*, 2885.
[295] Z. Wu, Z. Zou, J. Huang, F. Gao, *ACS Appl. Mater. Interfaces* **2018**, *10*, 26283.
[296] X. Wang, W. Ma, C. Din, Z. Xu, H. Wang, X. Zong, C. Li, *ACS Catal.* **2018**, *8*, 9926.
[297] Y. Li, B. Wei, Z. Yu, O. Bondarchuk, A. Araujo, I. Amorim, N. Zhang, J. Xu, I. C. Neves, L. Liu, *ACS Sustainable Chem. Eng.* **2020**, *8*, 10193.
[298] E. Detsi, J. B. Cook, B. K. Lesel, C. L. Turner, Y. Liang, S. Robbennolt, S. H. Tolbert, *Energy Environ. Sci.* **2016**, *9*, 540.
[299] X. Cheng, Z. Pan, C. Lei, Y. Jin, B. Yang, Z. Li, X. Zhang, L. Lei, C. Yuan, Y. Hou, *J. Mater. Chem. A* **2019**, *7*, 965.
[300] G. Qian, J. Chen, L. Luo, T. Yu, Y. Wang, W. Jiang, Q. Xu, S. Feng, S. Yin, *ACS Sustainable Chem. Eng.* **2020**, *8*, 12063.
[301] C. Ray, S. C. Lee, B. Jin, A. Kundu, J. H. Park, S. C. Jun, *J. Mater. Chem. A* **2018**, *6*, 4466.
[302] W. Li, X. Gao, D. Xiong, F. Xia, J. Liu, W. Song, J. Xu, S. M. Thalluri, M. F. Cerqueira, X. Fu, L. Liu, *Chem. Sci.* **2017**, *8*, 2952.
[303] X. Wu, J. Li, Y. Li, Z. Wen, *Chem. Eng. J.* **2021**, *409*, 128161.
[304] S. Liu, R. Gao, M. Sun, Y. Wang, T. Nakajim, X. Liu, W. Zhang, L. Wang, *Appl. Catal., B* **2021**, *292*, 120063.
[305] G. Chen, Z. Hu, Y. Zhu, B. Gu, Y. Zhong, H. Lin, C. Chen, W. Zhou, Z. Shao, *Adv. Mater.* **2018**, *30*, 1804333.
[306] W. Li, X. Gao, D. Xiong, F. Wei, W. Song, J. Xu, L. Liu, *Adv. Energy Mater.* **2017**, *7*, 1602579.

Hongyuan Yang is currently pursuing his Ph.D. degree under the supervision of Dr. P. W. Menezes and Prof. Dr. M. Driess at the Department of Metalorganics and Inorganic Materials, Technical University of Berlin. He attained his master's degree in Materials Physicals and Chemistry from Fudan University, China in 2020. In 2017, he received his bachelor's degree in Inorganic Non-metallic Materials Engineering from Changzhou University, China. His current research interests focus on photo/electrocatalysis, especially for water splitting.

Matthias Driess is a Full Professor of metalorganics and inorganic materials at the Department of Chemistry of Technische Universität Berlin. He obtained his Ph.D. degree and completed his habilitation at the University of Heidelberg in Germany. He serves as a deputy of the Cluster of Excellence UniSysCat and is a Director of the UniSysCat-BASF SE joint lab BasCat, and of the Chemical Invention Factory (CIF) for Start-ups in Green Chemistry. He is a member of the German National Academy of Sciences (Leopoldina), the Berlin-Brandenburg Academy of Sciences and Humanities, and the European Academy of Sciences.

Prashanth W. Menezes received his Ph.D. in 2009 from the Max Planck Institute for Chemical Physics of Solids in Dresden, Germany, in solid-state and structural chemistry. He then joined the Technische Universität München in 2010 to work in the direction of inorganic chemistry with a focus on novel materials. In 2012, he joined Prof. Driess at the Technische Universität Berlin and since then serves as a group leader for inorganic materials. His research focuses on the design, development, and structural understanding of novel catalysts, especially in the area of redox oxygen catalysis, (photo)electrocatalytic water splitting and electrochemical redox reactions.